AD_____

AWARD NUMBER: W81XWH-06-1-0432

TITLE: A New In Vitro Model of Breast Cancer Metastasis to Bone

PRINCIPAL INVESTIGATOR: Andrea M. Mastro, Ph.D

CONTRACTING ORGANIZATION: Penn State University
University Park, PA 16802

REPORT DATE: April 2010

TYPE OF REPORT: Final

PREPARED FOR: U.S. Army Medical Research and Materiel Command
Fort Detrick, Maryland 21702-5012

REPORT DOCUMENTATION PAGE

Form Approved
OMB No. 0704-0188

1. REPORT DATE	2. REPORT TYPE	3. DATES COVERED
1 April 2010	Final	15 Mar 2006 – 14 Mar 2010

4. TITLE AND SUBTITLE

A New In Vitro Model of Breast Cancer Metastasis to Bone

5a. CONTRACT NUMBER

5b. GRANT NUMBER
W81XWH-06-1-0432

5c. PROGRAM ELEMENT NUMBER

6. AUTHOR(S)

Andrea M. Mastro, Ph.D.; Erwin A Vogler, Ph.D., Carol V. Gay, Ph.D.

E-Mail: a36@psu.edu

5d. PROJECT NUMBER

5e. TASK NUMBER

5f. WORK UNIT NUMBER

7. PERFORMING ORGANIZATION NAME(S) AND ADDRESS(ES)

Penn State University
University Park, PA 16802

8. PERFORMING ORGANIZATION REPORT NUMBER

9. SPONSORING / MONITORING AGENCY NAME(S) AND ADDRESS(ES)
U.S. Army Medical Research and Materiel Command
Fort Detrick, Maryland 21702-5012

10. SPONSOR/MONITOR'S ACRONYM(S)

11. SPONSOR/MONITOR'S REPORT NUMBER(S)

12. DISTRIBUTION / AVAILABILITY STATEMENT
Approved for Public Release; Distribution Unlimited

13. SUPPLEMENTARY NOTES

14. ABSTRACT
Osteoblasts (OB) grew into bone-like tissue in a 3D model system. Pre-OB matured to OB and eventually to osteocyte-like cells. These cells met the criteria of osteocytes based on shape and protein expression. In addition, the density was similar to that reported for calvaria bone. The 3-D system was used to examine the interaction of metastatic breast cancer cells, MDA-MB-231, with OB. The cancer cells brought about profound effects on the osteoid tissue. The OB changed from cuboidal to spindle shape.The cancer cells aligned into an "Indian filing" pattern, and penetrated the osteoid. Metastasis suppressed MDA-MB-231-BRMS cells attached loosely to the osteoblasts but did not colonize or penetrate the tissue. Using RT-PCR, we found that metastatic cancer cells downregulated OB differentiation proteins but increased inflammatory cytokines. We have tried to modify these effects by changing the oxidative status of the microenvironment with selenium and by adding drugs commonly used to treat metastatic breast cancer, zoledronc acid (ZOL). ZOL's main known target is the osteoclast but we found that it clearly affects osteoblasts and cancer cells. The OB morphology changes were inhibited. Selenium supplementation caused changes in the osteoblast cell morphology and permitted cancer cell growth but in a different pattern than seen in the deficient cultures. In summary the model mimics in vivo bone metastatic colonization. The results show that the osteblasts are a major target.

15. SUBJECT TERMS
3D model, osteoblasts, metastatic breast cancer, bone

16. SECURITY CLASSIFICATION OF:			17. LIMITATION OF ABSTRACT	18. NUMBER OF PAGES	19a. NAME OF RESPONSIBLE PERSON
a. REPORT	b. ABSTRACT	c. THIS PAGE			USAMRMC
U	U	U	UU	90	19b. TELEPHONE NUMBER *(include area code)*

Table of Contents

Final Report: A New In Vitro Model of Breast Cancer Metastasis to Bone

Andrea M. Mastro, Carol V. Gay and Erwin A. Vogler

INTRODUCTION:

Breast cancer frequently metastasizes to the skeleton where it disrupts the balance between osteoblasts and osteoclasts and leads to osteolytic degradation (Bussard et al. 2008). The objective of this study was to test the hypothesis that osteolytic bone metastases results partly from the affect of the cancer cells on the osteoblasts, i.e. the cancer cells prevent osteoblasts from accreting mineralized tissue ultimately leading to accelerated skeletal degradation. In order to test this idea, we proposed to develop an existing three-dimensional culture system into an *in vitro* test system for studying the interactions between osteoblasts and metastatic breast cancer cells. The objectives were to characterize the morphology and physiology of osteoblasts (MC3T3-E1) cultured as a 3D osteoid in a bioreactor and to determine how they reacted to the presence of human metastatic breast cancer cells (MDA-MB-231). In addition we proposed to determine how this interaction was affected by changing the oxidative state of the microenvironment with selenium supplementation. We also used this system to determine how the currently used drugs, e.g. zoledronic acid, affected osteoblasts and cancer cells in the 3D model.

BODY:

Task 1. To determine the effects of metastatic breast cancer cells on the physiology of osteoblasts cultured in a long term culture system that fosters growth in three-dimensions.

a. Establish cultures of MC3T3-E1 cells in bioreactors and add metastatic breast cancer cells at various times after the establishment of culture (4,7,15,30 days). Periodically sample the secreted materials in the growth chamber that will indicate osteoblast function. ELISA or RIA will be carried out for OCN, IL- 6, MIP-2, MCP-1. Alkaline phosphatase will be assayed by a biochemical assay. Culture medium from cells grown in standard tissue culture will be compared. For control cells in selected assays, a human immortalized nontumorgenic cell line, such as hTERT–HME1 will be used.
b. Establish cultures of MC3T3-E1 cells in bioreactors and add metastatic breast cancer cells at various times after the establishment of culture bioreactors as in task 1-a. Terminate the cultures periodically to assay the cells for cell associated alkaline phosphatase, Type I collagen, mineralization (alizarin red, von Kossa) and for apoptosis (TUNEL).

Task 2. To determine the effects of metastatic breast cancer cells on osteoblast morphology in a long term bioreactor culture system that fosters growth in 3-dimensions.

a. Co –cultures of osteoblasts and breast cancer cells will be prepared as in task 1. The stage of differentiation of the osteoblasts and the time of the addition of the cancer cells will be decided based on the results of task 1. Co-cultures from the bioreactor and conventional cultures will be fixed to preserve morphological detail.

b. Part of each culture will be fixed with paraformaldehyde following a protocol to preserve GFP. These cultures will be imaged with confocal fluorescence microscopy to detect the metastatic breast cancer cell migration.

c. Part of each culture will be prepared for detection of apoptosis (TUNEL). The GFP tag of the cancer cells will allow us to distinguish apoptotic cancer cells from apoptotic osteoblasts.

d. Part of each culture will be prepared for scanning electron microscopic observation. We anticipate that we will be able to distinguish cancer cells from osteoblasts in these preparations based on size and shape.

e. Part of each culture will be prepared for the transmission electron microscopy. We will view the cells with an eye to fine structural detail.

Summary of the results

Parts of tasks 1 and 2 were pursued in parallel to maximize efficiency in achieving aims of the proposed work and to provide internal consistency in the work by using live cells/biological materials in a conserved timeframe. Much of this work is published; each publication is referred to.

Main finding: Osteoblasts, both lines and primary cells, grew in a specialized bioreactor where they differentiated and formed osteoid and bone-like tissue. They expressed characteristic differentiation genes and secreted osteoblast molecules and cytokines. In long term cultures the osteoblasts differentiated into osteocytes and bone depositions occurred. Metastatic cancer cells grew in co-culture with the osteoblasts; they penetrated and degraded the osteoid tissue. The cancer cells caused the osteoblasts to undergo a morphological change from cuboidal cells to spindle-shaped cells. The osteoblasts showed reduced production of differentiation proteins, e.g. OCN, ALKP, but increased production of inflammatory molecules such as IL-6. Metastasis suppressed isologous cells only loosely attached to the osteoblasts and grew very slowly. They did not affect osteoblast differentiation or cause an inflammatory response.

Dhurjati, R, et al. Extended-Term Culture of Bone Cells in a Compartmentalized Bioreactor. *Tissue Engineering*. 12: 3045-3054, 2006. (appended)

We developed a bioreactor based on the principle of simultaneous growth and dialysis (Figure 1) which we used to culture lines of murine (MC3T3-E1, calvaria, pre-osteoblasts) and human (hFOB1.19, embryonic osteoblasts) for extended periods, i.e. up to 10 months. The cells proliferated and grow into tissue consisting of 6-8 cell layers of mature osteoblasts in the bioreactor. This growth pattern was not achievable with these cells in standard tissue culture plastic (see also Shuman et al. manuscript appended and discussion below). Although similar patterns were seen in the first 15 days of culture, but by 30 days the tissue culture plastic cultures had become unstable, while those in the bioreactor continued to differentiate and lay down an extracellular matrix (ECM). Light microscopy and scanning and transmission electron microscopy were used to phenotype the cultures. The images showed mutilayers of osteoblasts embedded in an ECM (Figure 2). The cells differentiate as evidenced by expression of bone alkaline phosphatase and staining with alizarin red. The murine cells also showed mineralization based on von Kossa staining and mineralized nodules visible by electron microscopy (Table 1).

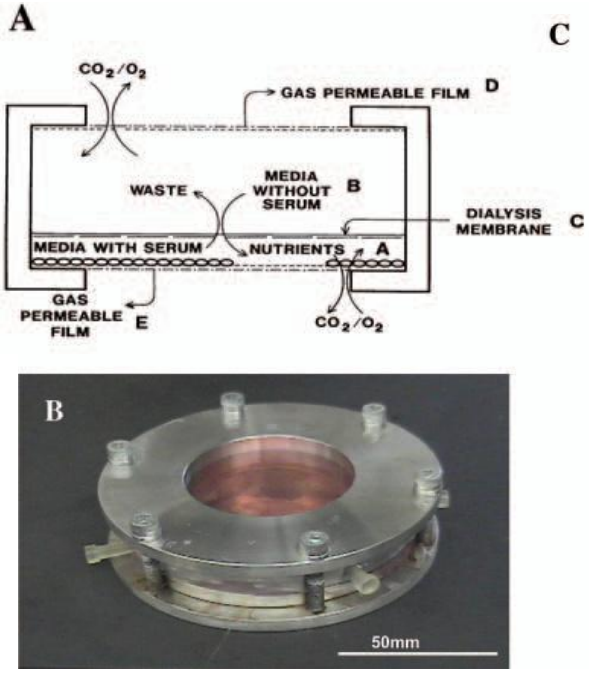

Figure. 1. Compartmentalized bioreactor design. (A) is a cross-sectional diagram through the device showing separation of the cellgrowth space (A) from the basal-medium reservoir (B) by a dialysis membrane (C). Cells are grown on gas-permeable but liquidimpermeable film (E). The device is ventilated through film (D), which is the same material as (E) as described herein, but can be different. The whole device is brought together in a liquid-tight fashion using screws shown in the laboratory implementation (B) and (C), which is an exploded view identifying separate components. Liquid-access is through luer taper ports (J, K) which mate to standard pipettes. See Materials and Methods for theory of operation. Color images available online at www.liebertpub.com /ten.

Table 1: MC3T3-E1 Cells in Conventional Culture Compared with Those in Compartmentalized Bioreactor

	Conventional Culture		***Compartmentalized Bioreactor***				
Days in culture	15	30	15	30	60	90	120
Number of cell layers	1-2	1-2	1-2	4-6	4-6	4-6	4-6
Alkaline Phosphatase[a,b]	1.14±0.01	1.27±0.17	2.94±0.05	6.88±0.55	ND	ND	ND
Alizarin red[c] (μmol)	4.59±0.12	5.07±0.09	5.28±0.05	6.88±0.55	ND	ND	ND
Von Kossa[c]	+	+	+	++	++	++	++
Mineralized nodules	-	+/-	+	++	++	++	++

[a] Measures of osteoblast maturity.
[b] nmol/mg protein per min.
[c] Extent of Mineralization.

+ observed
- not observed
ND not determined

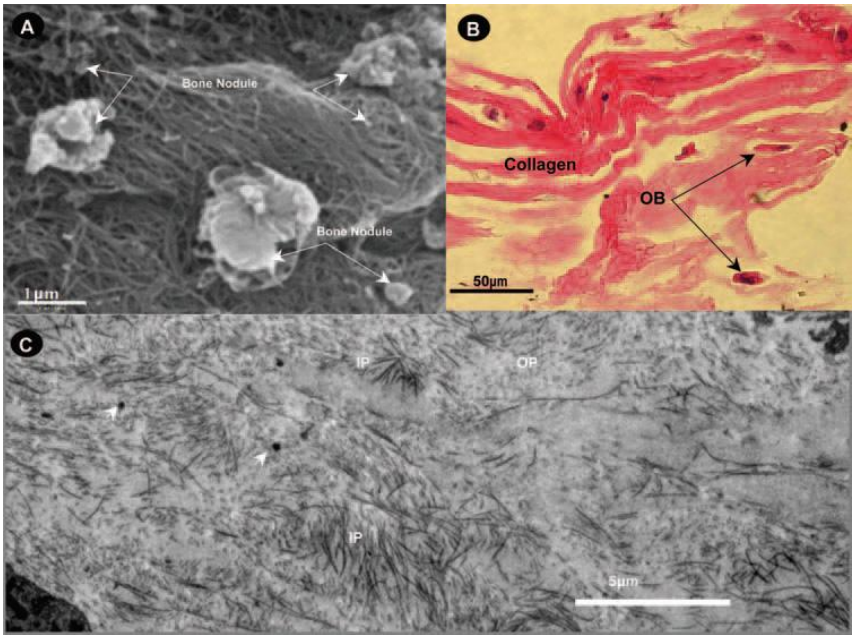

Figure. 2. Microscopic examination of matrix derived from MC3T3-E1 cultured in a bioreactor for 70 days. (A) Scanning electron microscopy of the outer layer showing a highly fibrous network with bone nodules. (B) Optical micrograph of a histologic workup showing layers of collagen with imbedded osteoblasts. (C) Cross-sectional transmission electron microscopy showing mineralized fibers running in (IP annotation) and out (OP annotation) of the plane.

Liu, X. et al. Influence of substratum surface chemisty/energy and topography on the human fetal osteoblastic cell line hFOB1.19: Phenotypic and genotypic responses observed *in vitro*. *Biomaterials* 28: 4535-4550, 2007 (appended)

The initial bioreactor growth patterns were based on testing the influences of various substrates on the phenotypic and genotypic responses of a human osteoblast line, hFOB1.19, in vitro. These studies aided in the choice of appropriate materials to use in the bioreactors system.

Krishnan, V, R. Dhurjati, E.A. Vogler and A. M. Mastro. Osteogeneis in vitro: from pre-osteoblasts to osteocytes. *In Vitro Cell Dev. Biol.- Animal* 46: 28-35, 2010. (appended)

When the osteoblasts were cultured in the bioreactor for extended periods, i.e. up to 10 months, they transitioned to osteocytes. (Figure 3). After inoculation into the bioreactors, the osteoblasts appeared as fibroblast-like cells, but as culture progressed they became more “cobblestone” in appearance. Over about two months, the density of cells increased. Over this time, the number of cell layers also increased. As the culture time continued, the cell layers decreased again to a monolayer of osteocyte-like cells. (Figure 4), These cultures expressed osteocyte differentiation proteins such as E-11, DMP-1 and scherostin (Table 2.) This is the first evidence of this differentiation process in culture. We also counted

the cells to determine how the numbers compared with those in human bone. We estimated that there were about $3.4x10^4$ osteocytes/mm^3 which compares favorably with $1.3X10^4$ osetocytes/mm^3 reported for human bone (Sugawara et al. 2005).

We also noted that with extended time in culture, mineralization sometimes occurred. Mineral chips taken from a 10 month culture were analyzed by x-ray diffraction or FITR. The patterns were similar to bovine bone, used for comparison (Figure 5). We do not yet understand all the parameters involved in the formation of the bone chips.

Task 2. To determine the effects of metastatic breast cancer cells on osteoblast morphology in a long term bioreactor culture system that fosters growth in three dimensions.

Dhurjati, R, V. Krishnan, L.A. Shuman, A. M. Mastro and E. A. Vogler. Metastatic breast cancer cells colonize and degrade three-dimensional osteblastic tissue in vitro. *Clin Exp Metastasis* 25: 741-752, 2008. (appended) *(This publication was cited by The Faculty of 1000, Medicine, a literature-awareness service that identifies the most important publication in medicine).*

Osteoblasts grown in the bioreactor for several months were challenged in human metastatic MDA-MB-231 cancer cells which are known to invade the skeleton in a xenograft mode (Phadke et al. 2006)**l.** 1. The cancer cells attached to the osteoblast tissue and formed colonies (Figure 6). The cancer cells penetrated the osteoid tissue with long processes (Figure 6, B) and also exhibited "single cell, aka "Indian Filing", (Figure 6, C). Exposure of the osteoblasts to conditioned medium from the cancer cells also disrupted actin organization (Figure 6, D,E). In addition, we saw that the osteoblasts in the presence of the cancer cells for just 3 days, changed shape from cuboidal to elongated. They aligned themselves in parallel arrays. The cancer cells lined up in the same direction along the arrays (Figure 7). Again, the age of the osteoblast culture was important. The younger the osteoblast culture, the more the cancer cells appeared to proliferate, but the older the culture the more the cancer cells behaved like aggressive tumors, i.e. penetration and single cell filing (Figure 8). Metastasis suppressed MDA-MB-231BRMS behaved very differently (Figure 9). These cells attached loosely to the osteoblast layer and did not form large colonies. After several days some appeared to undergo apoptosis perhaps due to anoikis. This finding is consistent with their behavior in vivo.

Table 2: Temporal gene expression of differentiation markers in MC3T3-E1 cultured in the bioreactor

Markers	*Months in culture*			
	0.7	1	2	10
Osteocalcin	0.54[a]	0.14	0.55	0.015
Osteonectin	0.53	0.53	0.34	0.19
Osteopontin	0.21	0.054	0.51	0.11
Type I Collagen	1.49	1.36	1.21	0.76
MMP13	0.11	0.23	1.46	Na
E-11	1.15	0.93	1.01	0.78
DMP-1	0.09	0.04	0.63	0.06
Sclerostin	Nd	Nd	*	*
Yield of RNA	1100 ng/uL	160 ng/uL	180 ng/uL	12 ng/uL

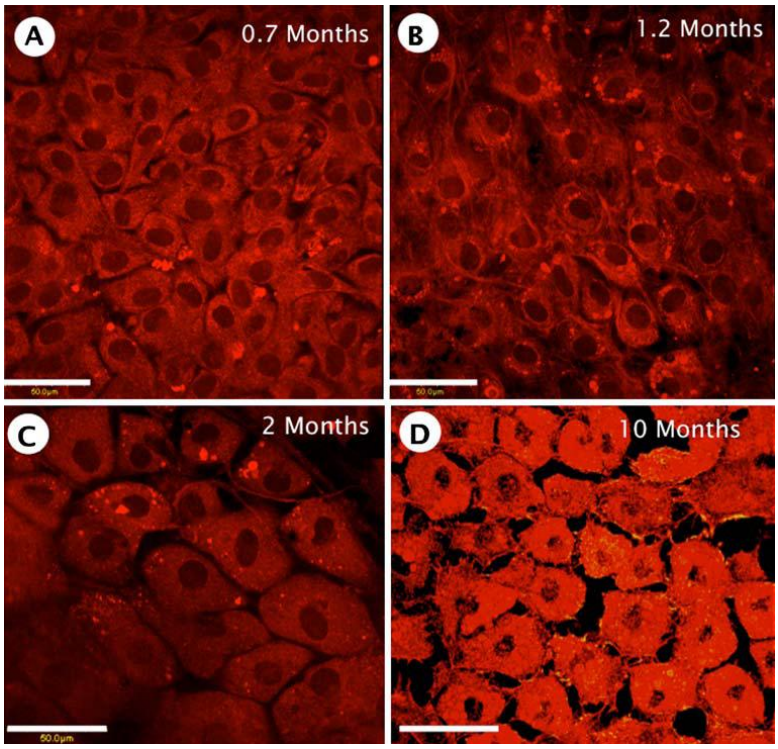

Figure 3: Progression in cell morphology monitored by confocal microscopy of Alexa Fluor 568 phalloidin stained MC3T3E-1 within the bioreactor over 10 mo of culture (compare with Fig. 2). (A) "Cobblestone"-shaped osteoblast-like cells matured from fibroblastic pre-osteoblasts within 3 wk. (B) Elongated cells appeared with development of many cellular processes within 1.2 mo. (C) Density of cells enmeshed in a dense collagenous matrix (appears black and see Figs. 4 and 8 in Dhurjati et al. (2006)) decreased over 2 mo. (D) One to two layers of stellate cells with many intercellular contacts after 2–10 mo of continuous culture. Scale bar represents 50μm.

Figure 4: Phenotypic maturation of MC3T3E-1 within the bioreactor over 10 mo continuous culture. An exponential-like decrease in the number of cell layers with time (left-hand axis) translated into a linearlike decrease in cell-layer/tissue-thickness ratio (right-hand axis). This finding was consistent with the process of bone maturation that resulted in transformation of proliferating pre-osteoblasts into nondividing osteoblasts that become engulfed in mineralized matrix and mature into osteocytes (Eriksen et al. 2007). Data within gray box were previously reported in (Dhurjati et al. 2008).

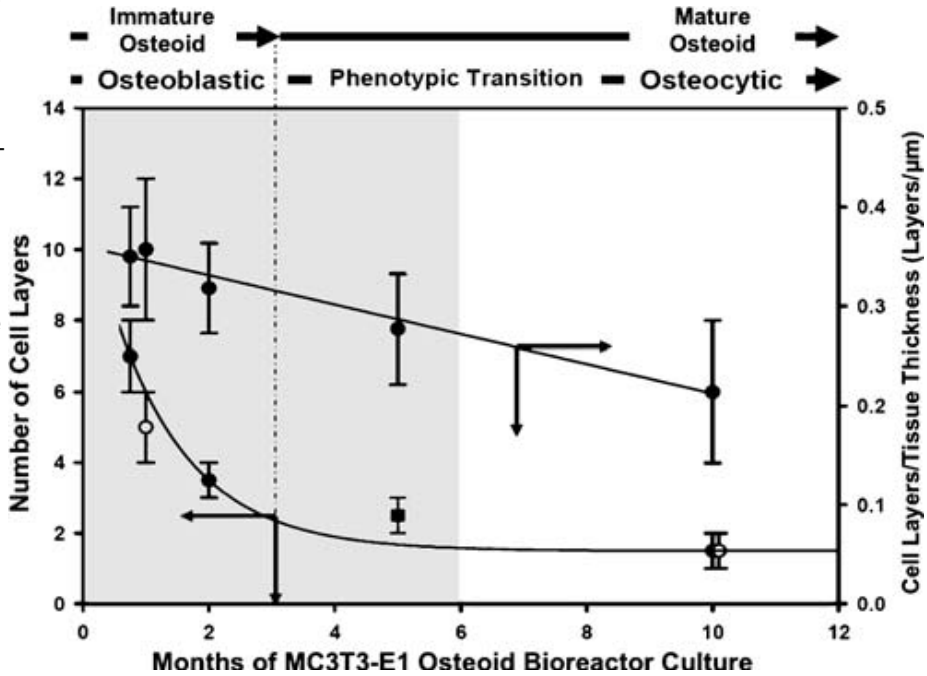

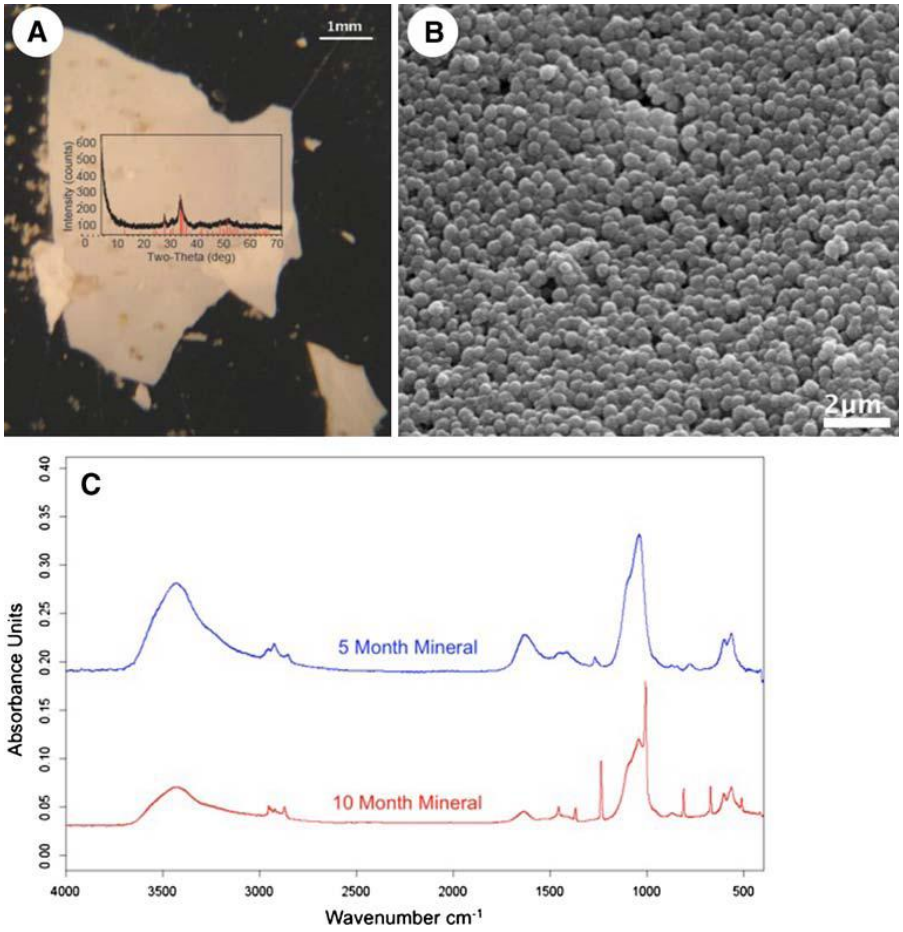

Figure 5: Macroscopic mineral deposits on the growth chamber side of the bioreactor dialysis membrane. Mineral chip taken from a 10-mo bioreactor dialysis membrane were prepared for Xray diffraction or FTIR spectral analyses as described in the "Materials and Methods" section. (A) The X-ray diffraction pattern was similar to bovine bone (inset). (B) The chip was comprised of close-packed spherical nodules. (C) FTIR spectra of chips recovered from 5 and 10 mo bioreactors showing changes in chemical composition with deposition time.

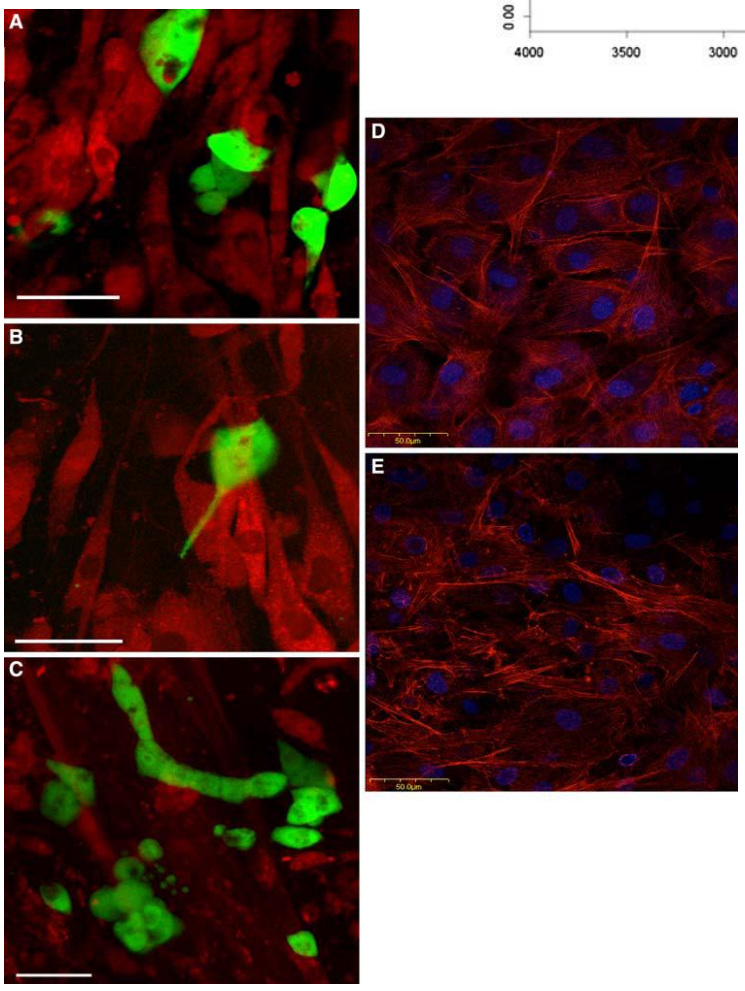

Figure 6: Fig. 3 MDA-MB-231GFP breast cancer cell invasion of MC3T3-E1 derived OT grown for 5 months within the bioreactor. OT (stained with Cell Tracker OrangeTM) was cocultured with MDA-MB-231 breast cancer cells (BCs) genetically engineered to produce GFP. Confocal images (scale bar = 50 lm, magnification = 409) were collected over 3 days (Panels A–C). These representative images are interpreted as stages of BC adhesion (Panel A, day one), penetration (Panel B, day two), and replication/ organization into characteristic filing patterns (Panel C, day three), respectively (see also Fig. 4). Phalloidin-stained OT grown for 16 days in the bioreactor (Panel D) was compared to similar tissue exposed to MDA-MB-231 conditioned medium for 2 weeks (Panel E, scale bar = 50 lm, magnification = 409). Note that exposure to conditioned media disrupted actin fiber organization in OT. Draq5 (Biostatus, Shepshed, UK) stained nuclei (blue) reveal concomitant nuclear shrinkage.

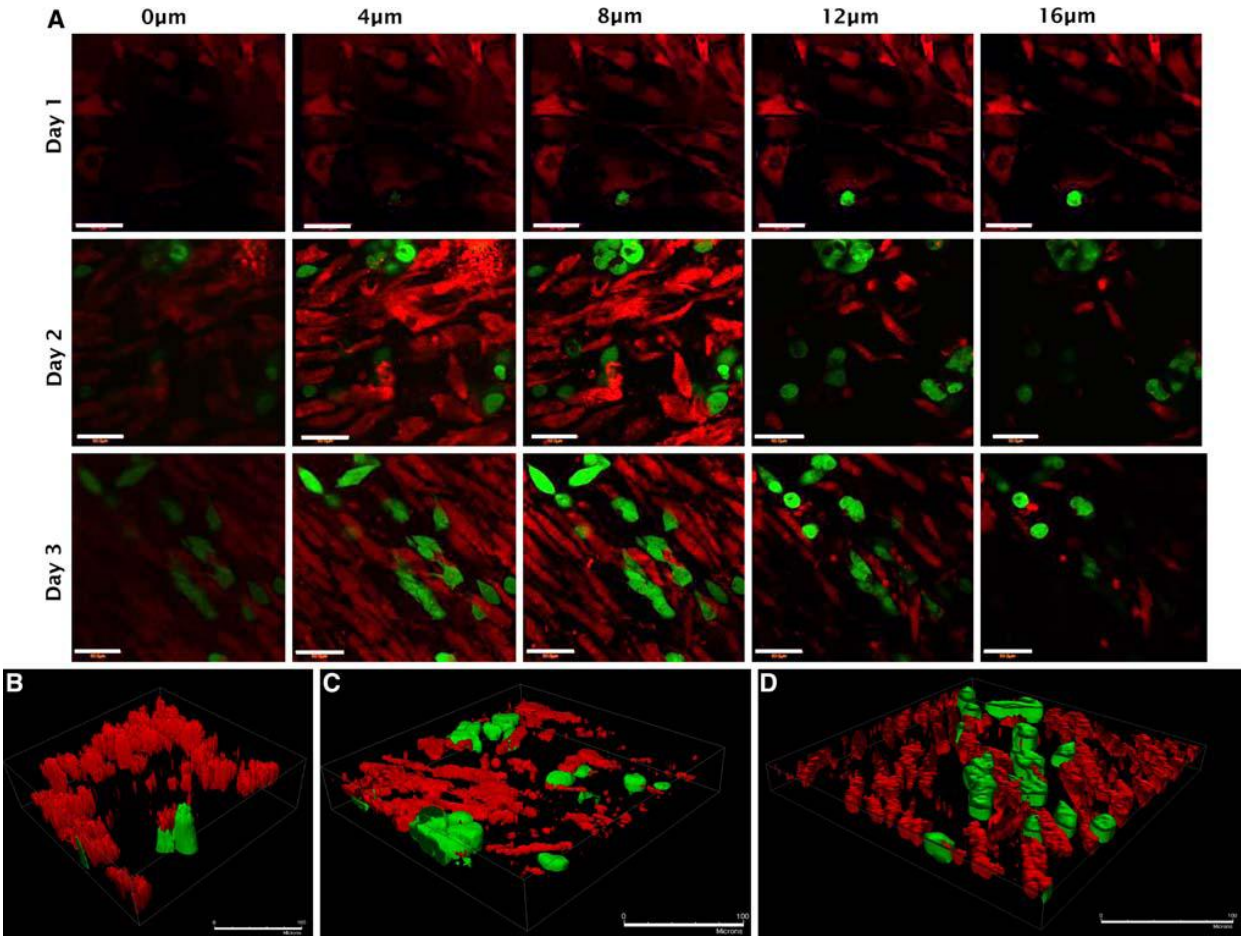

Figure 7: Fig. 4 MDA-MB-231 breast cancer cell (BC) invasion of MC3T3-E1 derived OT grown for 5 months the bioreactor (see also Figs. 1, 3). BCs were added to a 5 month OT culture as described as in the legend to Fig. 3. Optical sections (409, scale bar = 50 lm) at various depths within OT at successive days in culture were collected by laser scanning confocal microscopy. It appeared that BCs fully penetrated OT only in a few locations within day 1 of coculture. Penetration increased over days 2 and 3. Linear-like organization of breast cancer cells and osteoblasts within the tissue was evident beginning at day 2 but more obvious at day 3. Optical reconstructions of serial sections over 3 days (Panels B–D respectively, 409) revealed significant reorganization and permeablization of OT.

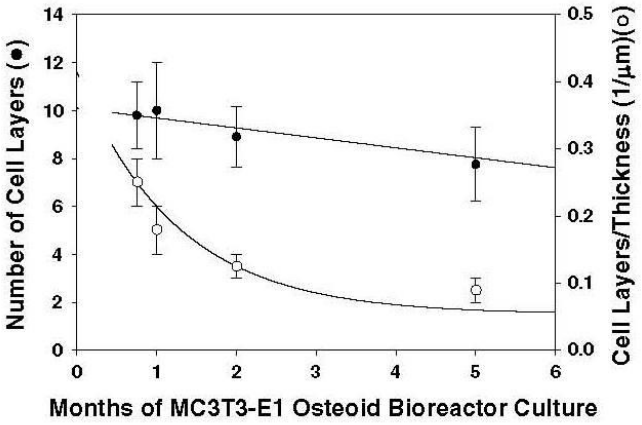

Experimental Parameter @ BC:OB=1:10	Months of Bioreactor Culture			
	0.75	1	2	5
BC Colonization	(+++)	(++)	(+)	(+)
Tissue Penetration	(-)	(+/-)	(+)	(+)
BC Filing	(-)	(+)	(++)	(++)
Tumor Formation	(-)	(+)	(++)	(++)

Figure 8: Qualitative aspects of MDA-MB-231 metastatic breast cancer cell (BC) interaction correlate with MC3T3-E1 derived OT maturity. An exponential-like decrease in the number of cell layers with time (left-hand axis, graph) translated into a linear-like decrease in cell layer/tissue-thickness ratio (right-hand axis, graph). This observation was consistent with the process of bone-tissue maturation that resulted in transformation of proliferating pre-osteoblasts into non-dividing osteoblasts that become engulfed in mineralized matrix and mature into osteocytes through a process of phenotypic transformation marked by increased osteoblast apoptosis [31]. The data presented in the summary table suggested that declining rates of BC colonization and increasing efficiency of tissue penetration, cell organization into chains, and colony formation were related to OT maturity

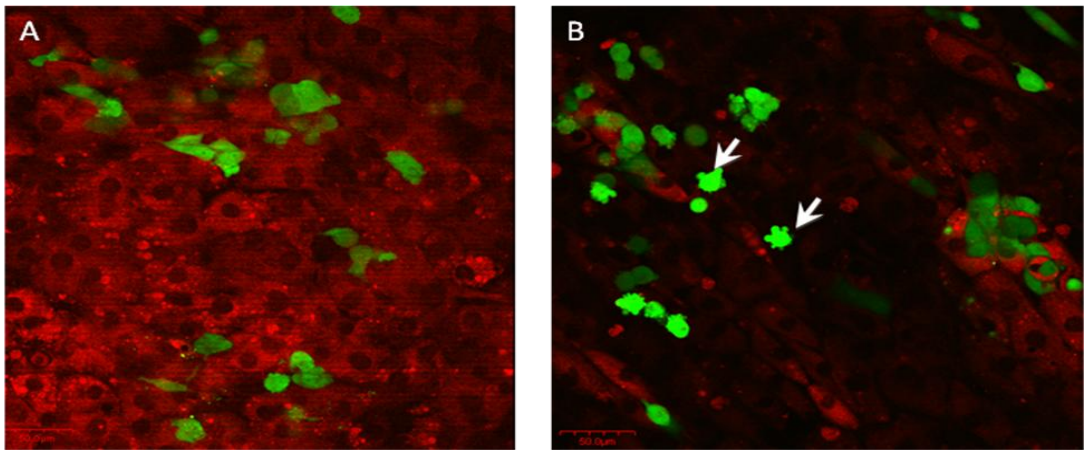

Figure 9: MDA-MB-231-BRMS ^{GFP} , metastasis suppressed cancer cells were added to MC3T3-E1 osteoblasts (stained red with Cell Tracker Orange^{TM}) that had been cultured for 2 months in a bioreactor. (A) After 3 days of co-culture, the MDA-MB-231-BRMS were seen to be loosely attached. (B) By 7 days of co-culture, there was indication that the BRMS cells were undergoing anoikis (arrows). There was no tumor cell invasion of the osteoblast tissue; however, some of the osteoblast appeared to become more spindle shaped.

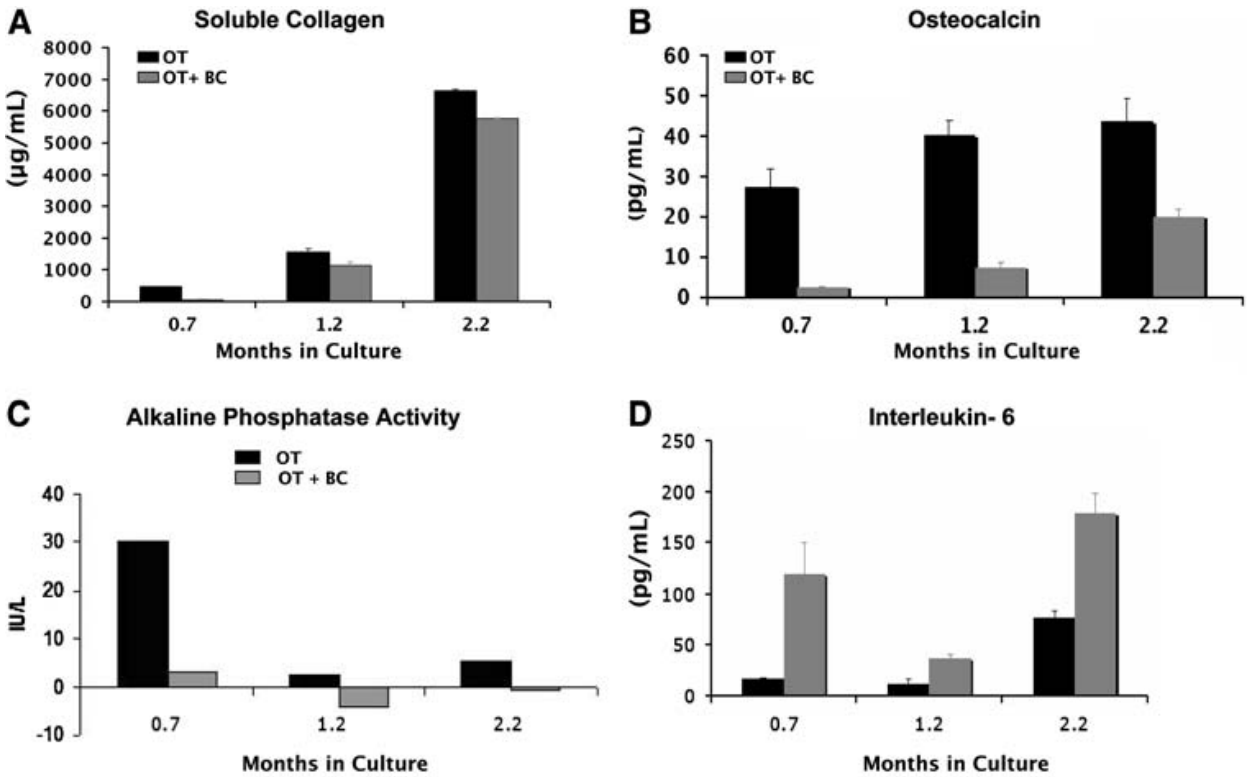

Figure 10: Osteoblasts cocultured with MDA-MB-231 metastatic breast cancer cells (BC) showed a reduction in the production of osteoblast maturation proteins and an increase in IL-6. MC3T3-E1 derived osteoblast tissue (OT) were grown in the bioreactor for 0.7, 1.2, and 2.2 months before breast cancer cells (BC) were injected onto OT at a 1:10 BC-to-osteoblast cell ratio and cocultured for 7 days. OT with no added BC served as controls. Levels of soluble collagen secreted by osteoblasts into the medium in the presence and absence of breast cancer cells were quantified using SircolTM Assay (Biocolor) (n C 2) (Panel A). Levels of osteocalcin (OCN) secreted into the medium in the presence and absence of breast cancer cells were quantified using multiplex ELISA assay (LINCOplexTM Mouse Bone Panel 2B, Millipore). Shown are averages of duplicate sample determination. (Panel B). Alkaline phosphatase activity was quantitated using the QuantiChromTM Alkaline Phosphatase Assay Kit (DALP-250), Bio- Assay Systems, Hayward, CA as indicated in the methods section. Each sample was tested three times (Panel C). Levels of murine IL-6 released into the culture media were determined with a multiplex ELISA assay (LINCOplexTM Mouse Bone Panel 2B, Millipore). Shown are averages of duplicate sample determinations (Panel D)

We assayed the culture supernatant for indications of differentiation. Collagen synthesis, alkaline phosphatase activity and osteocalcin, markers of osteoblast differentiation, were reduced in the presence of cancer cells (Figure 10 A, B). On the other hand, there was an increase in the osteoblast inflammatory response as indicated by IL-6 production (Figure 10 C, D). These data taken together suggest that metastatic breast cancer cells disrupt the osteoblast community. The osteoblasts stop production of matrix associated molecules and instead produce molecules that recruit and activate osteoclasts.

Andrea M. Mastro and Erwin A. Vogler. A Three-Dimensional Osteogenic Tissue Model for the Study of Metastatic Tumor Cell Interactions with Bone. Cancer Research 69: 4097-4100, 2009.

We were invited to submitted for peer evaluation a review article on this work**.** In this short article we summarized the major findings relative to cancer cells and osteoblasts in the bioreactor.

Comparison of metastatic and metastasis-supressed breast cancer cells in standard tissue culture with those grown in tissue culture plastic.

Shuman, L., V. Krishnan, D.M. Sosnoski, E.A.Vogler, and A.M. Mastro. A 3D culture reveals osteoblast-breast cancer cell interactions similar to those seen in vivo. (Manuscript in preparation,).

MDA-MB-231 cells and their metastasis-suppressed counterparts, MDA-MB-231BRMS1, were co-cultured with osteoblasts under standard, 2D, tissue culture (TC) conditions. They also were co-cultured with osteoblasts that had developed into osteoblastic tissue in a stable, 3D, bioreactor system. In both culture systems, the osteoblast grew and differentiated as evidenced by the expression of characteristic osteoblast proteins (Figure 11A). The gene expression pattern in tissue culture indicated the early stages of osteoblast differentiation while the bioreactor enabled us to maintain the cells for much longer periods during which time the same differentiation genes were expressed (Figure 11A). Both cultures indicated deposition of an extracellular matrix (ECM) (Figure. 11B). MMP-13, an indicator of ECM turnover, was expressed under both culture conditions but was highest in the bioreactor at 60 days (Figure. 11B).

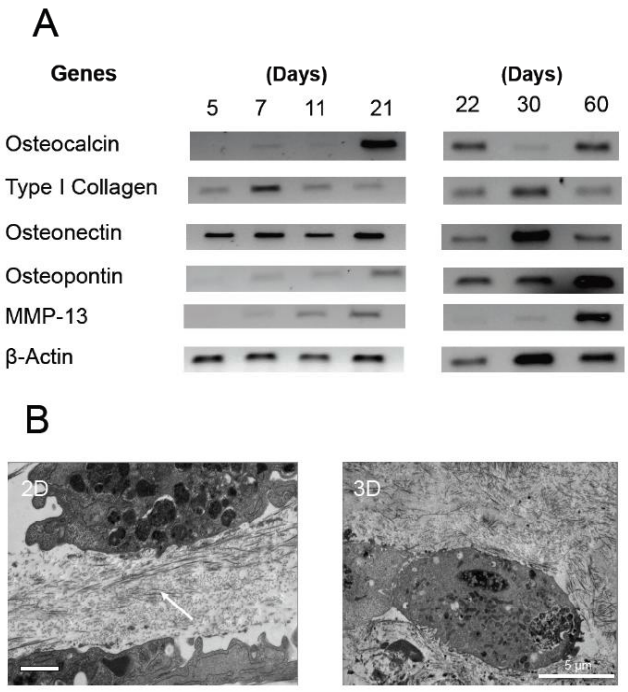

Figure 11. Expression of osteoblast differentiation genes over time. (A) MC3T3-E1 cells were cultured in a bioreactor (3D) or in Tissue culture polystyrene (2D) as described in the materials and methods section. At indicated times (22, 30, 60 days for the bioreactor samples and 5, 7, 11, and 21 days for cell culture samples), the cells were harvested for RNA isolation (RNeasy kit, Qiagen). RT-PCR was carried out using the primers listed in Table 1. Shown are representative amplicons bands. (B). TEM of MC3T3-E1 cultured in TCP (2D) for 15 days and in the bioreactor (3D) for 30 days. Arrows indicate the secreted extra-cellular matrix. The 3D culture shows that cells are packed in fine filaments, whereas in 2D, the cells are seen sitting on the substrate.

MDA-MB-231^{GFP} cells were added to osteoblasts that had been cultured for 4, 14 or 24 days in standard tissue culture (TC). These times are indicative of early, intermediate and late stages of differentiation. Breast cancer cells were added and co-cultured for 7 days at ratios of 1 cancer cell per 10, 100, 1000 osteoblasts.. The cultures were imaged by confocal microscopy at 1, 3 and 7 days after the addition of the cancer cells. In all cases the breast cancer cells attached to the osteoblast cell layer and proliferated. However cancer cell coloization was affected by the differentiation stage of the osteoblasts (Figure 12). Generally the less mature osteoblasts (day 4) more readily supported the breast cancer cell colonization (Figure 12A) compared with 14 and 24 day osteoblasts (Figure 12A). This pattern was true whether the cancer cell innoculum was 1:10, 1:100 or 1:1000 (Figure 12A).

We maintained 24 day osteoblasts in co-culture for an additional 7 days, i.e. 14 days total. During this extended co-culture time, the cancer cells grew to colonies covering >30% of the osteoblast culture (Figure 12B).

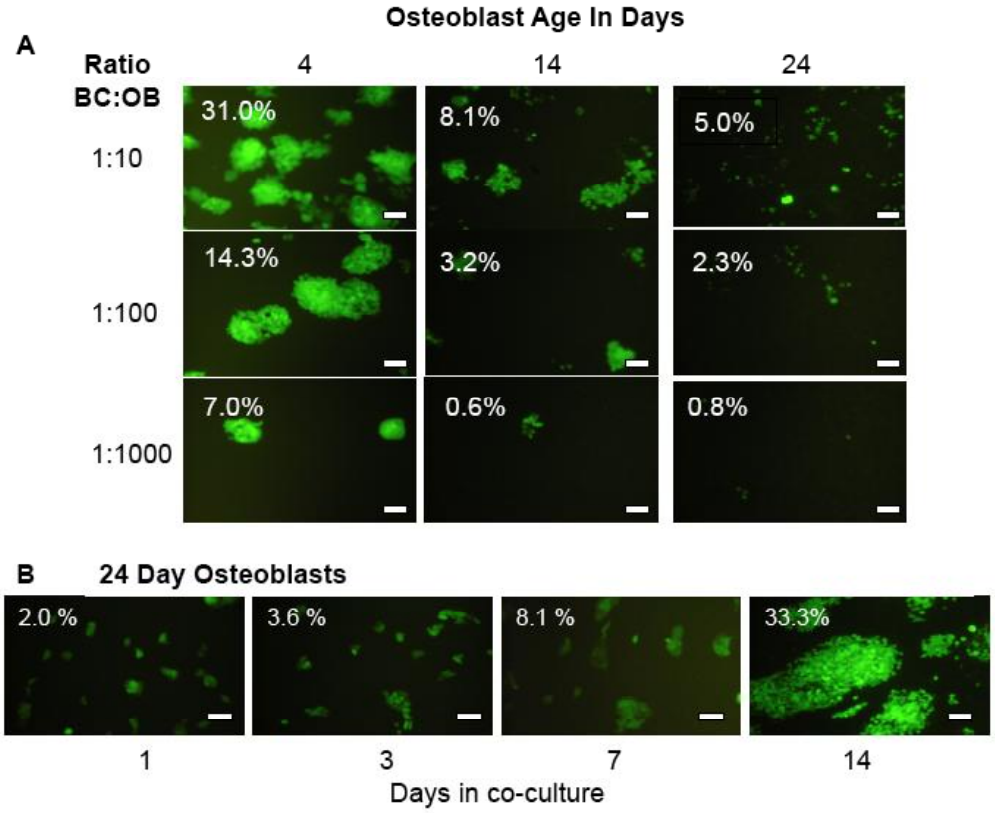

Figure 12. Co-culture of MC3T3-E1 osteoblasts with metastatic breast cancer cells, MDA-MB-231^{GFP}, in conventional cell culture. At various stages of osteoblast growth / differentiation (day 4, 14, or 24), breast cancer cells (BC) were added to osteoblasts (OB), at one of three ratios of BC to OB (1:10, 1:100, and 1:1000). Co-culture was carried out for 7 days. Shown are the fluorescence microscopic images of co-cultures. Values indicate percentage of culture area occupied by the breast cancer BC cells as calculated by the Image J analysis program (NIH). Three fields were viewed and analyzed at each point. Shown is a representative image with the corresponding percent culture area occupied by breast cancer BC cells. Three plates of each condition were cultured at least three separate times. Co-cultures were imaged after 1, 3, 7, and 14 days. Magnification bars indicate 100 µm on all images.

The age of the osteoblast culture also affected the ability of cancer cells to penetrate the tissue. In the older cultures, the cancer cells were found throughout the osteoblast layers from top to bottom (Figure 13). This pattern was not apparent in the younger cultures. Morphological changes of osteoblast from cuboidal to spindle were observed in the 3D bioreactor co-culture, but only to a very limited extent in the TCP cultures. The cancer cells in the 3D culture exhibited a distinct alignment with the long axis of the osteoblasts. This specific arrangement of cancer cells, often referred to as „single cell or Indian cell filing' by pathologists, is characteristic of tumor invasion in tissue in vivo. This cell-cell interaction was not seen in the standard TC plates. This finding suggests that, in the 3D model, cancer cells invade the osteoblastic tissue in a physiologically relevant manner. Metastasis suppressed MDA-MB-231-BRMS^{GFP} which form primary tumors but only show very limited metastases, (Phadke et al. 2008) were also tested.

These cells loosely attached to the osteoblasts but did not form large colonies (see Figure 9). After 3 days of co-culture, they did not bring about changes in osteoblast morphology or form single cell files. The MDA-MB-231-BRMS^{GFP} cells appeared to undergo anoikis after 7 days of co-culture. They did not invade the osteoblast tissue; however, the osteoblast became more spindle shaped. In constrast, in 2D (tissue-culture polystyrene dish) cultures, the MDA-MB-231-BRMS ^{GFP} cells attached and proliferated. By day 7 the cells had significantly colonized the osteoblast tissue (see Figure 5, Shuman et al, Appended manuscript titled „A 3D culture reveals osteoblast-breast cancer cell interactions similar to those seen in vivo'. We assayed the culture medium from the TC samples as well as the co-cultures in the bioreactor with murine specific reagents to determine if there were changes in the expression of osteoblast secreted proteins including inflammatory molecules. Using OCN as an indicator of differentiation, we found a decrease when the osteoblasts were co-cultured with MDA-MB-231 cells. In contrast there was an increase in the inflammatory cytokine, IL-6 (Figure 14). We did not see these changes in the presence of the metastasis suppressed cells.

A comparison of osteblasts grown under the two culture conditions indicated that the osteoblasts proliferated and differentiated in both cases (Table 3) but that only in the 3D system did the cells form multiple layers and an osteoid tissue that matured into a mineralized matrix. Breast cancer cells colonized osteoblasts under both conditions but only formed single cell files and penetrated the tissue in the 3D cultures. Only in the bioreactor did the osteoblasts show a strong response in shape change. Under both conditions they decreased expression of differentiation proteins but increased expression of inflammatory molecules.

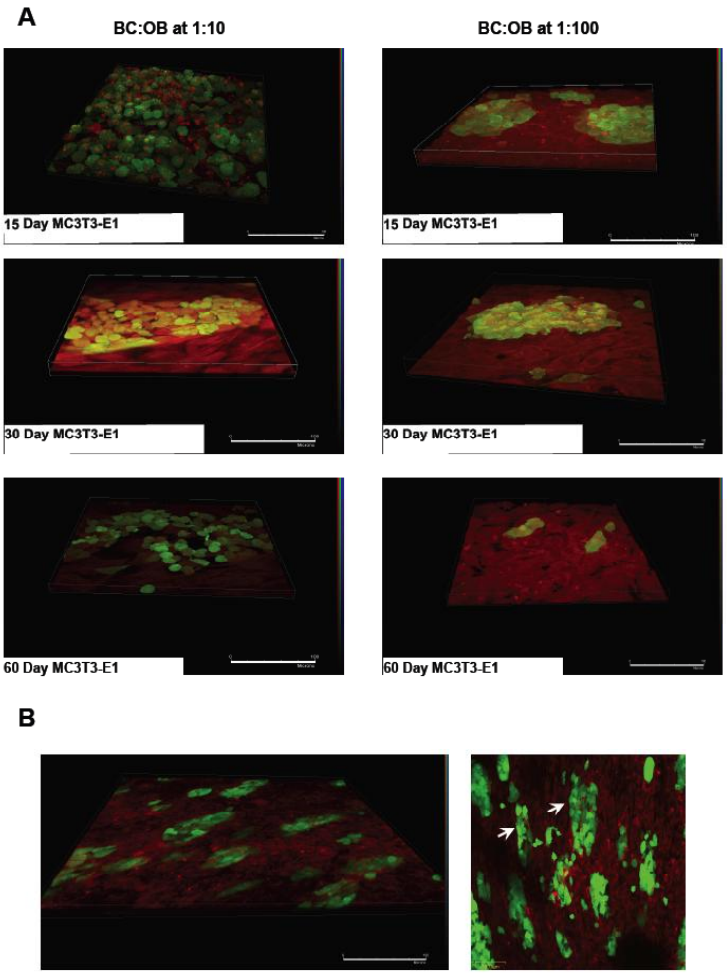

Figure 13. Breast cancer colonization of various ages of osteogenic tissue cultured in the bioreactor. (A). MC3T3E1 of various ages (15, 30 60 days) were co-cultured with MDA-MB-231^{GFP} breast cancer cells at different ratios in the bioreactor. The cultures were viewed with confocal microscopy. Shown are 3D reconstructed confocal images of z-stacks. Osteoblasts were fixed and stained with Alexa Fluor 568. The cancer cells fluoresce green. (B). visualization of „single cell filing' in 2 month osteblast culture (stained with cell tracker orange) co-cultured with breast cancer for 3 days. Cancer cells align along the osteoblast cell in an organized fashion (left panel). Formation of single cell filing (arrows, right panel)

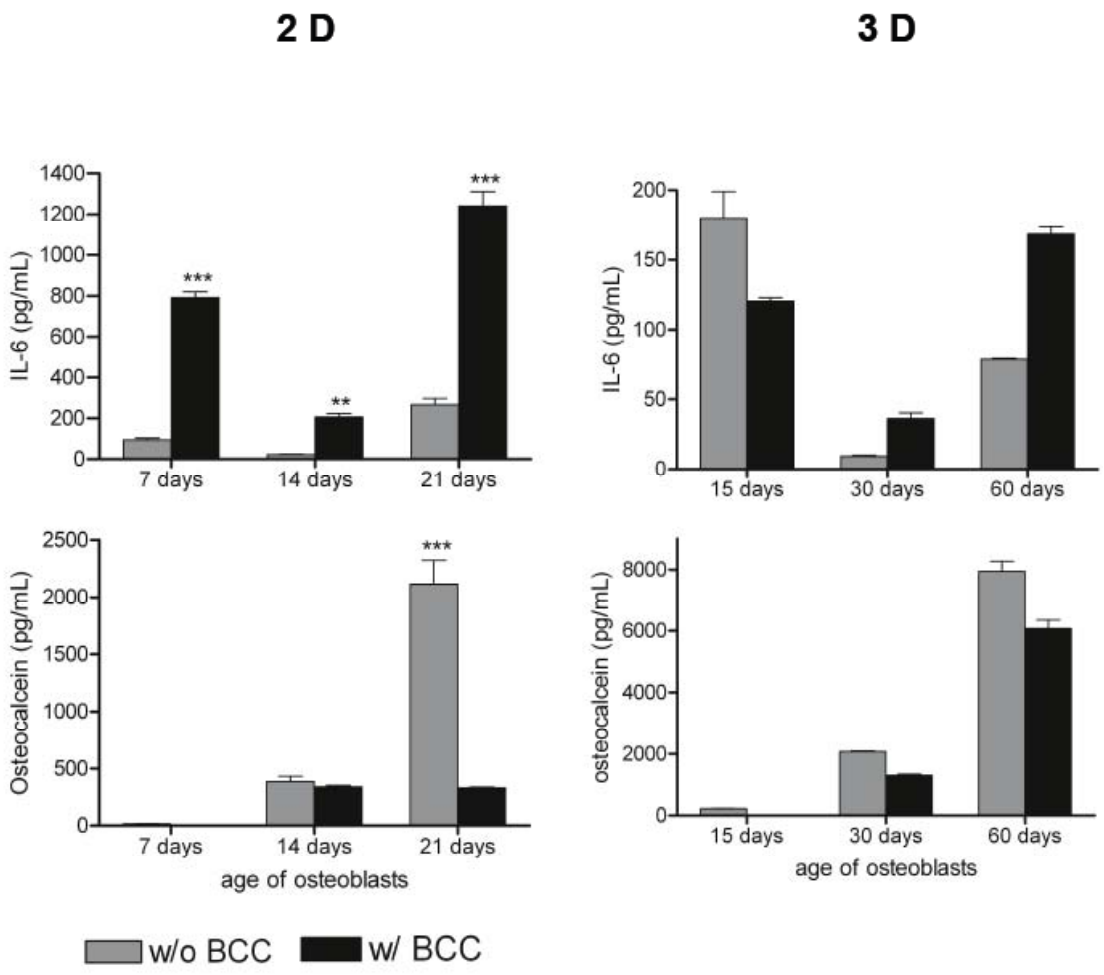

Figure 14. Expression of osteocalcin and IL-6 in the presence or absence of metastatic breast cancer cells. Quantitative plot of secreted osteocalcin protein from osteoblasts of various ages compared to osteoblasts cultured with breast cancer cells for a coculture period of 7 days in standard cell culture (A) or in the bioreactor (B). Levels of the pro-inflammatory cytokine, IL-6, secreted by the osteoblasts in the presence and absence of metastatic breast cancer cells grown in standard cell culture (C) or in the bioreactor (D). IL-6 and osteocalcin protein levels were quantified in duplicate using an ELISA assay from Millipore (LINCOplex™ Mouse Bone Panel 2B). Shown are average values of biological duplicates.

Table 3. Comparison between breast cancer and osteoblast interactions in 2D to 3D culture

	Experimental Parameter	Culture Method					
A.	**Osteoblasts**	**2D**				**3D**	
	Proliferation	++				+++	
	Maturation	++				+++	
	Number of cell layers	1 to 2				4 to 8	
	Mineralization	++				+++	
B.	**Co-Culture at BC:OB = 1:10**	**Age of OB (Days)**					
		4	**14**	**24**	**15**	**30**	**60**
	BC Colonization	+++	++	+	+++	++	+
	BC penetration of OB tissue	-	-	-	-	(-/+)	+
	BC single Cell Filing	-	-	-	-	+	++
	OB Response						
	Change in Morphology	++	+	+	+	++	++
	Collagen synthesis	ND	ND	ND	-	--	--
	Secreted osteocalcin decrease	ND	+	++	+	+	++
	IL-6 Increase	(-/+)	++	+	+	++	++

Abbreviations- OB: Osteoblasts, BC: Breast Cancer Cells, NC: No change, '+': degree of effect, „-„: no effect

In summary, in both tissue culture (2D) and in the bioreactor (3D), osteoblasts proliferate and differentiate (Table 3). However, life span of the 2D cultures is limited to about a month; whereas, 3D cultures have been maintained for at least 10 months. By this time osteocyte-like cells have developed. When osteoblasts of either condition were co-cultured with metastatic breast cancer cells, the cancer cells grew and formed colonies (Table 3). However, only in the 3D cultures did the cancer cells exhibit traits seen in pathological sections such as single cell filing and penetration of the cell layers.

Task 3. To test known stimulators and/or protectors of osteoblast function in the presence and absence of breast cancer cells in order to develop a means of blocking the destructive effects of breast cancer cells have on bone forming osteoblasts.

Establish cultures of osteoblasts at various stages of differentiation in the presence and absence of metastatic breast cancer cells as determined in task 1.

Main findings

The bisphosphonate, zoledronic acid (ZOL), when added to a bioreactor in the presence of cancer cells, had an obvious impact on the cancer cells in the co-culture system. The cancer cells formed smaller colonies and did not form projections or penetrate the matrix as seen with cultures without ZOL. The gene expression of the cancer cells and osteoblasts is currently underway. Further analyses are in progress. Selenium supplementation appeared to affect the osteoblasts more than the cancer cells. The osteoblast appeared to have long cell extensions. The cancer cells colonized the osteoblast tissue of the Se deficient and supplemented cultures but with different patterns.

1. The Selenium concentration was increased or reduced (by used of selenium-depleted serum) and the cultures were followed as described in task 1.

Selenium supplementation

Based on our findings in task 1 and a series of cell culture studies, we grew MC3T3-E1 cells in the bioreactor under low Se conditions or supplemented with 2 µm methylseleninic acid (MeSa). Selenium was reduced to < 20 nM by using 5% serum. We based this choice of a selenium supplement and concentration on reports in the literature and on experiments carried out in our laboratory with MC3T3-E1 in standard culture dishes ((Chen, Y-C, Carcinogenesis, 2009). This concentraton of MeSa was not toxic

to either the MC3T3-E1 or to the MDA-MB-231 cells. Under both conditions the osteoblasts grew and differentiated; i.e. alkaline phosphatase production and von Kossa staining, in standard cell culture.

We added MDA-MB-231GFP cells to bioreactors of MC3T3-E1 that were approximately 2.5 months old. The osteoblasts were first labeled with Cell Tracker Orange™ in order to visualize them with the confocal microscope (Figure 15). We noticed that the Se supplemented cells did not take up the dye as well as those grown in under conditions of low Se. We monitored the cultures by confocal microscopy for a week. We saw that cancer cells attached and grew under both conditions. Unlike our previous observations (Dhurjati et al. 2008) with Se adequate medium, the cancer cells failed to align themselves into single file and the osteoblasts did not change from cuboidal to spindle shape. Rather the Se supplemented osteoblasts formed long processes (Figure 15E). They also did not appear as well-defined microscopically (cf Figure 15 A with D, G). The cancer cells in the Se deficient medium formed colonies (Figure 15 C), as previously seen. In the presence of MSA, they grew more randomly and covered the osteoblast tissue (Figure 15 F). This pattern of growth was reminiscent of that seen with cancer cells and osteoblasts that were relatively undifferentiated after 15 days of culture in the bioreactor. It is possible that the MSA supplementation affected osteoblast differentiation in the bioreactor in spite of the fact that in standard culture plates, the osteoblasts with MSA produce alkaline phosphatase. The RNA and cell culture supernatants from the bioreactors have been collected. RT-PCR will be carried out to measure gene expression patterns of the osteoblasts and cancer cells under both

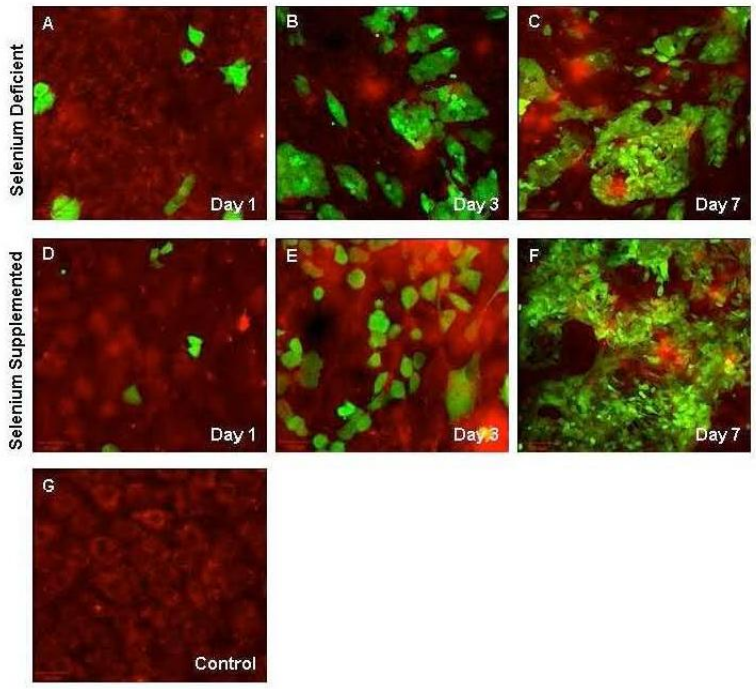

Figure 15: Confocal micrography of Selenium deficient (A, B, C) and selenium supplemented (D, E, F) MC3T3-E1 (red) co-cultured with MDA-MB-231-GEP for a period of 7 days. Representative images indicate breast cancer cell adhesion (A, D), proliferation (B, E) and colonization (C, F). Panel G is a representative image of osteoblast cells cultured without any cancer cells in deficient medium.

2. Bisphosphonates

Miller, G. Bisphosphonate Effects on Breast Cancer Colonization of Three-Dimensional Osteoblaststst Tissue. McNair Scholars Research Report. Penn State University. 2009. (appended)

We also tested compounds currently being used to treat patients with bone metastatic breast cancer. Bisphosphonates are synthetic analogues of inorganic pyrophosphates, normal regulators of bone mineralization (Rogers, Gordon et al. 2000).

Bisphosphonates are widely used to treat metastatic breast cancer as well as prostate cancer and other cancers that metastasize to the skeleton. Zoledronic acid (Zoledronate, ZOL), a nitrogen containing analogue of inorganic pyrophosphate, is one of the most aggressive in targeting bone metastasis.

Bisphosphonates bind strongly to bone mineral particularly where there is bone turnover. In the process of bone resorption, osteoclasts internalize the molecule which then inhibits certain critical enzymes and processes such as geranylgeranylation and farnesylation, molecules and processes required for post-translational prenylation (transfer of long chain isoprenoid lipids) of proteins. Although these drugs are effective against osteoclasts, they may affect cancer cells and OBs since prenylation is not limited to osteoclasts. The extent of these other-cell effects and mechanisms are not known.

The theory is that once bone degradation is inhibited, growth factors released in the process of bone resorption will no longer be available to stimulate cancer cell growth. The “vicious cycle” of bone metastasis will be stopped (Mundy 2002). There is evidence to suggest that in bone, bisphosphonates might also inhibit tumor growth directly, although this does not seem to be the case for metastases to soft tissues. What effect does this class of molecule have on osteoblasts?

Studies have been carried out *in vitro* with cell lines in standard tissue culture or *in vivo* in a mouse model. The *in vitro* studies may not impart a complete representation of how OBs or cancer cells react in the bone microenvironment. *In vivo* it is very difficult to separate the effects that numerous cell types have upon others. There are numerous studies of the effects of bisphosphonates on OBs (Reinholz, Getz et al. 2000; Chaplet, Detry et al. 2004; Pan, Farrugia et al. 2004). The results vary, possibly due to the type and age of OBs used. Several studies lead to the conclusion that ZOL enhances OB anabolism and causes increased bone formation. Some report that human primary OBs increased in differentiation in culture in the presence of ZOL. There was increased expression of OCN, bone morphogenic protein 2 and mineralization. They found no increase in the message for RANKL or OPG but there was an increase in OPG secretion and a decrease in transmembrane RANK-L expression possibly due to the effects of prenylation and expression of a metalloprotease (TACE). In contrast they report no effect of ZOL on differentiation of human mesenchynal derived OB but did see a drop in OB calcium deposition.

From these few examples, it is clear that ZOL and other bisphosphonates affect OBs. Do they affect tumor cells? It has been found that bisphosphonates have cytostatic and pro-apoptotic effects on myeloma, prostate and breast cancer cells. Other steps in the metastatic process, *i.e*. tumor cell adhesion and invasion, were inhibited by bisphosphonates. Some of these effects are believed due to metalloproteinase (MMP) activity. The blockage of cytokine secretions by OBs, stromal cells and monocytes may also be relevant to tumor cell growth.

In summary, there are numerous studies *in vivo* and *in vitro* with N-bisphosphonates, especially ZOL, to indicate that these drugs inhibit osteoclastic activity. The effects on OBs and other cells including tumor cells are not as clear. *In vitro* studies have yielded conflicting results with regard to OB differentiation is increased but some find a decrease. Tumor cells may be directly affected but there may indirect effects related to bone-tumor microenvironment.

We examined the effects of these molecules in the bioreactor. We first conducted a series of cell culture studies to determine the concentrations to use. In vivo, ZOL binds to the bone matrix so there is an initial blood level and then a concentrated amount in the bone. These studies were carried out by a honors student in bioengineering as part of her McNair fellowship research program. Appended is the paper that she wrote at the end of the summer 2009, program.

We tested ZOL on osteoblast proliferation (Figure 16 below from Miller) with an MTT assay. We tested continuous exposure to the drug at 0.05, 0.5 and 5.0 μM over 96 hours. MTT at 5 mg/ml was added to the cultures and incubated for 2 hours. MTT is reduced to formazan by living cells. Formazan crystals were solubilized and samples were read on a spectrophotemer. We found that 0.5 and 5.0 μM inhibited proliferation but 0.05 μM had no significant effects on OBs.

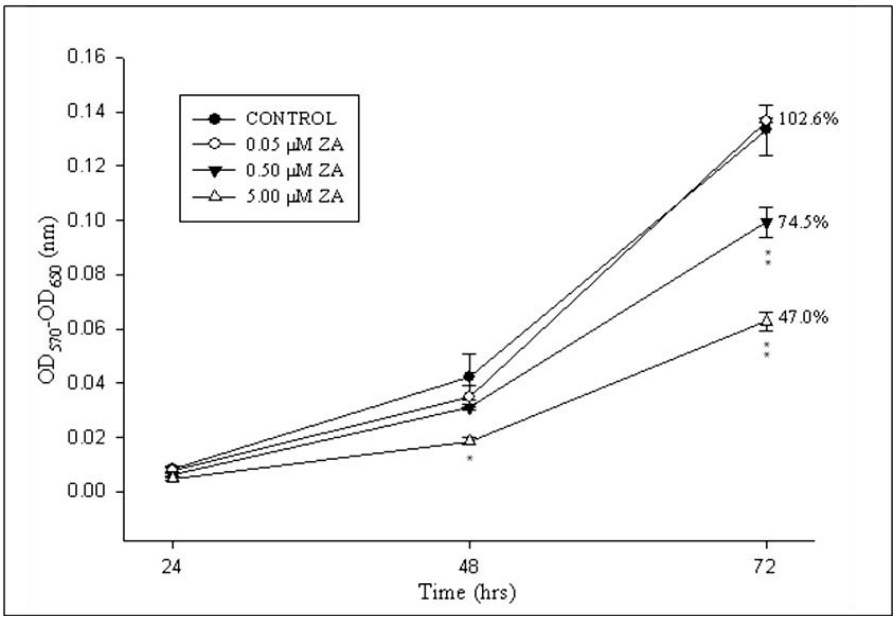

Figure 16. Effect of zoledronic acid (ZOL) on osteoblast proliferation. MC3T3-E1 were plated at 10^4 cells/cm^2, incubated overnight, and treated with ZOL at 0.05, 0.50 and 5.00 µM concentrations for 24, 48, and 72 hours (control cells were untreated). Cell proliferation was assessed with an MTT assay. Results are reported as mean ± SEM, n=3. Significant difference from control was assessed using a two-way ANOVA: $^{*}p<0.01$, $^{**}p<0.001$. Percentages are of control after 72 hour treatment with ZA.

We also tested ZOL on osteoblast differentiation and mineralization (Figure 17). Mature OBs were treated with 0.05, 0.5 and 5.0 µM ZOL for 7 days. Differentiation was assessed with a stain for alkaline phosphatase activity, and mineralization was determined by von Kossa staining. Again, we found that the low (0.05 µM) concentration of ZOL had minimal inhibitory effects on OB differentiation and mineralization.

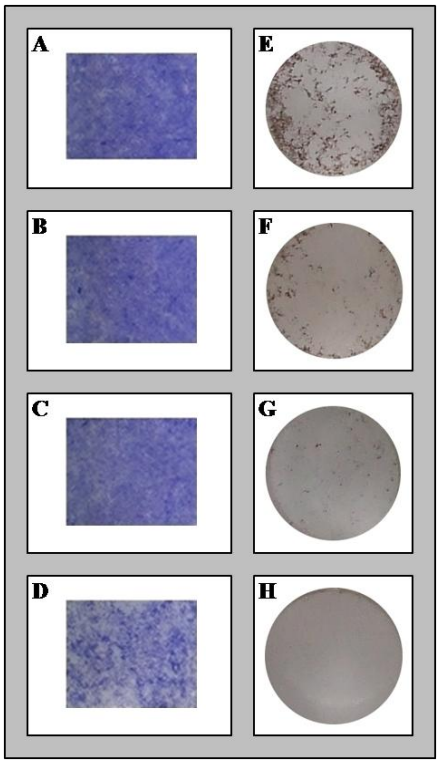

Figure 17. Effect of zoledronate on osteoblast differentiation and mineralization. MC3T3-E1 were plated at 10^4 cells/cm^2 in differentiation medium and allowed to grow for 14 days (A-D) or 28 days (E-H) with periodic medium changes. Cells were then continuously treated with ZA at 0.05 (B,F), 0.50 (C,G) and 5.00 (D,H) µM concentrations for 8 days. Control cells (A,E) were untreated. Cell differentiation was assessed by alkaline phosphatase activity (A-D). Mineralization was determined with a Von Kossa stain (E-H).

Based on the assumption that the concentrations of ZOL in 2 month cultures of osteoblasts in the bioreactor might be different than those found in cells grown under standard tissue culture conditions, we added either 0.05 μM or 0.5 μM to the cell chambers. As the ZOL diffused into the upper reservoir, over time the final concentrations reached 7 nM and 70 nM. We followed the cultures by confocal microscopy for several days and noted several parameters (Figure 18 and Table 4). The results are summarized in Table 4.

• In the presence of ZOL, fewer colonies of breast cancer cells formed.
• The colonies that formed with ZOL were more rounded and showed fewer elongated processes.
• The cultures treated with ZOL showed less cancer cell alignment.
• We saw what appeared to be lysed or broken cancer cells in the cultures treated with ZOL.
• The osteoblasts in the culture with ZOL did not show the modified spindle shape that they normally acquire in the presence of cancer cells.
• The cancer cells in the presence of ZOL did not appear to penentrate through the osteoblast multilayer as they did without the ZOL.

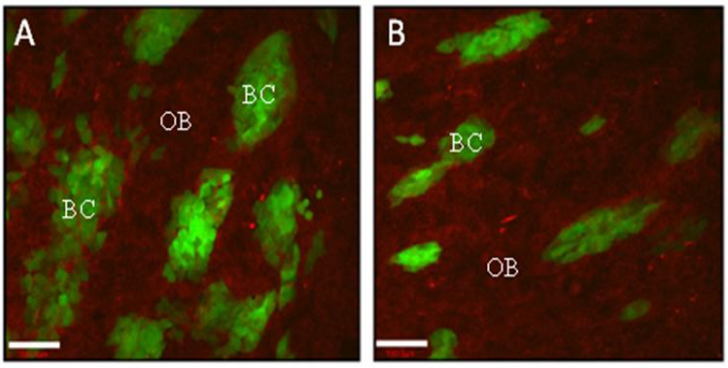

Figure 18. Qualitative analysis of the effects of zoledronic acid (ZOL) on MDA-MB-231 metastatic breast cancer cell (BC) colonization of osteoblast (OB) tissue. Cancer cells (green) were observed to penetrate and colonize OB tissue (red) in the bioreactor (A). Addition of ZOL to co-cultures in the bioreactor resulted in reduced BC colony formation and disruption of BC alignment with OB tissue (B – 0.50μM ZOL, 24 hour exposure). ZOL delayed BC penetration of OB tissue and OB retained characteristic cuboidal shape consistent with controls. Scale bar = 100μM.

Table 4. The effects of zoledronic acid on the interaction of breast cancer cells with osteoblasts in a 3D culture system.

Experimental Parameter	Culture/Treatment			
	OB	OB + BC	OB + BC + 0.05 μM ZOL	OB + BC + 0.5 μM ZOL
BC Colony Formation	n/a	+++	+	++
BC Processes	n/a	+++	+	+
Rounded BC Morphology	n/a	+	+++	++
BC Alignment	n/a	+++	+	++
Ruptured BC Cells	n/a	-	++	++
Spindle-shaped OB Morphology	---	+++	+	+
Tissue Penetration	n/a	+++	+	++

The RNA from these co-cultures has been isolated and we will be used to carry the effects of ZOL on the osteoblast differentiation proteins. Because both the human cancer cells and the murine osteoblasts contributed to the RNA, we have designed primers to distinguish murine from human RNA. We will use a housekeeping gene to normalize the RNA to account for differences in cell numbers.

In summary, ZOL affected the interaction of breast cancer cells and osteoblasts in the absence of osteoclasts. The next step is to examine the effect of docetaxel on two month cultures of OB grown in the bioreactor. We would expect docetaxel to block the proliferation of dividing cells. However, the two month cultures will be non-dividing and well differentiated. Thus we expect there to be little effect on the osteoblasts. In contrast, the cancer cells in the cultures continue to divide. We anticipate that the cancer

cells will be affected. There are reports that cancer cells in co-culture with normal cells are protected from cytoxic agents. We will first test a range of concentrations of docetaxel for cytotoxicity of cancer cells grown alone or co-cultured with differentiated cultures of osteoblasts in standard culture. Based on the results, we will choose a concentration to test in the bioreactor culture. We anticipate that we will be able to selectively affect the cancer cells. The final step will be to combine treatments with ZOL and docetaxel.

Future Goals

As we have presented this work at meetings and conferences it has become clear that a culture that included osteoclasts as well as osteoblasts would be very valuable. These together would comprise a " bone remodeling unit." To that end, a graduate student has been learning to differentiate both human and mouse osteoclasts in culture. We are currently writing proposals to obtain funding for this work.

He has successfully cultured human osteoclasts (Lonza) in the bioreactor and shown them to be functional osteoclasts (Figure 19). They developed into multinucleated cells that stained with acridine orange, indicative of an acid cytolplasm (Figure 19 A). They stained with TRAP and also formed actin rings, indicative of mature osteoclasts (Figure 19, B,C). When cultured on a bone slice, these cells degraded the bone as evidenced by formation of "resorption pits."

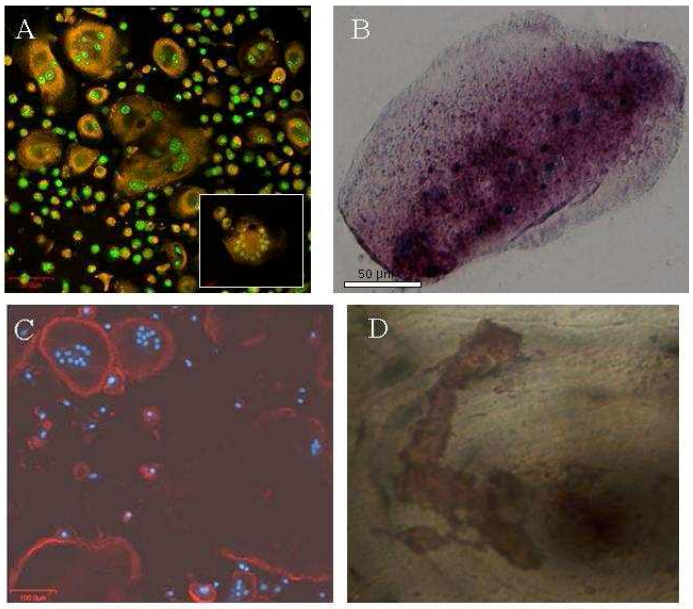

Figure 19 : Micrographs of Human pre-osteoclasts cultured for 7 days in Bioreactor (A, B) and 96 well tissue culture dishes (C, D)- (A) Acid compartments (orange) of mature multi-nucleated (green) osteoclasts visualized using acridine orange staining. Inset shows staining for actin ring on cells that were also stained for acridine orange. (B) TRAcP positive mature osteoclasts that were stained for acridine orange and actin ring. (C) Phalloidin stained multi-nucleated (blue) osteoclast depicting actin-ring (red) formation. (D) Phase image of osteoclast-made resorption pit on bovine cortical bone slice.

KEY RESEARCH ACCOMPLISHMENTS

- Primary osteoblasts and the MC3T3-E1 osteoblast line can be grown for extended periods in the specialized bioreactor.
- The osteoblasts differentiated and underwent an osteogenesis program from pre-osteoblasts to mature osteoblasts to osteocytes. Gene expression and morphology indicated this progression. Cells resembled in vivo calvaria osteocytes.
- Metastasis suppressed MDA-MD-231 BRMS1 cells only slowly grew in the bioreactor. They did not penetrate the tissue nor did they cause changes in osteoblast morphology or gene expression
- MDA-MB-231 metastatic breast cancer cells when co-cultured with the osteoblasts, caused a change in morphology of the osteoblasts. The cancer cells aligned themselves in a manner reminiscent of "Indian Filing."
- With both the primary osteoblasts and the MC3T3-E1 cell line, the cancer cells inhibited osteoblast differentiation genes. On the other hand they stimulated expression of inflammatory cytokines.
- The currently used drug, zoledronic acid, when added to co-cultures, prevented the cancer cells from forming large colonies and from pentrating the osteoid.
- Selenium supplementation of the cultures affected osteoblasts and cancer cells.
- Osteoclasts can be cultured in the bioreactor.

REPORTABLE OUTCOMES
Manuscripts (inclusive for project; appended)

Liu, X., J.Y. Lim, H.J. Donahue, R. Dhurjati, A.M. Mastro, E.A. Vogler. Influence of substratum surface chemistry/energy and topography of the human fetal osteoblastic cell line. 2007. Biomaterials. hFOB1.19: phenotypic and genotypic responses observed in *in vitro*. 28:4535-4550.

Kinder M, E. Chislock, K.M. Bussard, L. Shuman, and A. M. Mastro. Metastatic breast cancer induces an osteoblast inflammatory response. 2008. Experimental Cell Research. 314 173-189.

Dhurjati, R., V. Krishnan, L.A. Shuman, A. M. Mastro, and E.A. Vogler. Metastatic Breast Cancer Cell Colonization Degrades Three-Dimensional Osteoblast Tissue *In Vivo. 2008* Clinical and Experimental Metastasis 25: 741-752.

Bussard, K.M.,C. V. Gay, A. M. Mastro. The bone microenvironment in metastasis: what is special about bone? 2008. Cancer Metastasis Reviews. 27:41-55.

Mastro, A.M**.**, E. A. Vogler. 2009. A 3D Osteogenic-Tissue Model for the Study of Metastatic Tumor-Cell Interactions with Bone (minireview). 2009 Cancer Research 69: 4097 - 4100

Krishnan, V, R. Dhurjati, E.A. Vogler and Andrea. M. Mastro. Osteogenesis *In Vitro*: From Pre-Osteoblasts to Osteocytes. 2010. In vitro Cell Dev. Biol. – Animal. 46: 28-35

Shuman, L., V. Krishnan, D.M. Sosnoski, E.A.Vogler, and A.M. Mastro. A 3D culture reveals osteoblast-breast cancer cell interactions similar to those seen in vivo. (Manuscript in preparation).

Miller, G.N. Bisphosphonate Effects on Breast Cancer Colonization of Three-Dimensional Osteoblastst Tissue. McNair Scholars Research Report. 2009.

Abstracts/Presentations

Shuman, L.A., R. Dhurjati, X. Lui, C.V. Gay, E.A. Vogler, and Andrea M. Mastro. 2006. "A New In Vitro Model of Breast Cancer Metastasis to Bone." 97th Annual Meeting of the American Association for Cancer Research, Proceedings. 47:

Dhurjati R., L.A. Shuman, C.V. Gay, Andrea M. Mastro, and E.A. Vogler. 2006. "Indefinite-Term Culture of Bone Cells in a Compartmentalized Bioreactor." Pennsylvania State University Regenerate World Congress on Tissue Engineering and Regenerative Medicine, April 25 - 27, 2006 in Pittsburgh, Pennsylvania.

Dhurjati R., L.A. Shuman, C.V. Gay, Andrea M. Mastro, and E.A. Vogler. 2006. "Compartmentalized Bioreactor for Long-term Culture of Bone Cells." Pennsylvania State University Annual Meeting and Exposition of the Society for Biomaterials, April 26 - 29, 2006 in Pittsburgh Pennsylvania.

Andrea M. Mastro, L. S. Shuman, R. Dhurjati, X. Lui, C. V. Gay and E. A. Vogler. "A New In Vitro Model of Breast Cancer Metastasis in Bone." The 11th Congress of the Metastasis Research Society, September 3-6, 2006 in Tokushima, Japan. Abstract PD6-8 p 119.

Ravi Dhurjati, L. A. Shuman, V. Krishnan, Andrea M. Mastro, C. V. Gay and E. A. Vogler. "Compartmentalized Bioreactor: In Vitro Model for Osteobiology and Osteopathology." 28th Annual Meeting of the American Society for Bone and Mineral Research, September 15-19, 2006 in Philadelphia, PA. Vol. 21, Suppl 1, ps 349 #MO87.

Dhurjati R.; Shuman L.A.; Krishnan V., Gay C.V., A.M. Mastro and Vogler E.A. Compartmentalized Bioreactor: In Vitro Model for Osteogenesis and Breast Cancer Metastasis to Bone. Orthopedic Research Society Meeting, February 2007.

Shuman, L.A., Dhurjati, R., Krishnan, V., N., Gang, Vogler, E.A., Gay, C.V., A.M. Mastro. Use of Qtracker™ 655 to monitor the interaction of metastatic breast cancer cells with osteoblasts in co-culture. The American Association for Cancer Research Conference, Los Angeles, CA, April 2007; vol. 48: #2805.

Ravi D., Shuman LA., A.M. Mastro, Gay CV. and Vogler E.A, Compartmentalized Bioreactor: In Vitro Model of Osteogenesis and Cancer Metastasis to Bone. ASBMR 28th Annual Meeting, Philadelphia, PA; September 2006.

Ravi D., Shuman L.A., Krishnan V., A.M. Mastro and Vogler E.A., Metastatic Colonization of Bone Tissue by Breast Cancer In Vitro. 53rd Annual Conference of the American Society for Artificial Internal Organs, Chicago; June 2007

Ravi D., Krishnan V., Shuman L.A, A.M. Mastro and Vogler E.A., On the Permanent Life of Bone Tissue Outside the Organism. Gordon Research Conference on Bones and Teeth Biddeford, ME; July 2007

A.M. Mastro, Shuman, L.A., Dhurjati, R., Lui, X., Gay, C.V., Vogler, E.A. A new in vitro model of breast cancer metastasis in bone. Clin. Exp. Metastasis (2007) 24:385. Proceedings of the 11th International Congress of the Metastasis Research Society.

Krishnan V[1], Ravi D[2], Vogler EA[1,2], and A.M. Mastro[1,3]. Osteoblast Maturity Modulates Metastatic Breast Cancer Colonization in a Novel Bioreactor. PAGET Foundation Symposium: Skeletal Complications of Malignancy V, Philadelphia, PA October 25 – 27, 2007. Poster Presentation

V. Krishnan[1], D. Ravi[2], L. A. Shuman[1], A. M. Mastro[1] and E. A. Vogler[1,2]. 2007. On the Permanent Life of Tissue Outside the Body. Annual Meeting of American Association for the Advancement of Science, February 2007 in San Francisco, CA.

V. Krishnan[1], D. Ravi[2], L. A. Shuman[1], E. A. Vogler[1,2] and A. M. Mastro[1,3]. System in Crisis: In Vitro Model of Breast Cancer Colonization of Bone. Bones and Teeth, Gordon Research Conference, July 2007, University of New England, Biddeford, ME.

Liu, X., Lim, J.Y., Donahue, H.J., Dhurjati, R., A.M. Mastro, Vogler, E.A. 2007. Influence of Substratum surface chemistry/energy and topography of the human fetal osteoblastic cell line hOB1.19: Phenotypic and genotypic responses observed in vitro. Biomaterials 28:4535-4550.

Shuman, L.A., Krishnan, V., Dhjurati, R., Sosnoski, D.M., Vogler, E.A., and A.M. Mastro. A physiologically relevant 3D in vitro tissue culture system for monitoring the interaction of metastatic breast cancer cells with osteoblasts The Annual Meeting of the American Association for Cancer Research , San Diego, CA, April 2008. Proceedings of the 98th Annual Meeting vol 49.

Shuman, Laurie A. and Mastro, Andrea M. Mechanisms By Which Metastatic Breast Cancer Cells Initiate an Osteoblast Inflammatory Response, 27th Annual Summer Symposium, Penn State University, University Park, PA June 18 – 21, 2008 *Poster Presentation*

Miller, Genevieve. 2008 Penn State McNair Summer Research Conference "Bisphosphonate and taxane effects on osteoblast proliferation and differentiation." July 20, 2008.

Miller, Genevieve. "Bisphosphonate and taxane effects on breast-cancer cell colonization of osteoblast tissue." McNair & Summer Research Opportunities Program (SROP) Alumni Gathering. Penn State, February 26, 2009.

Miller, Genevieve. Becoming an Effective Presenter of Engineering and Science: Guidelines and Video Examples. "The role of the bioreactor in breast cancer research." Leonhard Center for Enhancement of Engineering Education, Penn State.

Mastro, A. M. Bone metastasis. Invited speaker, The International Metastasis Research Society Meeting / AACR Conference "Metastasis to Bone." Vancouver, British Columbia, August 2008.

Krishnan, V., E. A. Vogler, A. M. Mastro. “3D in vitro model of breast cancer colonization of bone” 100th Annual Meeting of the American Association for Cancer Research, Denver Colorado, April 2009.

Krishnan,V, E. Vogler, A.M. Mastro. A 3-D Bone-Remodeling Unit for the Study of Metastic Breast Cancer Colonization. Gordon Research Seminar on Bones and Teeth, Univ Of New England, Biddeford, ME July 2009.

Miller, G.N., V. Krishnan, A.M. Mastro, and E.A. Vogler. Bisphosphonate Effects on Breast Cancer Colonization of Three-Dimensional Osteoblastic Tissue. The IX International Meeting on Cancer-Induced Bone Disease. October 18-3011, 2009. Arlington, VA.

Miller, G.N., V. Krishnan, A.M. Mastro, and E.A. Vogler. Bisphosphonate Effects on Breast Cancer Colonization of Three-Dimensional Osteoblastic Tissue. Biomedical Engineering Society Annual Fall Scientific Meeting. October 7-9, 2009. Pittsburgh, PA.

Miller, G.N. The effect of a bisphonate, zoledronic acid, on osteoblasts in vitro. Penn State McNair Summer Research Conference. July 17-19, 2009. University Park, PA.

Krishnan,V, E. Vogler, A.M. Mastro. 2010. The Interaction of Breast Cancer Cells with osteoblasts and osteoclasts in a 3-D in vitro model. 101st annual Meeting of the American Association for Cancer Research, Proceedings

Mastro, A.M. 2010. An in vitro model of the vicious cycle of cancer metastasis in bone. MRS-AACR Joint Conference on Metastasis and the Tumor Microenvironment. Philadelphia, PA. September 12-15, 2010. (presentation)

Thesis

Genevieve Nicole Miller. The Effects fof Comination Zoledronate and Docetaxel Therapy on Breast Cancer Colonization of Three-Dimensional Osteoblastic Tissue. The Pennsylvania State Univeristy Schreyer Honors College. Spring 2010.
Ms Miller has received an NSF pre-doctoral fellowship and has accepted a graduate student postion at Columbia University beginning in the Fall of 2010.

Applications for Funding based on this work

Miller, Genevieve. 2009 The effect of combination bisphonates and taxane therapy on breast cancer cell colonization of osteoblast tissue. Undergraduate Summer Discovery Grant from Penn State University. Awarded.

Miller, Genevieve. Pennsylvania Space Grant Consortium Sylvia Stein Memorial Scholarship for undergraduates, pending.

Based on our results thus far, the following proposals were submitted. However, none were funded. We are in the process of writing more!

Agency: NASA
Project title: Gravitational Effects on the Osteoblastic Inflammatory Response
Principal Investigator: Erwin Vogler
Co-Investigator: A. Mastro

Agency: NIH
Project title: Growing Osteocytes *in vitro*
Principal Investigator: Erwin Vogler
Co-Investigators: A. Mastro

Agency: NIH
Project title: An *in vitro* model of Cancer in Bone

Principle Investigator: E. Vogler
Co-Investigators: A. Mastro

Agency: NSF
Project title: *In vitro* chromatic non-linear optical Microscope of living bone Tissue
Principle Investigator: Venkatraman Gopalan
Co-Investigators: A. Mastro, E. Vogler
Submitted and pending Review

Agency: NIH (U01 Grant, Collaborative Research in Integrative Cancer Biology and The Tumor Microenvironment)
Project title: Experimental and Mathematical Models of Drug Treatment of Multiple Myeloma.
Principle Investigator:John Wikswo (Vanderbelt), Claire Edwards (Vanderbelt), Andrea Mastro (Penn State), Bruce Ayati (Univ. Iowa)
Co-Investigators: James Edwards, Lisa Mc Carvley, Glenn Webb (Vanderbelt), Erwin Vogler (Penn State)

Agency: NIH
Project title: Modeling the Vicious Cycle of Cancer in Bone
Principle Investigator: E. Vogler
Co-Investigators: A. Mastro

Agency: US Army Medical and Materiel Research Command, Breast Cancer Research Program Idea Expansion Award
Project title: An in *vitro M*odel of the Vicious Cycle of Metastatic Breast Cancer in Bone.
Principle Investigator: A. Mastro
Co-Investigators: E. Vogler

Agency: NIH
Project title: Imaging Cancer In bone
Principle Investigator: E. Vogler
Co-Investigators: A. Mastro, Venkatraman Gopalan, Zhiwen Liu

CONCLUSIONS

We used a specialized bioreactor to test the hypothesis that metastatic breast cancer cells affect osteoblast morphology and physiology. The bioreactor allowed us to grow osteoblasts into 3D bone-like tissue. Growth for a few months produced multilayers of osteoblasts emeshed in extracellular matrix. In longer cultures, i.e. 10 months, the osteoblasts gradually differentiated into osteocytes. Metastatic breast cancer cells, MDA-MB-231, were added to the osteoblast cultures at various times. We found that osteoblast gene expression was profoundly affected by metastatic breast cancer cells. There was a reduction in expression of differentiation genes, e.g. alkaline phosphatase, osteocalcin, collagen Type 1 synthesis. In contrast the osteoblast increased their production of inflammatory cytokines such as IL-6 and MCP-1. The cancer cells adhered to the osteoblasts and continued to grow. Within a few days the osteoblasts changed shape from cuboidal to spindle. The cancer cells aligned themselves in a single file (Indian File) along the osteoblasts. Eventually the cancer cells formed colonies and penetrated the osteoid tissue. They caused degradation of the extracellular matrix. Co-culture with metastasis suppressed MDA-MB-231 cells did not cause these changes. These cells grew poorly in the bioreactor (as they do in bone) and did not affect osteoblast differentiation or inflammation. We testing selenium supplementation of the culture as a way to lower oxidative stress. Supplementation alone affected osteoblast morphology. It did not inhibit cancer cell growth completely, but they no longer formed colonies. We also tested the effects of a bisphosphonate, zoledronic acid, used for treatment of bone metastasis in the clinic. Although this drug is used to target osteoclasts, we saw that in the osteoblast, cancer cell co-culture, it lead to smaller colonies of cancer cells and less penetration of the extracellular matrix.

REFERENCES

1. Bussard, KM. C.V. Gay, A.M. Mastro. The bone microenvironment in metastasis: what is special about bone? Cancer Metastasis Reviews. 2008; 27:41-55.

2. Dhurjati R, Liu X, Gay CV, Mastro AM, Vogler EA. Extended-Term Culture of BoneCells in a Compartmentalized Bioreactor. Tissue Engineering 2006;12:3045-3054.

3. Kinder, M., E. Chislock, K.M. Bussard, L. Shuman, and Andrea M. Mastro. Metastatic breast cancer induces an osteoblast inflammatory response. Exp, Cell Res. 2008; 314:173-189.

4. Liu, X., J.Y. Lim, H.J. Donahue, R. Dhurjati, A.M. Mastro, E.A. Vogler. Influence of substratum surface chemistry / energy and topography of the human fetal osteoblastic cell line. Biomaterials. hFOB1.19: phenotypic and genotypic responses observed in *in vitro*. 2007;28:4535-4550.

5. Mastro,A.M. and Vogler E.A. A three-dimensional Osteogenic Tissue Model for the Study of Metastatic Tumor Cell Interaction with Bone. Cancer Research. 2009. 69" 4097-4100

6. Krishnan, V, R. Dhurjati, E.A. Vogler and A.M. Mastro. Osteogenesis in vitro: from pre-osteoblasts to osteocytes. In Vitro Cell Dev. Biol – Animal 2010: 46: 28-35

7. Miller, G.N. Bisphosphonate Effects on Breast Cancer Colonization of Three-Dimensional Osteoblastst Tissue. McNair Scholars Research Report. 2009.

OTHER REFERENCES CITED

Chaplet, M., C. Detry, et al. (2004). Zoledronic acid up-regulates bone sialoprotein expression in osteoblastic cells through Rho GTPase inhibition. Biochem J 384(Pt 3): 591-8.

Chen, Y., D. Sosnoski, L. Novinger, U. H. Gandhi, K.S. Prabhu, A.M. Mastro. 2009 Selenium Modifies the Osteoblast Inflammatory Stress Response to Bone Metastatic Breast Cancer. Carcinogenesis, 11:1941-48. PMCID: PMC2791325 (2009 Sept 16 Epub ahead of print).

Erickson, E.F.; G.Z. Eqhbali-Fatourechi et.al. (2007). Remodeling and Vascular Spaces in Bone. J. Bone Miner Research 22:1-6

Green, J. R. (2003). Antitumor effects of bisphosphonates. Cancer 97(3 Suppl): 840-7. Mundy, G. (2002). Metastasis to bone: causes, consequences and therapeutic opportunities. Nat Rev Cancer 2: 584-593.

Mundy, G.R. (2002). Metastasis to Bone: Causes, Consequences and Therapeutic Opportunities. Nat. Rev. Cancer 2:584-93.

Pan, B., A. N. Farrugia, et al. (2004). The nitrogen-containing bisphosphonate, zoledronic acid, influences RANKL expression in human osteoblast-like cells by activating TNF-alpha converting enzyme (TACE). J Bone Miner Res 19(1): 147-54.

Reinholz, G. G., B. Getz, et al. (2000). Bisphosphonates directly regulate cell proliferation, differentiation, and gene expression in human osteoblasts. Cancer Res 60(21): 6001-7.

Rogers, M. J., S. Gordon, et al. (2000). Cellular and molecular mechanisms of action of bisphosphonates. Cancer 88(12 Suppl): 2961-78.

Sugawara, Y, H. Kmioka et al. (2005) Three-dimensional reconstruction of chick calvarial osteocytes and their cell processes using confocal microscopy. Bone 36: 877-883

TISSUE ENGINEERING
Volume 12, Number 11, 2006

Extended-Term Culture of Bone Cells in a Compartmentalized Bioreactor

RAVI DHURJATI, M.S.,[1] XIAOMEI LIU, Ph.D.,[2] CAROL V. GAY, Ph.D.,[3] ANDREA M. MASTRO, Ph.D.,[3] and ERWIN A. VOGLER, Ph.D.[1,2,4]

ABSTRACT

A specialized bioreactor is used to grow mineralizing, collagenous tissue up to 150 μm thick from an inoculum of isolated murine (mouse calvaria MC3T3-E1, American Type Culture Collection (ATCC) CRL-2593) or human (hFOB 1.19 ATCC CRL-11372) fetal osteoblasts over uninterrupted culture periods longer than 120 days (4 months). Proliferation and phenotypic progression of an osteogenic-cell monolayer into a tissue consisting of 6 or more cell layers of mature osteoblasts in the bioreactor was compared with cell performance in conventional tissue-culture polystyrene (TCPS) controls. Cells in the bioreactor basically matched results obtained in TCPS over a 15-day culture interval, but loss of insoluble extracellular matrix and an approximate doubling of apoptosis rates in TCPS after 30 days indicated that progressive instability of cultures maintained in TCPS with periodic refeeding but without subculture. In contrast, stable cultures were maintained in the bioreactor for more than 120 days, suggesting that extended-term tissue maintenance is feasible with little or no special technique. Transmission electron microscopy ultramorphology of tissue derived from hFOB 1.19 recovered from the bioreactor after only 15 days of culture showed evidence of osteocytic-like processes and gap junctions between cells like those observed *in vivo*, in addition to elaboration of the usual osteoblastic markers such as alkaline phosphatase activity and mineralization (alizarin red). Thus, the bioreactor design based on the principle of simultaneous growth and dialysis was shown to create an extraordinarily stable peri-cellular environment that better simulates the *in vivo* condition than conventional tissue culture. The bioreactor shows promise as a tool for the *in vitro* study of osteogenesis and osteopathology.

INTRODUCTION

CELLS EXTRACTED FROM THE NATIVE, *IN VIVO* PHYSIOLOGICAL state and placed into a culture system undergo adaptive responses often referred to as "culture shock.[1] The effect and duration of culture shock depend on the stability of the pericellular (micro) environment, the extent to which this microenvironment simulates the *in vivo* condition, and the ability of cells to actively interact and transform the pericellular milieu by secreting a variety of macromolecules found in extracellular matrix (ECM).[2,3] Indeed, culture shock and the accumulated damage cells sustain in culture has long been thought to limit cell viability *in vitro*.[4,5] Thus, one of the bioengineering objectives for any *in vitro* culture device is to create a stable pericellular environment simulating the *in vivo* condition in a manner that mitigates, rather than amplifies, the effect of culture shock. The conventional tissue-culture approach is to surround cells held in dishes or flasks with a buffered medium containing various nutrients (e.g., amino acids, glucose, serum proteins, vitamins). As cells grow, nutrients are depleted, waste products accumulate (especially lactic acid), and pericellular pH decreases to unacceptable levels. The typical solution to this problem is to exchange spent growth medium with fresh, on a continuous

Departments of [1]Materials Science and Engineering, [2]Bioengineering and [3]Biochemistry and Molecular Biology, Materials Research Institute, and [4]the Huck Institutes of Life Sciences, Pennsylvania State University, University Park, Pennsylvania.

basis (perfusion) or as a matter of scheduled maintenance. A decided disadvantage with either of these approaches is that the aforementioned secreted macromolecules are removed along with waste products. In the case in which periodic media exchanges are employed, the resulting oscillation in pH and nutrient concentrations imparts an instability in cultures that can lead to excessive cell vacuolization, ruffled cell margins, and increasing rates of cell-surface detachment. Thus, conventional tissue-culture strategies, especially the flask-and-dish type serviced with periodic media exchanges, fail to maintain the stable pericellular environment that is critical to recovery from culture shock. As applied specifically to the culture of bone cells *in vitro*, continuous removal or periodic exchange of growth medium also means that cell- and protein-mediated dissolution–precipitation reactions involved in mineralization-resorption are likewise perturbed. Thus, it is difficult to simulate the natural developmental sequence of bone cells that includes proliferation, post-mitotic expression of a differentiated phenotype, ECM formation, and mineralization. As an example relevant to this work, transformation of mature osteoblasts into an osteocytic phenotype *in vitro* has not been reported to our knowledge.

More than a decade before widespread use of conventional tissue culture in biotechnology, G. G. Rose pioneered the "simultaneous growth and dialysis" method[6] by culturing cells beneath a cellulosic membrane (commercial cellulose wrapping film in Rose's implementation). The core idea was to continuously feed cells with low-molecular-weight metabolites by dialysis through a cellulose membrane that also retained secreted high-molecular-weight macromolecules within the growth space created by the bounding membrane. Metabolic waste products such as lactic acid were dialyzed out of the pericellular space and into the basal medium, where waste could be removed without perturbing cells by wholesale growth-medium removal. Rose's idea languished in the literature until its rediscovery more than 20 years later, when simultaneous growth and dialysis was bioengineered into a routinely usable compartmentalized culture device,[7,8] one version of which is shown Fig. 1. It was found that this bioreactor facilitated a number of advantages in the culture and maintenance of soft-tissue and hybridoma cells, perhaps most notable of which was the ability to sustain cells for more than 30 days without user intervention and the accumulation of biosynthesized macromolecules (such as immunoglobulin G) within the growth space for periodic harvest.[8] Unpublished work (Vogler) suggests advantages in the culture of recalcitrant primary cells and *in vitro* immunization as well.

Our interest in the development of improved orthopedic biomaterials and scaffolds for orthopedic tissue engineering[9–11] has led to the need for *in vitro* test vehicles that permit

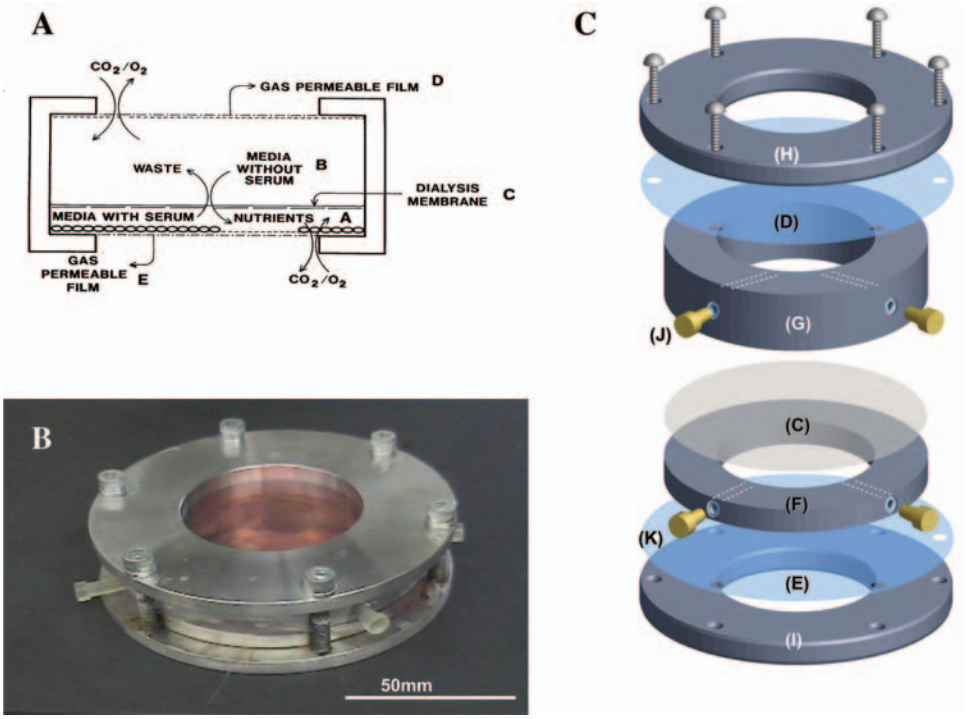

FIG. 1. Compartmentalized bioreactor design. (**A**) is a cross-sectional diagram through the device showing separation of the cell-growth space (A) from the basal-medium reservoir (B) by a dialysis membrane (C). Cells are grown on gas-permeable but liquid-impermeable film (E). The device is ventilated through film (D), which is the same material as (E) as described herein, but can be different. The whole device is brought together in a liquid-tight fashion using screws shown in the laboratory implementation (**B**) and (**C**), which is an exploded view identifying separate components. Liquid-access is through luer taper ports (J, K) which mate to standard pipettes. See Materials and Methods for theory of operation. Color images available online at www.liebertpub.com/ten.

extended-term (>30 days) contact of osteoblasts, osteoclasts, and co-cultures thereof with candidate biomaterials. Finding many limitations with conventional culture, not the least of which was loss of culture integrity over long culture intervals, we were motivated to use the compartmentalized bioreactor for bone–cell culture. Herein we report phenotypic development of 2 continuous osteoblast cell lines from an osteogenic-cell monolayer to a mineralizing, collagenous tissue: mouse calvaria MC3T3-E1 (American Type Culture Collection (ATCC), Manassas, VA, CRL-2593) and human fetal osteoblasts (hFOB 1.19, ATCC CRL-11372). Transmission electron microscopy (TEM) ultra-morphology of hFOB 1.19–derived tissue recovered from the bioreactor after 15 days shows evidence of osteocytic-like processes and regions of intercellular contacts between cells, suggesting that osteoblasts undergo complex phenotypic development within the bioreactor like that observed *in vivo* when osteoblasts are engulfed in a mineralizing tissue. Thus, the compartmentalized bioreactor shows promise as a tool for the *in vitro* study of osteogenesis and osteopathology.

MATERIALS AND METHODS

Bioreactor design and implementation

The compartmentalized bioreactor (Fig.1A) separates a cell-growth space (A, 5 mL) from a larger-volume medium reservoir (B, 30 mL) with a dialysis membrane (C). Cells were cultured on a transparent, liquid-impermeable film (E) selected for cytocompatibility[12–14] and gas (oxygen and carbon dioxide (CO_2)) permeability (see further below). During culture, cells were continuously bathed in pH-equilibrated and oxygenated medium dialyzing from the reservoir (B). At the same time, metabolic waste products such as lactic acid dialyzed out of the growth compartment (A), maintaining low pericellular concentrations. Serum constituents or macromolecules synthesized by cells with molecular weights in excess of the dialysis-membrane cutoff (6–8 kDa in our implementation) were retained and concentrated within the growth compartment. The entire vessel was ventilated through transparent gas-permeable films bounding cell growth and reservoir compartments (D,E). The assembled bioreactor had a 25 cm^2 cell-growth area. The medium reservoir volume was designed for medium-replenishment intervals ranging from 15 to 45 days, depending on the metabolic activity of the cells. Access to the cell-growth space and medium reservoir was through luer taper ports (Fig. 1C; J,K) using standard pipettes. The bioreactor was designed to work with most standard inverted phase-contrast microscopes with minor stage modification and allowed adequate optical microscopy throughout the culture interval, although the development of a thick, collagenous multicellular tissue naturally compromised resolution at the cellular level. The bioreactor was machined from 316L stainless steel stock.[8] The body of the compartmentalized device consisted of 4 main rings (C; F,G,H,I). Two chambers (A,B) were created with 3 films (C,D,E) sandwiched between inner rings (F,G). The device was held together in a liquid-tight fashion using 6 stainless steel screws, as can be seen in the laboratory implementation of Fig. 1B. Access to, and venting of, growth and reservoir chambers was through luer-taper ports (J,K). The gas-permeable films (G,H) forming the outer barriers for chambers a and b were approximately 3 mil thick and made by hot pressing Surlyn 1702 resin (DuPont, Wilmington, DE) using simultaneous application of heat (220°C) and pressure (245 Pa) in a laboratory hot press (Model 2699, Fred S. Carver Inc., Wabash, IN). The internal film barrier was cellulosic-dialysis membrane (Spectrapor-13266; Spectrum Medical Industries, Rancho Dominguez, CA) and was hydrated in de-ionized water for at least 1 h before assembly of the bioreactor. Fabricated bioreactors were filled with 0.1% sodium azide prepared in phosphate buffered saline (PBS), packaged in plastic bags, and sterilized using 10 Mrad γ-ray irradiation at the Breazeale Nuclear Reactor on the campus of the Pennsylvania State University. Sterile-packed bioreactors were opened within the confines of a laminar-flow biosafety cabinet, drained of azide storage solution, and rinsed 3 times with basal medium using conventional aseptic technique just before cell inoculation, as described below.

Cells and cell culture

Murine calvaria pre-osteoblasts (MC3T3-E1, ATCC CRL-2593) and human fetal osteoblastic cells (hFOB 1.19, ATCC CRL-11372) were obtained from ATCC. MC3T3-E1 were cultured in alpha minimum essential medium (α-MEM) supplemented with 10% charcoal-stripped fetal bovine serum and 1% penicillin-streptomycin. Post-confluent MC3T3-E1 were cultured in a differentiation medium also containing 50 μg/mL ascorbic acid and 10 mM β-glycerophosphate. hFOB 1.19 were cultured using Dulbecco's modified Eagle medium and Ham's F-12 (1:1) basal medium supplemented with 10% charcoal-stripped fetal bovine serum and 1% penicillin-streptomycin. Post-confluent hFOB 1.19 were cultured in a more-complex differentiation medium also containing 50 μg/mL ascorbic acid, 10^{-8} M 1,25-dihydroxy vitamin D3 and 10^{-8} M menadione.

The hFOB 1.19 line was conditionally immortalized by transfection with a gene encoding for the temperature-sensitive mutant (tsA58) of the SV40 large T antigen. Transfection confers a 33.5°C continuous proliferation "permissive" temperature and 39°C quiescent temperature at which cells stop proliferating without undergoing apoptosis.[15] We cultured hFOB 1.19 at 37°C and obtained a doubling time similar to that observed at the permissive temperature.[16]

Culture experiments were initiated in rinsed bioreactors (see above) by filling the growth compartment with approximately 5 mL of serum-containing medium containing a suspension of approximately 2×10^4 cells/mL (sub-confluent cell density). The reservoir was filled with serum-free basal

medium containing no proteins. Cells from the same inoculum were plated in 25-cm^2 standard tissue-culture polystyrene (TCPS) dishes (Corning Life Science) and served as the controls. Cultures were maintained in a water-jacketed 5% CO_2 incubator (Model 3110; Thermo Electron Corp., Waltham, MA) held at 37°C. After cells had reached confluence (3–5 days), growth medium was replaced with differentiation medium, and cells were permitted to grow in control plates and in the bioreactor without subculture. Medium was replaced in TCPS controls every 3 to 5 days as dictated by the color of the methyl red indicator, with a hint of yellow (acid indicator) leading to full exchange. Basal medium within the bioreactor reservoir (but not growth space) was refreshed every 15 to 30 days, again depending on the color of the pH indicator, with a hint of yellow leading to full exchange of only the reservoir contents. For example, 120-day MC3T3-E1 cultures in the bioreactor were sustained with 4 replacements of basal medium within the reservoir every 30 days.

Cell attachment and proliferation rates

Short-term ($0 < t < 3$ h) cell-attachment assays were performed as described previously.[16,17] Briefly, cells were plated onto 15 identically prepared plates at 2×10^4 cells/cm^2 in whole medium. TCPS culture dishes were the comparison controls. Dishes with the substratum used in the bioreactor were prepared by adhering Surlyn film onto the bottom of TCPS culture dishes using double-sided adhesive tape. Cells were allowed to adhere from the sessile medium while incubated at 37°C in a CO_2 incubator. At various intervals, a single plate was selected for destructive analysis (every 5 min from $0 < t < 30$ min, every 10 min from $30 < t < 60$ min, every 15 min for $60 < t < 120$ min, and every 30 min for $120 < t < 180$ min) by discarding the suspension medium and rinsing the substrata 3 times with PBS. Attached cells were released with trypsin and counted using hemacytometry.

Surfaces were analyzed in triplicate. Proliferation assays were performed in the same basic way, except that after 3 h of attachment time, substrata were rinsed with PBS to remove non-adherent cells and refreshed with growth medium. Remaining cells were allowed to proliferate for 6, 12, 24, 48, and 72 h before destructive analysis. Long-term ($\geq$15 days) proliferation was monitored using SYBR green nuclear staining. Duplicate TCPS and substrata removed from the bioreactor were fixed with 4% paraformaldehyde in PBS, permeabilized with 0.1% Triton X-100 in PBS, stained with 0.02% SYBR green in PBS (Molecular Probes; Invitrogen Corp., Carlsbad, CA), and examined using an Olympus BX-60 epi-fluorescent microscope (Olympus America Inc., Melville, NY). Average nuclei number was determined by counting 15 representative spots on each substrate using image analysis (ImagePro Software; MediaCybernetics, Inc., Silver Spring, MD).

Alkaline phosphatase activity

Alkaline phosphatase (ALP) activity was quantified at the end of each culture period using a chromogenic assay involving conversion of p-nitrophenyl phosphate to p-nitrophenol as described by Lim *et al.*[18] Briefly, cells washed in PBS were lysed by rinsing with PBS and 0.1% (w/v) Triton X-100 (Sigma) in PBS. Lysates were subjected to 2 freeze-thaw cycles, after which ALP reaction buffer (1:1 mixture of 0.75 M 2-amino-2-methyl-1-propanol and 2 mg/mL p-nitrophenol phosphate) was added and incubated at 37°C for 15 min. This reaction mixture was stopped with 0.05 N sodium hydroxide, and the absorption was measured at 410 nm with a Beckman Spectrophotometer (DU-70 series; Beckman Coulter Inc., Fullerton, CA). A calibration curve was prepared by serial dilution of p-nitrophenol standard solution. A portion of the reaction mixture was used to measure total protein concentration using a Bio-Rad protein assay kit (Bio-Rad Laboratories, Hercules, CA). ALP activity was normalized to total cell protein. Experiments were conducted in triplicate for duplicate cultures. Results are reported as means $\pm$ standard deviations (1σ).

Apoptosis

Cell apoptosis was analyzed using the enzyme terminal deoxynucleotidyl transferase (TUNEL) assay (Promega Corp., Madison, WI) to catalytically incorporate fluorescein-12-dUTP at 3′-OH deoxyribonucleic ends so that apoptotic cells fluoresced green. All cells were stained red with SYTOX Orange (Molecular Probes) so that apoptotic cells could be differentiated from normal using fluorescent microscopy. At the end of each growth period, duplicate cultures were rinsed twice with PBS, fixed with 4% paraformaldehyde, and permeabilized with 0.2% Triton X-100. Cells were then equilibrated in buffer for 5 to 10 min at room temperature, followed by incubation with terminal deoxytransferase (TdT) buffer (which included equilibration buffer, nucleotide mix, and TdT enzyme) in a humidified chamber for 60 min at 37°C. The reaction was terminated using 2 SSC washes (Invitrogen) for 15 min at room temperature according to the TUNEL assay protocol. Positive and negative controls were prepared in parallel. After removing un-incorporated fluorescein-12-dUTP, cells were stained with SYTOX Orange for 10 min at room temperature. After staining, substrata were mounted with ProLong Gold and photographed with a Laser Scanning Confocal microscope (Olympus Fluoview 300, Olympus America Inc.). Images were analyzed using ImagePro software. The percentage of apoptotic cells in the whole cell population was calculated from 10 to 20 random spots on each substrate.

Insoluble ECM protein assay

Cells were incubated in a bioreactor or in TCPS for 15 and 30 days. After medium was removed, cell layers were washed twice with PBS and extracted in 4 M guanidine hydrochloride, 50 mM Tris-hydrochloric acid, 100 mM 6-aminocaproic acid, 5 mM benzamidine hydrochloride, and 1 mM phenylmethylsulfonyl fluoride, pH 7.4, at 4°C with constant rocking. Cells were separated from the extract using centrifugation

(2000 g×5 min; the extract was routinely checked for cell debris using microscopy with trypan blue staining to enhance visualization of cell debris). Protein concentration in the supernatant was quantified using Bio-Rad protein assay kit and normalized with cell number for each growth condition.

Hematoxylin and eosin staining

Tissue excised from the bioreactor was fixed in 2.5% glutaraldehyde. Dehydration and paraffin embedding were performed using an automated tissue processor (Citadel 2000, Thermo Electron Corp.). Five-μm sections were cut using a microtome (Model 2040; Leica Micro Systems, Bannockburn, IL) and mounted on glass coverslips. Hematoxylin and eosin staining was performed according to a standard protocol using automated staining equipment (Shandon Gemini, Thermo Electron Corp.), and the stained sections were observed under an optical light microscope (Olympus BX50, HiTech, Olympus America Inc.).

Scanning and transmission electron microscopy

Cultures were washed in buffer (0.1 M, pH 7.2 sodium cacodylate) and fixed overnight with 2.5% glutaraldehyde in cacodylate buffer at 4°C followed by staining with 1% osmium tetroxide in cacodylate buffer for 1 h at room temperature. Fixed cells were dehydrated using graded series of ethanol concentrations, dried in a critical point dryer (BALTEC SCD030, Techno Trade Inc.) using dry CO_2, mounted onto an aluminum stub, and sputter coated with 10 nm of gold/palladium in an automated sputter coater (BALTEC SCD030.). Cells were examined under a scanning electron microscopy (SEM, JSM 5400, JEOL, Peabody, MA) at an accelerating voltage of 20 kV. Energy dispersive x-ray analysis was performed using image analysis software (IMIX-PC v.10, Princeton Gamma Tech Inc.). For TEM, primary fixation with 2.5% glutaraldehyde and secondary fixation with 1% osmium tetroxide were followed by en bloc staining with 2% aqueous uranyl acetate for 1 h. Dehydration was performed using a graded series of ethanol concentrations followed by impregnation and embedding in Spurr's resin. Ultra-thin sections were cut with a diamond knife (Diatome Ultra 45) on a microtome (Ultracut UCT, Leica), placed on uncoated copper grids, and stained with 0.2% aqueous uranyl acetate and 0.2% lead citrate. The cross-sections were examined using TEM (JEM 1200 EXII, JEOL), and images were collected using an attached high-resolution camera (Tietz F224, Gauting).

RESULTS AND DISCUSSION

Tables 1 and 2 compile semi-quantitative cell-growth data over 30 days for hFOB 1.19 and 120 days for MC3T3-E1 cells, respectively, in the bioreactor and compare them with to data obtained in conventional TCPS. Neither cells grown on TCPS nor those grown in the bioreactor were subcultured over the entire culture interval (see Materials and Methods). For both hFOB 1.19 and MC3T3-E1, between 1 and 2 cell layers formed in TCPS, compared with 4 to 6 layers in the bioreactor over the 30-day culture interval (the exact number of layers varied with position in the bioreactor and how a cell layer was defined). ALP activity, which was positive for both cell lines in both culture devices, indicated evidence of a mature osteoblastic phenotype. Mineralization was especially evident using von Kossa and formation of nodules in the MC3T3-E1 case, but hFOB 1.19 did not mineralize as well in either culture device. Based on the data summarized in Tables 1 and 2, it is evident that performance of hFOB 1.19 and MC3T3-E1 in the bioreactor was similar to that of cells grown on TCPS in the first 15 days of culture. However, cell performance in the bioreactor clearly exceeded that for TCPS over a 15- to 30-day culture interval, with double the number of cell layers and greater ALP activity and alizarin red staining. TCPS controls were not maintained for more than 30 days because it was visually and quantitatively evident that these cultures were failing (see further below).

Fig. 2 compares attachment and growth dynamics of hFOB 1.19 in the bioreactor and with attachment and growth dynamics in TCPS over a 0- to 720-h culture period. In the short-term ($0 < t < 3$ h), there was approximately 2 times the

Table 1. Human Fetal Osteoblasts 1.19 Cells in Conventional Culture Compared with Those in Compartmentalized Bioreactor

	Conventional Culture		*Compartmentalized Bioreactor*	
Days in Culture	*15*	*30*	*15*	*30*
Number of cell layers	1–2	1–2	3–4	4–6
Alkaline phosphatase[a,b]	4.39 ± 0.26	4.47 ± 0.38	28.89 ± 1.99	5.79 ± 0.40
Alizarin red[c] (μmol)	2.89 ± 0.04	3.03 ± 0.02	2.97 ± 0.18	5.17 ± 0.14
von Kossa[c]	—	—	—	—
Mineralized nodules	—	—	—	—

[a]Measures of osteoblast maturity.
[b](nmol/mg protein/min).
[c]Extent of mineralization.
—, not observed.

Table 2. MC3T3-E1 Cells in Conventional Culture Compared with Those in Compartmentalized Bioreactor

	Conventional Culture		*Compartmentalized Bioreactor*				
Days in culture	15	30	15	30	60	90	120
Number of cell layers	1–2	1–2	1–2	4–6	4–6	4–6	4–6
Alkaline phosphatase[a,b]	1.14 ± 0.01	1.27 ± 0.17	2.94 ± 0.48	3.36 ± 0.46	ND	ND	ND
Alizarin red[c] (μmol)	4.59 ± 0.12	5.07 ± 0.09	5.28 ± 0.05	6.88 ± 0.55	ND	ND	ND
von Kossa[c]	+	+	+	++	++	++	++
Mineralized nodules	—	+/—	+	++	++	++	++

[a]Measures of osteoblast maturity.
[b]nmol/mg protein per min.
[c]Extent of mineralization.
+, observed; —, not observed; ND, not determined.

attachment preference for TCPS over the polymer-film substrata used in the bioreactor (see inset expanding time axis and expressing % inoculum on a linear axis; see also Vogler and Bussian[17] for more discussion of polymer-film cyto-compatibility). However, proliferation into confluent monolayer (on TCPS) from this sub-confluent cell density ($3 < t < 72$ h) and post-monolayer growth into multilayers ($72 < t < 720$ h) was nearly the same in TCPS and the bioreactor. In fact, actual growth rates k within $3 < t < 72$ h were statistically identical at 95% confidence intervals (TCPS $= 0.23 \pm 0.01 \times 10^{-2}$ h^{-1}; bioreactor $= 0.29 \pm 0.03 \times 10^{-2}$ h^{-1}). Data within the 72- to 720-h interval were too sparse for statistical comparison, but it is interesting that the total cell number (at constant surface area $= 25$ cm^2) continued to increase significantly within the bioreactor and TCPS at approximately the same rate, achieving a 5 times increase in total cell number over this time span. The data show that the initial 2-fold cell-attachment preference for TCPS persisted through the exponential-growth ($3 < t < 72$ h) and post-confluence expansion ($72 < t < 720$ h) phases.

Further interpretation in terms of the data in Table 1, this persistence attachment preference implies that more cells are packed into fewer cell layers on TCPS than within the bioreactor, consistent with the general observation that cells on TCPS appear thinner than in the bioreactor (compare, for example, Fig. 3A, C), although a focused study would be required to be definitive in this regard.

Despite the initial advantage of TCPS, hFOB 1.19 began to appear less robust than in the bioreactor within 720 h (30 days), as evidenced by TEM images showing numerous

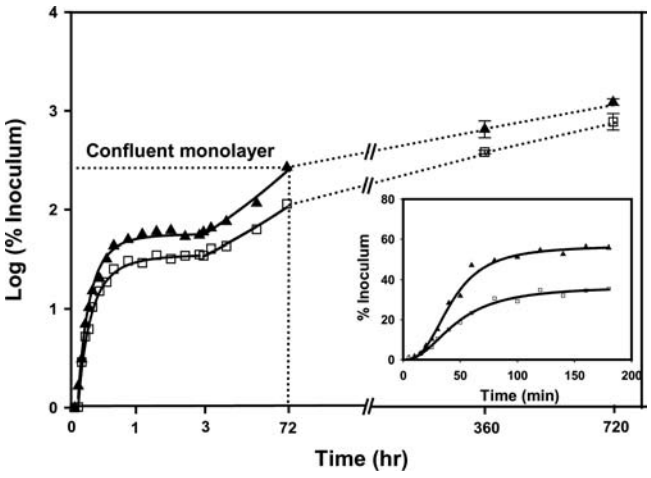

FIG. 2. Growth dynamics of human fetal osteoblasts on tissue-culture polystyrene (TCPS, filled triangles) controls, compared with those of the compartmentalized bioreactor (open squares; note logarithmic ordinate). Inset expands short-term attachment rates using a linear ordinate. The initial 2-fold cell-attachment preference for TCPS persists through the exponential-growth ($3 < t < 72$ h) and post-confluence expansion ($72 < t < 720$ h) phases.

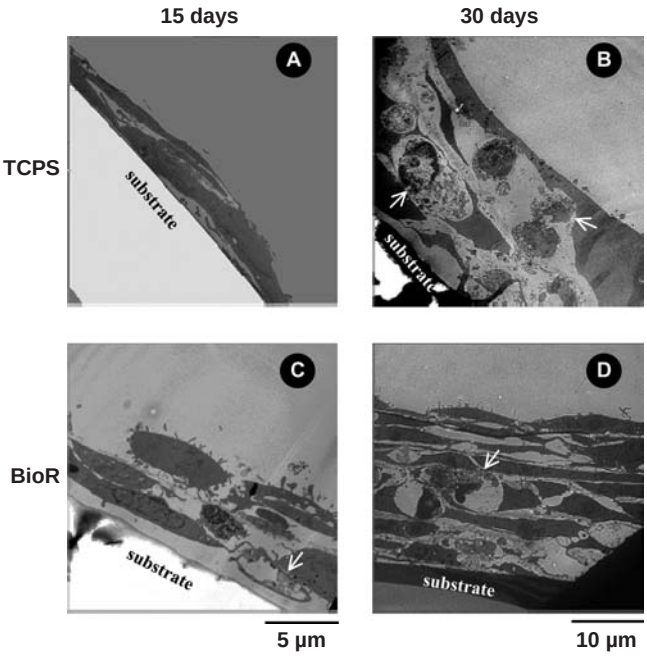

FIG. 3. Comparison of human fetal osteoblasts (hFOB 1.19) on tissue-culture polystyrene (TCPS) (**A, B**) and in the compartmentalized bioreactor (**C, D**) by cross-sectional transmission electron microscopy. Cell layers are thicker in the bioreactor than on TCPS (compare **A, B** to **C, D**) and formation of apoptotic bodies (arrows) after 30-day culture in TCPS.

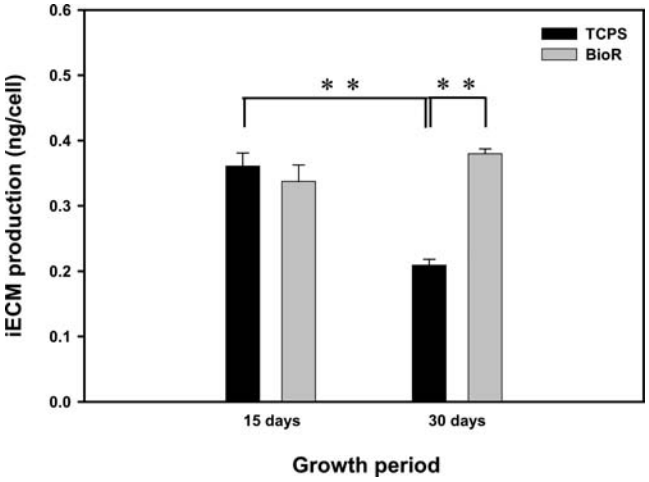

FIG. 4. Comparison of insoluble extracellular matrix (ECM) production by human fetal osteoblasts on tissue-culture polystyrene (TCPS, dark bar) and in the bioreactor (light bar). Insoluble ECM significantly decreased after 30 days on TCPS but remained constant in the bioreactor. Bar values are mean of duplicate samples measured in triplicate with standard deviation represented by error bars.

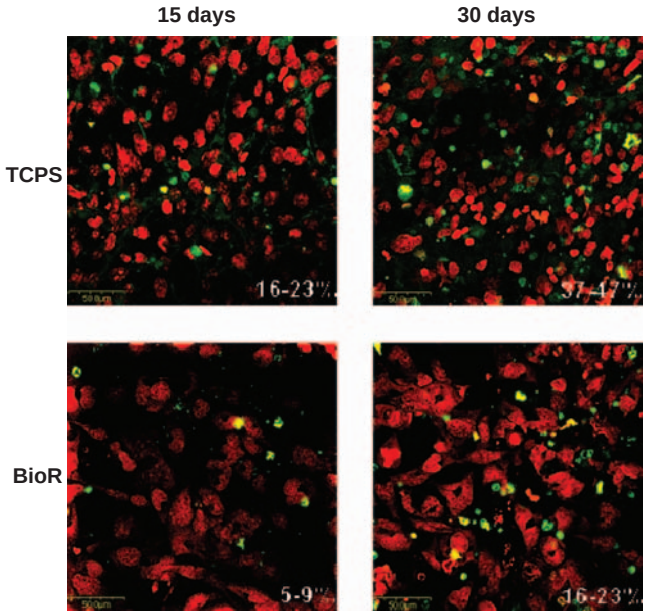

FIG. 5. Representative confocal image of apoptotic bodies (green stain) in tissue-culture polystyrene (TCPS) and in the bioreactor selected from 8 to 10 similar in-depth image planes probing human fetal osteoblast–derived tissue. All cells were stained red (Sytox Orange, scale bar = 50 μm). Percentages of apoptotic cells quoted in each panel are the range of values observed within the image planes.

apoptotic bodies, cytoplasmic vesiculation, and chromatin margination (Fig. 3) and a distinct loss of insoluble ECM (Fig. 4). TUNEL assay results (summarized in Fig. 5) confirmed that, at 30 days, apoptosis was approximately 2 times as great in TCPS as in the bioreactor (37–47% in TCPS versus 16–23% in the bioreactor), although 30-day apoptosis levels were roughly 3 times 15-day levels in both devices. Examination of hFOB 1.19 tissue recovered from the bioreactor after 15-day culture by cross-sectional TEM (Fig. 6A, B) revealed 3 to 4 layers of cells with many cytoplasmic protrusions (arrowheads) and healthy-appearing nuclei showing no evidence of apoptosis. The general impression derived from an examination of many such TEM cross-sections is that cells in the layers closest to the substratum (presumably older cells) were flatter and more dish-shaped than cells within the upper layers (presumably younger cells) that had a more cuboidal shape. No effort was made to quantify this visual interpretation. Arrow annotations on Fig. 6C point to what appear to be osteocytic-like processes between 2 cells, and Fig. 6D shows close contact between cells. Exocytosis of vesicles is evident in Fig. 6D.

Results obtained with MC3T3-E1 osteoblasts in TCPS and the bioreactor were similar to those seen for hFOB 1.19, with the notable exception that mineralization was much more striking with MC3T3-E1 cells. One of many large nodules (Fig 7A, SEM) that were found on and within MC3T3-E1 tissue after 70-day culture (see also Fig. 8A) was analyzed. Fig. 7B is a high-resolution cross-sectional view through a nodule similar to that shown in Fig. 7A. Nodules such as these proved positive for calcium and phosphorous according to energy-dispersive x-ray analysis (Fig. 7C, SEM/energy dispersive spectroscopy of a nodule taken from a 30-day bioreactor). These nodules were enmeshed in a fibrous, apparently collagenous, network that was evident in SEM preparations such as that shown in Fig. 8A. Histological preparations of MC3T3-E1 tissue recovered from 70-day bioreactors (Fig. 8B) confirm substantial matrix development, with osteoblasts oriented along sheets of matrix. TEM of von Kossa-stained 70-day tissue shown in Fig. 8C is consistent with collagen fibers running in (IP annotation) and along (OP annotation) the plane with interspersed mineral nodules (arrows). We estimated that tissue taken from a 120-day bioreactor was approximately 150 μm thick. After 120 days in culture, there was no indication that MC3T3-E1 tissue grown in the bioreactor was unstable and the absolute term of culture within the bioreactor is regarded as indefinite until experimentation finds an endpoint at which significant instability can be detected.

CONCLUSIONS

Evidence summarized in Fig. 2 and supporting micrographs (Figs. 3–8) show that long-term maintenance of hFOB 1.19 (ATCC CRL-11372) and MC3T3-E1 (ATCC CRL-2593) without subculturing leads to formation of cell multilayers within a thick, mineralized matrix that cannot be realized when cells are regularly passaged at confluence. Achievement and maintenance of such a 3-dimensional "tissue" that promotes cell-to-cell contact has been shown to be critical to the development of osteogenic cells into a

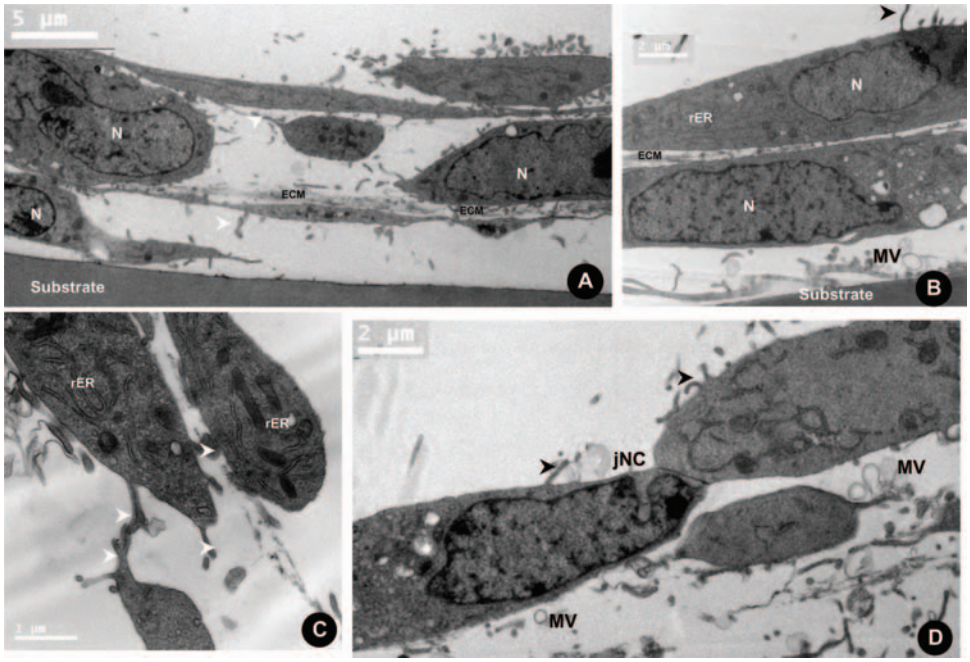

FIG. 6. Ultra-morphology of human fetal osteoblast–derived tissue (15 days) recovered from the bioreactor by cross-sectional transmission electron microscopy. Arrows point to cell protrusions that occasionally connect 2 cells, as shown in (**C**). jNC, gap junction; MV, matrix vesicles; N, nucleus; rER, rough endoplasmic reticulum.

fully differentiated osteoblast phenotype.[19–22] We demonstrated that such tissue can be grown and maintained long-term (>120 days) in a bioreactor based on the principle of simultaneous growth and dialysis with improved efficiency over conventional tissue-culture labware (TCPS). In fact, tissue maintained 30 days in TCPS with medium replacement every 3 days became unstable, with 2 times the apoptosis rates of cells grown in the bioreactor and loss of insoluble ECM, even though results obtained in TCPS and the bioreactor were similar in the first 15 days of culture.

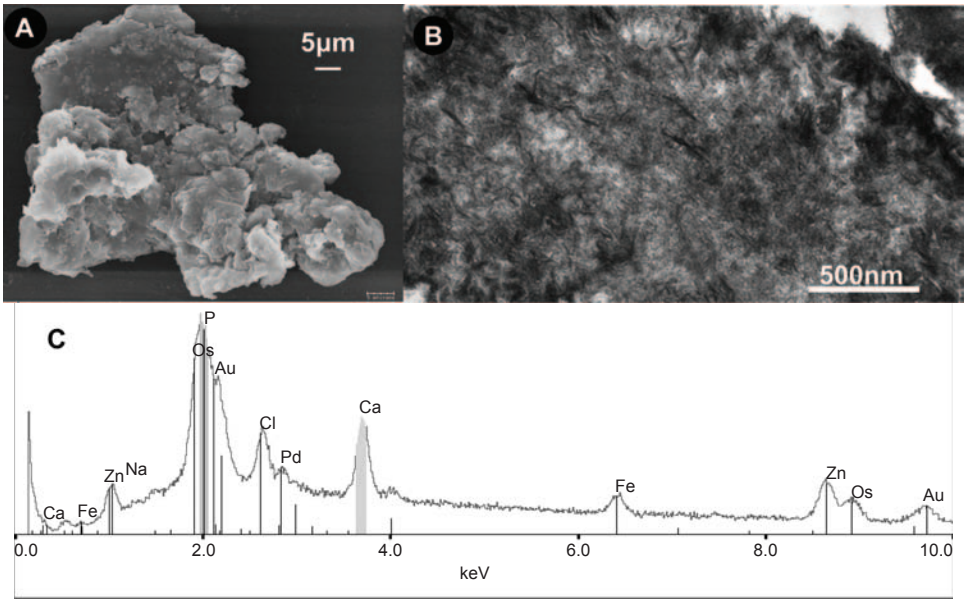

FIG. 7. Analysis of a mineral nodules taken from MC3T3-E1 cultured in a bioreactor. (**A**) Scanning electron microscopy (SEM) of a large nodule taken from a 70-day bioreactor. (**B**) High-magnification, cross-sectional transmission electron microscopy (TEM) of a similar nodule. (**C**) X-ray spectrum obtained using SEM/energy dispersive spectroscopy of a nodule taken from a 30-day bioreactor confirming Ca and P as major constituents.

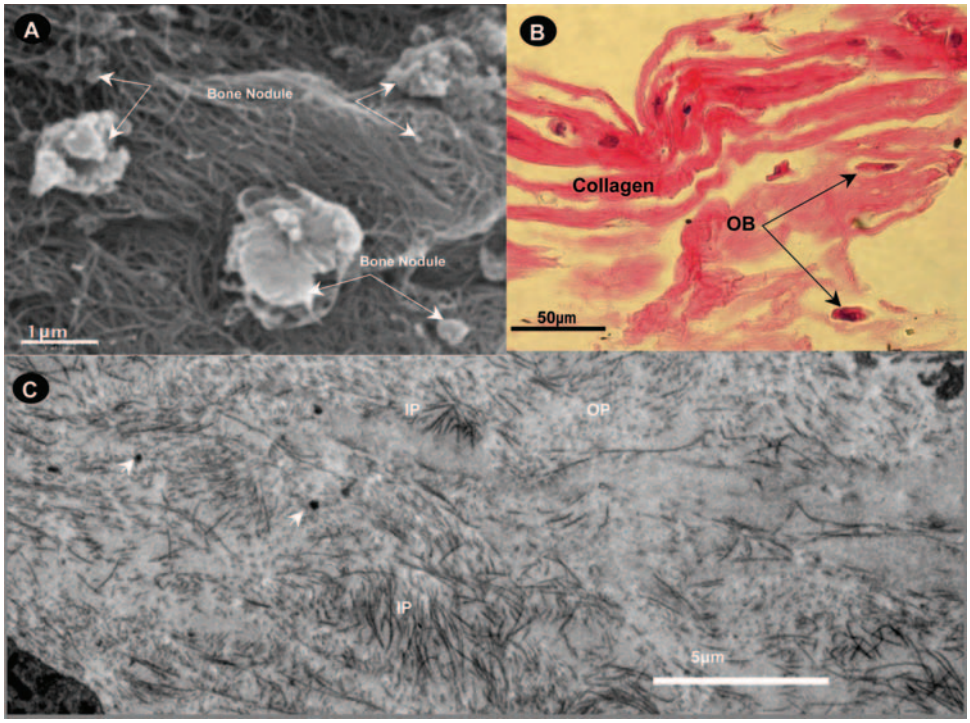

FIG. 8. Microscopic examination of matrix derived from MC3T3-E1 cultured in a bioreactor for 70 days. (**A**) Scanning electron microscopy of the outer layer showing a highly fibrous network with bone nodules. (**B**) Optical micrograph of a histologic workup showing layers of collagen with imbedded osteoblasts. (**C**) Cross-sectional transmission electron microscopy showing mineralized fibers running in (IP annotation) and out (OP annotation) of the plane.

Furthermore, morphology of cells grown in the bioreactor suggested development of an osteoid structure, with older cells taking on a flattened osteocytic-like phenotype with inter-cellular connections. The matrix surrounding up to 6 layers of cells was fibrous and mineralized. This comparison of the bioreactor with TCPS suggests that the eventual instability observed in TCPS was primarily due to the accumulated damage arising from periodic medium replacement that removes not only waste products, but also ''luxury macromolecules'' secreted by the cells. Hence, the standard cell-culture method tends to propagate, rather than mitigate, the effects of culture shock. By contrast, the simultaneous-growth-and-dialysis culture method maintained an extraordinarily stable pericellular environment. With neither subculturing steps to push cells closer and closer to the Hayflick limit[4] nor the environmental stress of an ever-changing pericellular milieu, tissue grown with the bioreactor is apparently stable for long periods of time, measured at least in months. Thus the compartmentalized bioreactor shows promise as a tool for the *in vitro* study of osteogenesis and osteopathology.

ACKNOWLEDGMENTS

This work was supported, in part, by a grant from the Pennsylvania Department of Health. The Pennsylvania Department of Health specifically disclaims responsibility for any analyses, interpretations, or conclusions. This work was also supported by the Pennsylvania State Tobacco Settlement Formula Fund, National Institutes of Health Grant AG13087–10, U.S. Army Medical Research and Material Command Breast Cancer Research Program WX81XWH-06-1-0432, and the Susan G. Komen Breast Cancer Foundation BCTR 0601044. The authors appreciate additional support from the Huck Institutes of Life Sciences, Materials Research Institute, and Departments of Bioengineering and Materials Science and Engineering of the Pennsylvania State University.

REFERENCES

1. Sherr, C., and DePinho, R. Cellular senescence: mitotic clock or culture shock? Cell **102,** 407, 2000.
2. Anselme, K. Osteoblast Adhesion on Biomaterials. Biomaterials **21,** 667, 2000.
3. Schnaper, H.W., and Kleinman, H.K. Regulation of cell function by extracellular matrix. Pediatr Nephrol **7,** 96, 1993.
4. Shay, J.W., and Wright, W.E. Hayflick, his limit, and Cellular Ageing. Nature **1**, 72, 2000.
5. Rubin, H. Telomerase and cellular lifespan: ending the debate? Nature Biotechnol **16,** 396, 1998.
6. Rose, G.G. Cytopathophysiology of tissue cultures growing under cellophane membranes. In: Richter, G.W., and Epstein, M.A., eds. International Review of Experimental Pathology. New York: Academic Press, 1966, pp. 111–178.

7. Vogler, E.A. Compartmentalized Cell-Culture Device and Method. U.S. Patent 4748124. DuPont de Nemours, Inc., Wilmington, DE, 1988.
8. Vogler, E.A. A compartmentalized device for the culture of animal cells. Biomater Artif Cells Artif Organs **17,** 597, 1989.
9. Donahue, H.J., Siedlecki, C.A., and Vogler, E. Osteoblastic and osteocytic biology and bone tissue engineering. In: Hollinger, J.O., Einhorn, T.A., Doll, B., and Sfeir, C., eds. Bone Tissue Engineering. Boca Raton, FL: CRC Press, 2004, pp. 44–54.
10. Lim, J.Y., Liu, X., Vogler, E.A., and Donahue, H.J. Systematic variation in osteoblast adhesion and phenotype with substratum surface characteristics. J Biomed Mater Res **68A,** 504, 2004.
11. Lim, J.Y., Taylor, A.F., Li, Z., Vogler, E.A., and Donahue, H.J. Integrin Expression and osteopontin regulation in human fetal osteoblastic cells mediated by substratum surface characteristics. Tissue Eng **11,** 19, 2005.
12. Vogler, E.A., and Bussian, R.W. Short-Term cell-attachment rates: a surface sensitive test of cell-substrate compatibility. J Biomed Mat Res **21,** 1197, 1987.
13. Vogler, E.A. Thermodynamics of short-term cell adhesion in vitro. Biophysical J **53,** 759, 1988.
14. Vogler, E.A. A thermodynamic model of short-term cell adhesion in vitro. Colloids Surfaces **42,** 233, 1989.
15. Harris, S.A., Enger, R.J., Riggs, B.L., and Spelsberg, T.C. Development and characterization of a conditionally immortalized human fetal osteoblastic cell line. J Bone Min Res **10,** 178, 1995.
16. Lim, J.Y., Liu, X., Vogler, E.A., and Donahue, H.J. Systematic variation in osteoblast adhesion and phenotype with substratum surface characteristics. J Biomed Mat Res **68A,** 504, 2004.
17. Vogler, E.A., and Bussian, R.W. Short-term cell-attachment rates: a surface-sensitive test of cell-substrate compatibility J Biomed Mat Res **21,** 1197, 1987.
18. Lim, J.Y., Taylor, A.F., Li, Z., Vogler, E.A., and Donahue, H.J. Integrin expression and osteopontin regulation in human fetal osteoblastic cells mediated by substratum surface characteristics. Tissue Eng **11,** 19, 2005.
19. Freed, L.E., and Vunjak-Novakovic, G. Culture of organized cell communities. Adv Drug Deliv Rev **33,** 15, 1998.
20. Gurdon, J., Lemaire, P., and Kato, K. Community effects and related phenomena in development. Cell **75,** 831, 1993.
21. Ferrera, D., Poggi, S., Biassoni, C., Dickson, G.R., Astigiano, S., Barbieri, O., Favre, A., Franzi, A.T., Strangio, A., Federici, A., and Manduca, P. Three-dimensional cultures of normal human osteoblasts: proliferation and differentiation potential in vitro and upon ectopic implantation in nude mice. Bone **30,** 718, 2002.
22. Gerber, I., and Gwynn, I. Differentiation of rat osteoblast-like cells in monolayer and micromass cultures. Eur Cell Mater **3,** 19, 2002.

Address reprint requests to:
Erwin A. Vogler
Penn State University
Depts. of Materials Science and Engineering
and Bioengineering
103 Steidle Bldg.
University Park, PA 16802

E-mail: eav3@psu.edu

Available online at www.sciencedirect.com
ScienceDirect
Biomaterials 28 (2007) 4535–4550
Biomaterials
www.elsevier.com/locate/biomaterials

Leading Opinion

Influence of substratum surface chemistry/energy and topography on the human fetal osteoblastic cell line hFOB 1.19: Phenotypic and genotypic responses observed *in vitro* ☆

Xiaomei Liu[a], Jung Yul Lim[b], Henry J. Donahue[b], Ravi Dhurjati[c], Andrea M. Mastro[d], Erwin A. Vogler[a,c,*]

[a]*Department of Bioengineering, The Pennsylvania State University, University Park, PA 16802, USA*
[b]*Division of Musculoskeletal Sciences, Center for Biomedical Devices and Functional Tissue Engineering and Department of Orthopaedics and Rehabilitation, College of Medicine, The Pennsylvania State University, Hershey, PA 17033, USA*
[c]*Department of Materials Science and Engineering, The Pennsylvania State University, University Park, PA 16802, USA*
[d]*Biochemistry and Molecular Biology, Materials Research Institute and the Huck Institutes of the Life Sciences, The Pennsylvania State University, University Park, PA 16802, USA*

Received 28 May 2007; accepted 13 June 2007
Available online 20 July 2007

Abstract

Time-dependent phenotypic response of a model osteoblast cell line (hFOB 1.19, ATCC, and CRL-11372) to substrata with varying surface chemistry and topography is reviewed within the context of extant cell-adhesion theory. Cell-attachment and proliferation kinetics are compared using morphology as a leading indicator of cell phenotype. Expression of (α_2, α_3, α_4, α_5, α_v, β_1, and β_3) integrins, vinculin, as well as secretion of osteopontin (OP) and type I collagen (Col I) supplement this visual assessment of hFOB growth. It is concluded that significant cell-adhesion events—contact, attachment, spreading, and proliferation—are similar on all surfaces, independent of substratum surface chemistry/energy. However, this sequence of events is significantly delayed and attenuated on hydrophobic (poorly water-wettable) surfaces exhibiting characteristically low-attachment efficiency and long induction periods before cells engage in an exponential-growth phase. Results suggest that a 'time–cell–substratum–compatibility–superposition principle' is at work wherein similar bioadhesive outcomes can be ultimately achieved on all surface types with varying hydrophilicity, but the time required to arrive at this outcome increases with decreasing cell–substratum–compatibility. Genomic and proteomic tools offer unprecedented opportunity to directly measure changes in the cellular machinery that lead to observed cell responses to different materials. But for the purpose of measuring structure–property relationships that can guide biomaterial development, genomic/proteomic tools should be applied early in the adhesion/spreading process before cells have an opportunity to significantly remodel the cell–substratum interface, effectively erasing cause and effect relationships between cell–substratum–compatibility and substratum properties.

Impact Statement: This review quantifies relationships among cell phenotype, substratum surface chemistry/energy, topography, and cell–substratum contact time for the model osteoblast cell line hFOB 1.19, revealing that genomic/proteomic tools are most useful in the pursuit of understanding cell adhesion if applied early in the adhesion/spreading process.

Keywords: Cell adhesion; Surface chemistry; Surface energy; Cell–substratum–compatibility; hFOB; Osteoblast

☆ *Editor's Note*: This paper is one of a newly instituted series of scientific articles that provide evidence-based scientific opinions on topical and important issues in biomaterials science. They have some features of an invited editorial but are based on scientific facts, and some features of a review paper, without attempting to be comprehensive. These papers have been commissioned by the Editor-in-Chief and reviewed for factual, scientific content by referees.

*Corresponding author. Department of Materials Science and Engineering, Pennsylvania State University, University Park, PA 16802, USA. Tel.: +1 814 863 7403; fax: +1 814 865 2917.
E-mail address: eav3@psu.edu (E.A. Vogler).

0142-9612/$ - see front matter © 2007 Elsevier Ltd. All rights reserved.
doi:10.1016/j.biomaterials.2007.06.016

1. Introduction

Adhesion and proliferation are fundamental eukaryotic (mammalian) cellular processes involved in embryogenesis, immune response, tissue maintenance, and wound healing [1]. Cell contact, attachment, and subsequent adhesion of anchorage-dependent cells are among the first phases of cell–material interactions [2,3] that profoundly influence integration with tissue and eventual success or failure of a broad range of implanted biomaterials. For these reasons, as well as a compelling need to understand prokaryotic adhesion and surface colonization, cell adhesion has been a focus of research for nearly 50 years. Cell-adhesion research has involved a unique collaboration between biologists and chemists/physicists specializing in material and surface sciences. As a consequence, a vast literature has arisen over these decades that has been the subject of a number of very good reviews (see, for examples, Refs. [2,4–13]). This literature attempts to find relationships between material properties (surface chemistry, energy, and morphology) and bioadhesive outcomes by integrating physicochemical and biological approaches to the problem. The widespread use of many different kinds of materials in biomedical, biotechnical, and engineering applications where cell adhesion is important bears witness to the significant progress that has been made in controlling cell adhesion. However, at a fundamental level, cell adhesion remains poorly understood. Cellomic, proteomic, and genomic tools offer new insights into changes in the regulation of the cell machinery responsible for observed adhesive outcomes in contact with different materials. This information will revolutionize our understanding of cell adhesion at the *intra-cellular level*. How this information might help interpret cell–substratum–compatibility (a.k.a. cytocompatibility) is a particular focus of this review.

As a means of making our objectives tractable, we focus on the specific case of osteoblast adhesion to different materials, which is of significance to the fast-growing fields of orthopedic biomaterials and musculoskeletal tissue engineering [14]. Rapid growth of these fields can be traced to the demographic facts that extended human life span and higher-activity levels at older age have greatly increased need for orthopedic healthcare [15–18]. Improved hard-tissue repair, augmentation, or replacement has thus become a very significant challenge for orthopedic biomaterials and orthopedic surgery [19–21]. Meeting these challenges depends, in part, on establishing firm relationships between implant success and orthopedic biomaterial properties (so-called structure–property relationships) that can guide the design process. These structure–property relationships critically depend on a thorough understanding of the adhesion of hard-tissue cells (osteoblasts, osteoclasts, chondrocytes, etc.) to artificial materials.

Various model osteoblasts have been introduced and used to gain insight into the bone–cell response to candidate orthopedic biomaterials *in vitro*. The most widely used model cells are primary cultures derived from normal human and rodent bone fragments, or osteosarcoma cell lines generated from human bone tumors. Each of these cell sources has strengths and limitations for studying the cell adhesion of osteoblasts *in vitro* [22–25]. For example, primary-human osteoblasts have a normal osteoblastic phenotype; but these cells are typically quite fastidious *in vitro*, grow very slowly, and have a limited life span when successfully brought into culture. Cultures derived from rodent generally circumvent these problems but may not be appropriate models for humans due to trans-species differences in phenotypic characteristics. Osteosarcoma cell lines derived from spontaneous tumors are readily grown *in vitro*, proliferate endlessly, but do not exhibit a normal phenotype. Worse perhaps, osteosarcoma cells respond abnormally to various hormones and cytokines compared to normal, differentiated human osteoblasts. In effort to overcome these limitations, Harris et al. [24] established a conditionally immortalized, human fetal-osteoblast cell line, hFOB 1.19 that was stably transfected with a gene coding for a temperature-sensitive mutant (tsA58) of the SV40 large T antigen. Resultant hFOB cells express osteoblast-specific phenotypic markers and mineralize extracellular matrix (ECM). Later, Subramaniam et al. [25] characterized hFOB 1.19 as an immortalized, but non-transformed cell line with minimal chromosome abnormalities and normal spectrum of matrix proteins. Because of these inherent qualities, we have chosen to restrict this review to the behavior of hFOB 1.19 in contact with substrata with different surface-chemical and topological features. This restriction has the obvious benefit of sharply focusing scope of the review to only a few investigators, but is at the acknowledged expense of excluding a burgeoning literature describing the behavior of other osteoblast cell types; especially the popular murine calvaria cell line MC3T3-E1 (ATCC, CRL-2593). We hope that these omissions do not seriously compromise utility of the work, which is as much aimed at finding new directions in cell adhesion as summarizing/condensing knowledge acquired over the last decade or so on osteoblast interactions with biomaterials.

We begin this review by broadly categorizing experimental and theoretical approaches to the cell-adhesion problem that have been taken over the years, attempting to place how genomics and proteomics can best provide new information in the prospective design of orthopedic biomaterials. Specific studies of osteoblast interactions with materials are then summarized with the objective of extracting insights into the short- and long-term influence surface properties can have on model osteoblasts. A general conclusion drawn from data at hand is that gene regulation responsible for adhesion selectivity among surface chemistries/energies is incisive at early stages (<3 days) of cell–surface interactions and will require focused experimental strategies to clearly observe.

2. A reflection on cell adhesion

2.1. Cell-adhesion theories

Fig. 1 coarsely categorizes different approaches that have been taken to the problem of cell adhesion, along with some early (but not necessarily first) literature citations that, in the authors' view, are archetypes for work that was to follow along the same theme. In the early years, say 1960s to mid 1980s, there was enthusiasm that cell adhesion could be substantially understood using colloid science, surface chemical, and surface thermodynamic principles (the pioneering 1924 work of Mudd and Mudd [26,27] in bacteria adhesion was possibly the first application of surface thermodynamics to cell adhesion). A number of imaginative physicochemical theories were developed to explain the cell-adhesion process [4–8,28–33] with the goal of establishing a predictive basis for optimizing biocompatibility—or at least a rational basis for explaining how substratum surface properties so profoundly affect cell–material interactions. Although some of these theories have been useful in separating and weighing the relative importance of various material properties (such as charge, wettability, surface density of cell-binding ligands, etc.), it seems clear now that cell–substratum interactions ranging from cell–surface contact through proliferation to chronic cell–material interaction are far too complex to be meaningfully embraced by relatively simple mathematical models.

Also in these early years, experiment revealed a strong dependence of cell adhesion/proliferation on substratum surface chemistry, giving rise to the expectation that cell adhesion could be understood using surface-chemical principles. Rappaport's [34] early 1970s work was among the earliest studying surface-chemical effects on mammalian cell adhesion. Soon after, a variety of surface-synthesis strategies were explored, ranging from use of liquid-phase chemical oxidants [35,36] to application of gas-discharge treatments [37] now commonly employed in the commercial production of disposable plastic tissue cultureware [38]. Evidence mounted supporting the idea that a particular surface functional group—hydroxyl or carboxyl for example—was particularly stimulatory to cell adhesion and proliferation [39–43] over other functional groups. However, it has proven difficult in subsequent research to clearly separate cause and effect in the cell-adhesion/proliferation process, especially in the ubiquitous presence of proteins, and by doing so, unambiguously separate surface chemistry from all other influences (such as surface energy/water wettability) [44]. The most general rule connecting material properties with cell–substratum–compatibility emerging from decades of focused research is that anchorage-dependent mammalian cells (those requiring substratum adhesion for proliferation) favor modestly water-wettable or hydrophilic surfaces exhibiting a water contact angle $\theta < 60^\circ$ [9,10,31,33,38,45–47]. No doubt, surface chemistry and wettability are inextricably convolved properties because it is the hydrogen bonding of water to surface functional groups that most profoundly influences wettability (see, as examples, Refs. [38,46,48]).

Viewed from a purely biological perspective, cell adhesion is all about how cells respond to different surfaces as measured by various morphological and/or phenotypic markers. Grinnell's [2] classic published in International Review of Cytology traced cell morphology and ultrastructure through different stages of adhesion and dependence on substratum properties. The role of various receptors and adsorbed ligands became evident in this era, ultimately identifying a pantheon of 'adhesins' that rather quickly dominated cell-adhesion thought [49–51]. Interest in, or even remembrance of, physicochemical and surface-science theories faded very quickly; even though it

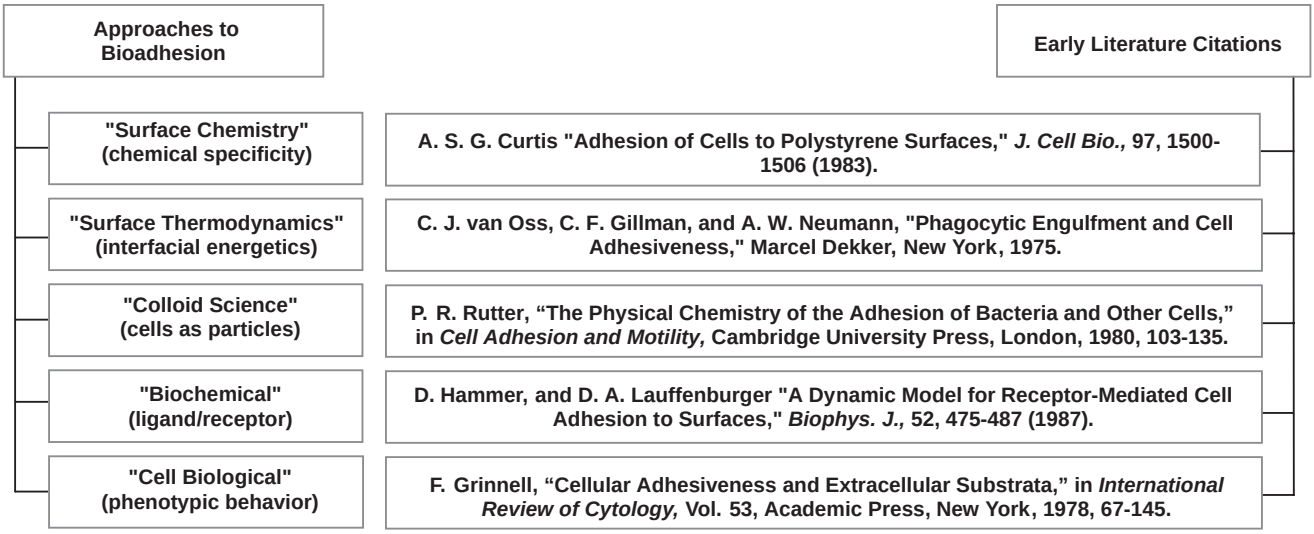

Fig. 1. Different approaches to cell adhesion with some archetypical literature citations. Each of these approaches effectively probe different phases of cell adhesion and describe cell adhesion in different terms.

is self-evident that biology, biochemistry, and physics are simultaneously operative at some level. Perhaps Hammer and Tirrell [11] captured it best with the words "…specific recognition between reactive biomolecules or receptors occurs against a backdrop of polymeric and long-range nonspecific forces."

Different approaches to cell adhesion captured in Fig. 1 effectively study different facets of a multi-faceted cell-adhesion problem that become more-or-less important at various stages of cell adhesion. For example, there can be little doubt that surface chemistry, colloid forces, and surface thermodynamics are more important earlier in the process than later. Thus, an unsolved problem in cell adhesion is to integrate these separated temporal views in a way that establishes how preceding stages of cell–surface interaction influence succeeding stages. Pursuing the example mentioned above a bit further to illustrate this latter point, it is evident that colloid science considers only forces between cell and surface that occur in close proximity—but not contact—whereas surface thermodynamics contemplates the energetics of interface formation and destruction commensurate with intimate cell–surface contact [38]. Thus, colloidal principles might speak volumes about the forces that bring cells to within a few tens of nanometers of a surface but colloid science is silent about the adhesion process itself. Conversely, surface thermodynamics might address cell–surface adhesivity but says nothing about getting the cell close enough to the surface to actually form a cell–surface interface. A connecting theory is required to bring these parts of the problem together and explain how the surface-contact step can influence final adhesion. Modified colloid and surface-thermodynamic theories might indeed build such a bridge [31,33], but the span between the physics and biology appears much, much broader. Worse, it is not yet apparent what kind of information can fill this physics–biology gap or how closure can be accomplished in terms that relate materials properties to cell–substratum–compatibility.

2.2. Cell attachment and proliferation kinetics

Cell biologists view the adhesion of anchorage-dependent mammalian cells to a substratum surface as occurring in four major steps that precede proliferation: protein adsorption, cell–substratum contact, cell–substratum attachment, and cell adhesion/spreading [2,9,31,33]. Protein adsorption is complex in its own right, involving molecular-scale interactions with a hydrated surface that no doubt transpire nearly instantaneously relative to the timeframe of cell adhesion (see, as examples drawn from many, Refs. [52,53]). Cell contact and attachment involve gravitation/sedimentation to within 50 nm or so of a surface whereupon physical and biochemical forces conspire to close the cell–surface distance gap. Initial cell contact with the substratum presumably occurs by extension of filopodia that penetrates an electrostatic barrier between cell and substratum surfaces that usually bears similar net-negative charges [2,38]. Filopodia attach firmly to the substrate and play an important role in orienting cells on the surface and begin the process of customizing the substratum for improved cell adhesion (see Refs. [2,54] for reviews). Time required to complete contact and attachment steps in a simple, stagnant culture-dish arrangement is usually of the order of 30 min for typical soft-tissue cells [45] (see also Fig. 2), but clearly depends on a complex interplay between cell, surface, and suspending fluid-phase composition [38] in a manner that has been only partially described by aforementioned colloid and surface-thermodynamic theories. Adherent cells then slowly (typically within hours) spread over the surface, depending on compatibility with the surface, expressing a strong 'biological component of adhesion' [38] that includes secretion of ECM and results in the flattening of cells on the substratum [2] (spread-cell length is about 3–10 times height [9]). Needless to say, (protein) composition of the fluid phase can greatly affect the entire cell-adhesion process [31,33,55–59]. Thus, it is apparent that the short-term (<3 days) cell-adhesion/proliferation process spans a broad range of time and length scales. As a consequence, the biophysics of cell adhesion is very complex and any successful model of cell adhesion must address this multi-scale aspect of the problem.

Fig. 2 sketches a generalized kinetic profile representing short-term cell adhesion/proliferation typically observed for the adhesion of mammalian cells to planar surfaces from a stagnant fluid phase (e.g. plating cells into petri dishes or tissue-culture flasks). Fig. 2 plots attached cell number (expressed as % of originating cell inoculum) as a function of time [14,45,46,60,61]. Annotations on Fig. 2

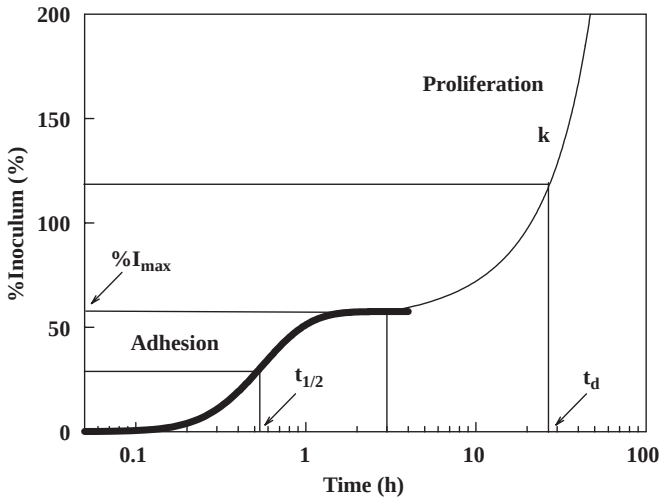

Fig. 2. Schematic illustration of cell adhesion and proliferation kinetics identifying quantitative parameters that can be extracted from measurement of number of attached cells (expressed here as percentage of (viable) cell inoculum; $\%I$) with time. $\%I_{max}$ is the maximum percentage of a cell inoculum that adheres to a surface from a sessile cell suspension and $t_{1/2}$ measures half-time to $\%I_{max}$. The proliferation rate (k) and cell-number doubling time (t_d) measure viability of attached cells (adapted from Ref. [60]).

indicate a number of quantitative parameters than can be extracted from experimental data comprising such a kinetic analysis. These parameters include time-to-half-maximal attachment $t_{1/2}$ and maximal attachment $\%I_{max}$. $\%I_{max}$ is defined by a steady-state attachment plateau that has been interpreted as either a pseudo-equilibrium partitioning between attached and suspended cells [38,45,62] or a kinetic-saturation phenomenon [63–66]. This steady state precedes cell spreading and, after a dwell time (which can also be quantified), adherent cells replicate with proliferation rate k and a characteristic population doubling time t_d. As will be discussed subsequently, each of these attachment/proliferation parameters is quite sensitive to surface chemistry and protein/surfactant composition of the fluid phase [31,33], as well as being diagnostic of cell–substratum–compatibility [45,46].

The whole kinetic process sketched in Fig. 2 is not frequently measured, especially the early attachment phase characterized by $t_{1/2}$ and $\%I_{max}$, because cell-enumeration protocols are quite labor intensive (there are a variety of cell-enumeration methods available including dye techniques [67–74], autoradiography [75], light and electron microscopy [76,78], Coulter counting [79], hemocytometry [80], spectrometry [81,82], nuclei number [83], total DNA [84], total protein concentration [78,85] that may or may not give similar results, depending on cell number and specific experimental conditions). Instead, a variety of experimental short cuts are taken, such as measuring attached cell number after some arbitrary cell–surface contact time [86–89]. In many instances, the fluid-phase composition is changed mid-way through the cell-attachment assay, as by discarding unattached cells or changing protein composition, which can completely change the biophysics of the adhesion process. The wide variety of methods used makes it very difficult to compare results from different protocols or research groups. It is thus not always clear how measured cell-adhesion parameters correlate, or even if these different parameters are at all related. This complexity in the literature is exacerbated by the fact that there are a number of methods of assessing cell–surface interaction that do not fall in the category of cell-attachment kinetics. These include measurement of cell spreading [90–92], cell interfacial energy [93], forces required to dislodge adherent cells [94–96], and use of detachment indices [97].

2.3. The cell morphological response to materials

The most obvious and striking difference in cell behavior on different materials is cell shape (morphology). Variations in cell morphology can be observed by light and electron microscopy assisted with various cytoskeletal stains such as actin and vinculin stains [61,77,89,98–102]. Morphological changes can be quantified by using image analysis that reports dimensional parameters such as cell area, perimeter, Feret's diameter, circularity, and coverage per unit surface area.

Anchorage-dependent cells attached to a surface that supports cell growth undergo a progressive process of flattening from a very-nearly spherical shape to discoid, as was well described in Grinnell's [2] 1978 review. During this shape change, adhesion to the surface is mediated by formation of focal adhesions and plaques constructed from an assembly of transmembrane integrins that anchor the cytoskeleton to ECM secreted by surface-bound cells. Related to Fig. 2, these events occur well after steady-state adhesion has been achieved but before the exponential-growth phase. Vogler [38] has emphasized that this 'biological component of the work of adhesion' expresses itself much later than the operative timeframe of physical forces that bring cells from suspension in media to the substratum surface. Using detergent solutions (Tween-80; polyoxyethylene sorbitan monooleate) to vary liquid-phase interfacial tension or to match that of serum-containing medium, it has been shown that all phases of cell contact through attachment observed in cell-culture medium could be observed in absence of proteins [31,33]. Of course, attached cells ultimately die in the absence of serum (or defined-media) proteins, but cells attached from detergent solutions apparently grow quite normally if the detergent solution is replaced with serum-containing medium soon after cells reach the attachment steady state (Vogler, unpublished work). All of this suggests that the early-attachment phase does not include significant ECM production but rather is dominated by physical forces.

Cell-attachment time is clearly an important variable in the correlation of cell morphology to substratum characteristics—chemical or topological. Our experience with hFOB summarized in the next section suggests that the general sequence of events, from round cells to flat, is substantially independent of the overall cell–substratum–compatibility. On surfaces exhibiting poor cell–substratum–compatibility (typically hydrophobic, see Figs. 3–5), cells remain rounded for an extended period of time compared to more compatible surfaces (typically hydrophilic). But if cells on poorly compatible surfaces survive, even if just barely, flattening and eventual population of the surface occur. Thus, expression of morphological traits may be viewed as delayed on poorly compatible surfaces, a kind of time–cell–substratum–compatibility–superposition principle that suggests cells are engaged in an extended process of secreting ECM to compatibilize the surface.

2.4. Genomic and proteomic tools in the study of cell adhesion

Modern genomic and proteomic tools offer unprecedented opportunity to directly measure changes in the cellular machinery that lead to the observed cell response to different materials. Perhaps, these powerful methods will provide new information that can fill the physics–biology gap mentioned above, or at least yield insights into how closure can be accomplished in terms that relate materials properties to cell–substratum–compatibility. The objective

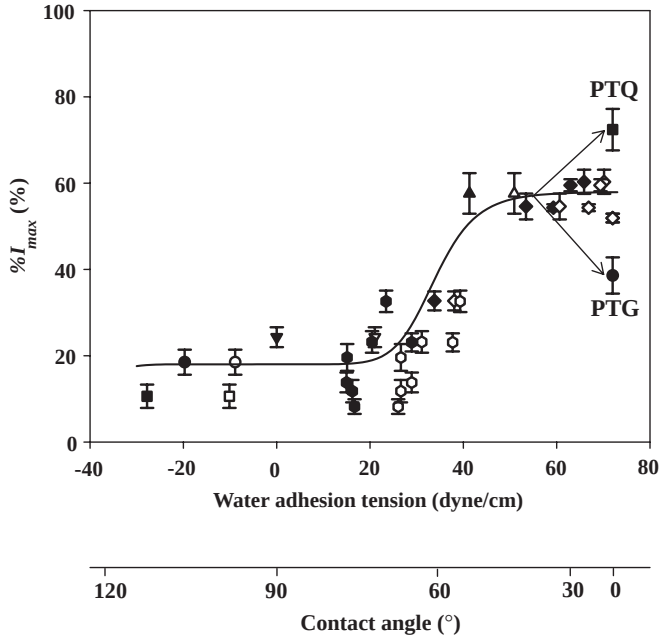

Fig. 3. Correlation of $\%I_{\max}$ (see Fig. 2) with substrata surface energy for hFOB. Surface energy is here measured by water adhesion tension $\tau^o = \gamma_{lv}^o \cos\theta$, where $\gamma_{lv}^o = 72.8$ dyne/cm at 20 °C for pure water and θ is the angle subtended by a water droplet on the surface understudy (advancing θ = filled symbols, receding θ = open symbols; adapted from Ref. [60]). Error bar represents standard deviation ($N \geqslant 3$). Trend-line through advancing and receding data is guide to the eye; ▲ = TCPS; ▼ = BGPS (bacteriological grade polystyrene); ● = glass; ■ = quartz; ◆ = PTPS (plasma-treated polystyrene); ⬢ = biodegradable polymers of PLGA 5/5 ($M_n = 80$ k), PLGA 7/3 ($M_n = 96$ k), PLA ($M_n = 160$ k), PCL ($M_n = 80$ k), PLCL 7/3 ($M_n = 82$ k), PLGCL 2.5/2.5/5 ($M_n = 60$ k), PLGCL 3.5/3.5/3 ($M_n = 54$ k). M_n = number-average molecular weight by GPC. PLGA = poly(lactide-*co*-glycolide); PLCL = poly(lactide-*co*-caprolactone); PLGCL = poly(lactide-*co*-glycolide-*co*-caprolactone). See Ref. [60] for details on materials preparation and characterization.

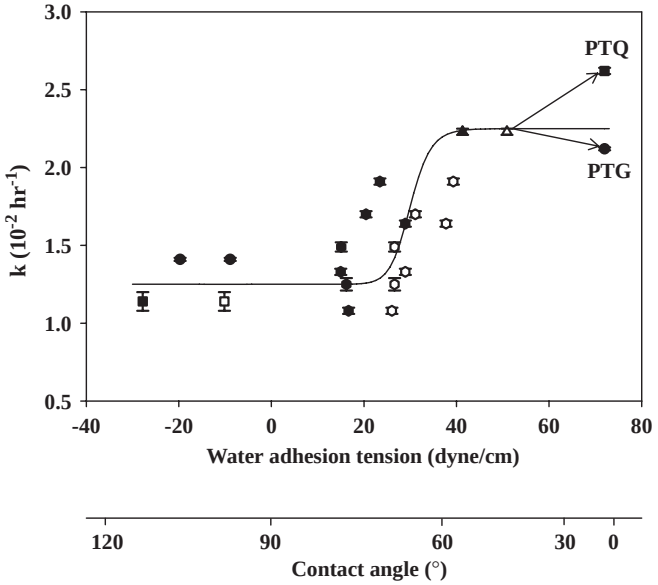

Fig. 4. Correlation of cell proliferation rate constant k with substratum surface energy for hFOB. Surface energy is here measured by water adhesion tension $\tau^o = \gamma_{lv}^o \cos\theta$, where $\gamma_{lv}^o = 72.8$ dyne/cm at 20 °C for pure water and θ is the angle subtended by a water droplet on the surface understudy (advancing θ = filled symbols, receding θ = open symbols; adapted from Ref. [60]). Error bars represent standard deviation of $N \geqslant 3$. Trend line through advancing and receding data is guide to the eye. Material identification is the same as in Fig. 3.

here is to systematically relate material properties to the regulation of important genes that ultimately control cell vitality and evolution of phenotype. But, before the genomic/proteomic revolution can transform our basic understanding of cell–substratum–compatibility, especially as it relates to material properties, we need to know which of the plethora of genes and proteins should be monitored and over what time frame.

Time quite clearly plays an important role in cell adhesion of mammalian cells. It seems safe to guess that gene regulation during these different phases of adhesion would be likewise quite different, leading directly to the expectation that the outcome of genomic/proteomic analysis will strongly depend on when in the cell-adhesion process these tools are used. For the purpose of illustrating this important point, it seems useful to speculate when genomic/proteomic studies might yield results that would correlate most strongly with substratum surface properties. According to the preceding discussion, biophysical chemistry dominates the initial phases of cell–surface contact and attachment, at least as it occurs in the highly simplified case of cell adhesion to a culture dish from a sessile fluid phase. Perhaps, cell machinery is in idle during this phase awaiting the signal to manufacture ECM and integrins that will mediate/moderate adhesion in subsequent stages of cell adhesion. If this is the case, little-or-no useful information from genomic/proteomic tools would be anticipated at this very early stage of cell adhesion (to say nothing of the experimental difficulties associated with data acquisition). Later, say within the first 4 h of attachment to a cell-compatible surface such as ordinary tissue-culture labware, strong up-regulation of genes responsible for production of ECM and various integrins would be anticipated. Perhaps, the extent of up-regulation would correlate with substratum surface properties in a manner that might suggest cause and effect relationships that can serve as the basis of material design. Still later, say within $4 < t < 72$ h when cells begin to proliferate and are consequently preoccupied with mitosis, substratum-specific gene regulation might be quite challenging to detect. But data summarized in Section 3.1 show there are significant differences in proliferation rates, at least for hFOB 1.19, suggesting that this phase of cell adhesion would nevertheless be a likely target for the application of genomic/proteomic tools. Finally, in the post-mitotic period ($t > 72$ h), when adherent cells begin to express normal physiological processes (such as mineralization of the surrounding ECM) surface properties might only weakly correlate with substratum surface properties. Here too, the time–cell–substratum–compatibility–superposition principle mentioned in preceding section should be borne in mind because timing of these phases of adhesion are accordingly shifted to longer times on poorly

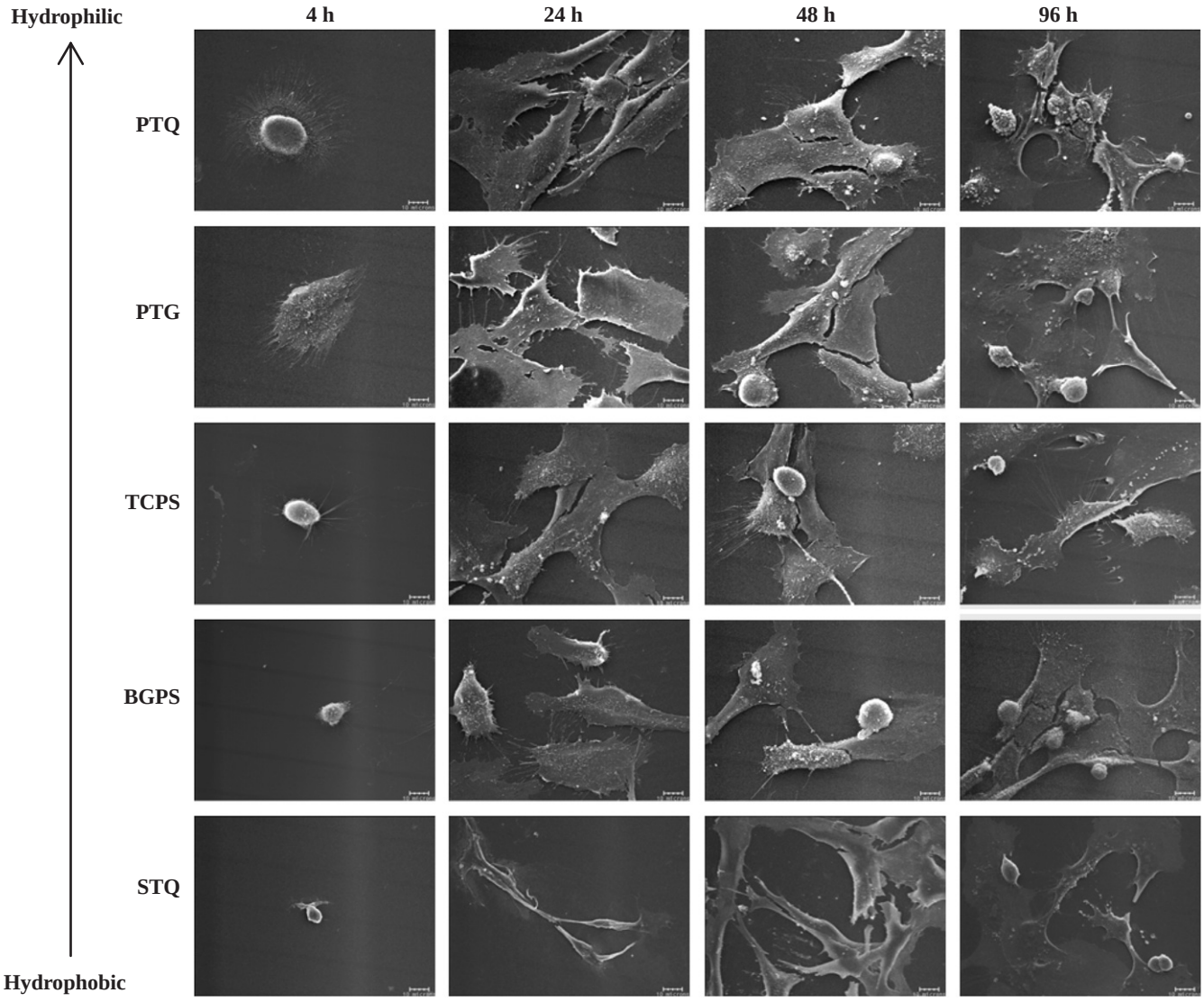

Fig. 5. Variation in hFOB morphology on different surfaces after 4, 24, 48, and 96 h of culture as assessed by SEM (hydrophilic surfaces: PTQ = plasma-treated quartz, PTG = plasma-treated glass, TCPS = tissue-culture grade polystyrene; hydrophobic surfaces: BGPS = bacteriological grade polystyrene, STQ = silane-treated quartz). Scale bar = 10 μm. Note that variation in cell morphology abates with time, especially for hydrophobic specimens.

cytocompatible surfaces and so gene regulation would presumably be shifted in time as well. Of course, all of this discussion is highly speculative because focused studies have not yet been carried out with any particular material, let alone with materials bearing systematically varied surface properties. Studies reviewed in the next section just begin to provide some of this information.

3. Influence of substratum surface chemistry/energy and topography on the adhesion of human fetal osteoblastic cell line hFOB 1.19

Time-dependent phenotypic response of hFOB 1.19 (ATCC, CRL-11372) to substrata with varying surface chemistry and topography is reviewed in this section in light of the cell-adhesion theory outlined in the preceding section. Osteoblasts exhibit many, if not all, of the general bioadhesive characteristics of other mammalian (soft tissue) cells, plus some interesting peculiarities presumably specific to osteoblasts. As a consequence, an implicit assumption prevailing in the literature is that surface-engineering methods applied to improve soft-tissue–cell adhesion (modification of surface chemistry, surface energy/wettability) can be likewise used to improve osteoblast adhesion to, and proliferation on, orthopedic biomaterials *in vivo*. In addition to these standard surface-engineering methods, precision engineering of surface topography is an alternative receiving considerable interest in orthopedic biomaterials because of the contemporaneity among nanoengineering, nanomedicine [103–105], and the demand for improved orthopedic healthcare mentioned in the introduction. In principle, surface topography and surface chemistry can be varied independently but, in practice, this is difficult to do and even more difficult to

prove that chemistry and topography are actually independent parameters. This latter issue has become a matter of academic interest in the emerging field of nanomedicine. Pragmatically, it may not be so important how cell–substratum–compatibility is influenced as long as this surface engineering reproducibly leads to improved material characteristics. But, for the purpose of prospective (rather than accidental) design of orthopedic biomaterials, it is critical to evaluate which of the aforementioned surface characteristics are most influential. Careful evaluation of cell-adhesion kinetics, morphology, and application of genomic/proteomic tools outlined in the preceding section are key to understanding osteoblast response to orthopedic biomaterial characteristics.

3.1. Short-term adhesion and proliferation of hFOB on different surfaces

Lim et al. [14,60,61] found that hFOB adhesion efficiency ($\%I_{max}$ indicated in Fig. 2) strongly correlated with substratum wettability, with high rates of cell attachment on relatively hydrophilic surfaces ($\tau^o > 30$ dyne/cm or a nominal contact angle $\theta < 65^\circ$) and low-attachment rates on hydrophobic surfaces ($\tau^o < 30$ dyne/cm or a nominal contact angle $\theta > 65^\circ$; where $\tau^o \equiv \gamma_{lv}^o \cos\theta$ is the adhesion tension of pure water with interfacial tension γ_{lv}^o subtending a contact angle θ on the substratum surface; see Refs. [38,48] for a discussion of biomaterial wetting properties and Ref. [106] for use of hydrophilic/hydrophobic terminology applied to biomaterials). A variety of materials were examined, including silane-treated glass and quartz (STG, STQ), polylactide/glycolide-based biodegradable polymers, bacteriological-grade polystyrene cultureware (BGPS), and tissue-culture grade polystyrene cultureware (TCPS). Lim et al. made no overt attempt to control surface texture in these studies, or any particular effort to characterize adventitious surface rugosity. It is probably safe to assume that these materials were rough at the sub-micron level and surface texture was more-or-less random. Lim's work has been confirmed by subsequent analysis that focused in the hydrophilic end of the wetting scale. Fig. 3 compiles unpublished results (Vogler) showing that incremental increase in PTPS wettability (by air-plasma-discharge treatment) over the range $42 < \tau^o \leqslant 72.8$ dyne/cm range did not measurably increase hFOB attachment efficiency over TCPS (Corning TCPS control surfaces exhibited an advancing water contact angle $\theta_a = 55^\circ$ and receding contact angle $\theta_r = 45^\circ$). In this regard, hFOB results mirror those obtained with epithelioid and fibroblastic soft-tissue cells [31,33,45]. However, a noticeable attachment preference of hFOB for fully water-wettable quartz (air-plasma treated, PTQ) and discrimination against fully water-wettable glass (air-plasma treated, PTG) relative to TCPS seems to be unique for hFOB compared with soft-tissue cells [60] and possibly generic to osteoblasts. This significant difference in hFOB attachment efficiency to surfaces exhibiting the same nominal surface wettability might be due to cytotoxicity of ordinary SiO_x glass [107,108] that inhibits early stages of cell adhesion. But the cause of the attachment preference for the quartz surface chemistry ($>99.99\%$ SiO_2) remains unresolved. Nevertheless, this glass/quartz difference is an example where substratum chemistry apparently plays an important role in cell adhesion, quite independent of water wettability.

Interestingly, cell-proliferation rates also correlated with substratum surface wettability, as shown in Fig. 4. This correlation suggests that the cellular machinery responsible for replication is affected by surface chemistry/energy, well after the contact and attachment phase occuring within the $0 \leqslant t \leqslant 2$ h timeframe (see also Fig. 2). No doubt gene regulation associated with proliferation is in high gear, leading to the speculation that many interesting differences in the cell–substratum–compatibility of various materials could be detected using genomic/proteomic tools within this early phase of cell–surface interaction, as discussed in Section 2.4. The word "speculation" is purposefully chosen here because, although it makes intuitive sense that gene regulation at this stage in cell–substratum interaction should be quite different from that observed in confluent cells, to our knowledge no such measurements have actually been made. The reward for such experimentally challenging research should be observation of large differences among cells on different materials that is not observed at later times; even at the extremes of surface energy. That is to say, the opportunity to correlate material properties with expression of proteins important in the adhesion process may be in the exponential-growth phase that follows steady-state attachment (see Fig. 2).

Returning to Fig. 4, it is interesting to note that whereas the proliferation rate k on PTQ was measurably faster than TCPS, reflecting differences observed in attachment rate discussed above, proliferation on PTG was approximately the same as TCPS. Perhaps, this suggests that attachment efficiency $\%I_{max}$ and proliferation rate k are independent parameters in certain circumstances measuring different aspects of cell–surface compatibility. Stepping back from these details momentarily, it is quite striking from Figs. 3 and 4 that hFOB response to surface energy pivots near $\tau^o \sim 30$ dyne/cm ($\theta \sim 60^\circ$), as has been observed for a variety of soft-tissue cells (and some prokaryotes, see Refs. [46,47]). Vogler attributes this to the behavior of water at surfaces [47] that profoundly influences protein adsorption, among other important physicochemical phenomenon. Perhaps, vicinal water is the medium through which cells sense physical properties of articifical surfaces in forced contact: surface chemistry/energy affects the aqueous pericellular milieu immediately contacting attached cells and cells respond accordingly (see Ref. [47] for more disucssion). Clearly, this will remain only so much speculation until we can measure the intra-cellular response to different materials to see if there is any correlation with contacting surface energy and behavior of water at these surfaces [46,47].

Hendrich et al. [74] were among the first to measure osteoblast response to purposely textured surfaces. They found measurably higher hFOB proliferation on a relatively smooth titanium surface and lower cell proliferation on relatively rough CoCrMo alloy surfaces. However, hFOB was found to proliferate at similar rates on CoCrMo and stainless steel surfaces, even though these two surfaces had significantly different roughness. Hao et al. [109] studied hFOB proliferation on Ti–6Al–4V titanium alloy surfaces with different rugosity, modified either mechanically or with a high-power diode laser. Cell growth increased considerably on the laser-treated titanium alloy surfaces and slightly on the mechanically roughed surface (compared to untreated surfaces). However, it was observed that contact angles decreased (water wettability increased) with either laser or mechanical treatment (presumably due to an increase in oxygen content on treated surfaces), indicating both topographic and surface-chemical modification. Lim et al. [110,111] recently reported studies of hFOB adhesion and proliferation on polymer systems with varying surface texture, chemical composition, and wettability. As surfaces varied from smooth to textured with different topographic feature scale, hFOB adhesion was observed to exhibit statistically significant differences in cell–substratum–compatibility; although the full range in adhesion efficiency varied only about 20% among surfaces studied. Authors noted that "…various biomaterial characteristics (topography, surface, and chemistry/energy) are intercorrelated", emphasizing the point made early in this section that it is difficult to deconvolve impact of topography from surface chemistry/energy on cell-adhesion/cell–substratum–compatibility.

3.2. Morphological response of hFOB to different surfaces

Lim et al. [61] examined differences in cytoskeletal features of hFOB cultured on surfaces with different surface energy at different culture intervals (3 h, 1 day, 3 days) by actin/integrin immunofluorescence staining. This work demonstrated remarkable morphological difference between cells on hydrophilic and hydrophobic substratum at equivalent times. Cells cultured on plasma-treated quartz (PTQ, hydrophilic) displayed distinct, large plaques of integrins (α_v and β_3 subunits) co-localized with actin stress fibers whereas there was much less development of these adhesion structures on silane-treated quartz (STQ, hydrophobic). These observations motivated further examination of cell morphology on substrata with varying surface energy and as a function of time in an attempt separate surface energy and time-in-culture effects. Fig. 5 compares hFOB cultured on PTQ, PTG, TCPS (relatively hydrophilic), BGPS, and STQ (relatively hydrophobic) for 4, 24, 48, and 96 h (compare to cell attachment kinetics of Figs. 2 and 3). Initially attached cells observed by light microscopy were distributed randomly on all surfaces (not shown). After 4 h, hFOB reached maximal attachment on all surfaces and were found to be significantly more spread on PTQ and PTG than on TCPS, BGPS, and STQ. Notice from Fig. 5 that attached-cell shape is dramatically affected by surface energy, increasing in size with hydrophilicity from a dimension similar to that of a cell in suspension ($\leqslant 10\,\mu m$) on STQ. Filopodia extend in all directions from hFOB on PTQ, PTG, and TCPS but there were relatively fewer filopodia extending from hFOB on hydrophobic BGPS and STQ that were more directionally oriented as if emanating from a single point of attachment. Examination of a large number of such micrographs revealed that hFOB morphology on PTG was more variable than on other surfaces, as illustrated in Fig. 6, possibly correlating with the observed cytotoxicity of glass mentioned in Section 3.1. After 24 h, hFOB on all surfaces became more elongated and flattened. Cells were fully spread and in close contact by extended filopodia on PTQ, PTG, and TCPS, but some cells on BGPS remained rounded and not fully extended. Fig. 7 uses image analysis (ImageJ, National Institute of Health) of Coomassie-blue-stained cells to quantify this visual assessment of hFOB morphology on PTQ and STQ and TCPS. In our hands, % coverage and occupied area were the two most sensitive parameters that seemed to correlate with SEM.

Cells on STQ were the most extended and longitudinally oriented of the group, and retained a spindle-like shape up to 48 h. Within 48 h, cell rounding associated with cell division was observed on all surfaces except on STQ, indicating delayed cell proliferation on STQ consistent with the reduced hFOB doubling time on hydrophobic surfaces reported by Lim et al. [60]. Morphological differences among cells on the various surfaces all but disappear after 48 h contact, except perhaps hFOB on STQ that retained a spindle-shaped morphology up to 96 h. Nevertheless, it is clear that extremes in surface energy (that quite nearly lead to life-to-death differences in short-term viability) were substantially remediated after a relatively short culture period. In this regard, it is interesting to note that evolution of morphology on hydrophobic surfaces is slower, but otherwise not remarkably different than that observed for hFOB on more hydrophilic surfaces—an example of the time–cell–substratum–compatibility–superposition principle mentioned previously. For example, images of hFOB on BGPS at 48 h or on STQ at 96 h might well be traded with that of hFOB on TCPS for 24 h without significantly changing perception of trends.

Fig. 8 expands on the work of Lim et al. [61] discussed above using actin and vinculin immunostaining to visualize evolution of cytoskeleton and focal adhesions of hFOB on TCPS, PTQ and STQ by comparing 3 and 24 h culture intervals. hFOB on PTQ and TCPS displayed actin bundles at 3 h, whereas actin was much more diffuse in hFOB on STQ. This is quite consistent with the gross morphology observed using SEM (Fig. 5) from which it appeared that hFOB on STQ was attached only at a single point. Vinculin plaques were also distinct at the leading edge of hFOB on PTQ and TCPS, which was not at all the case of STQ. At 24 h of cell culture, differences among surfaces were even

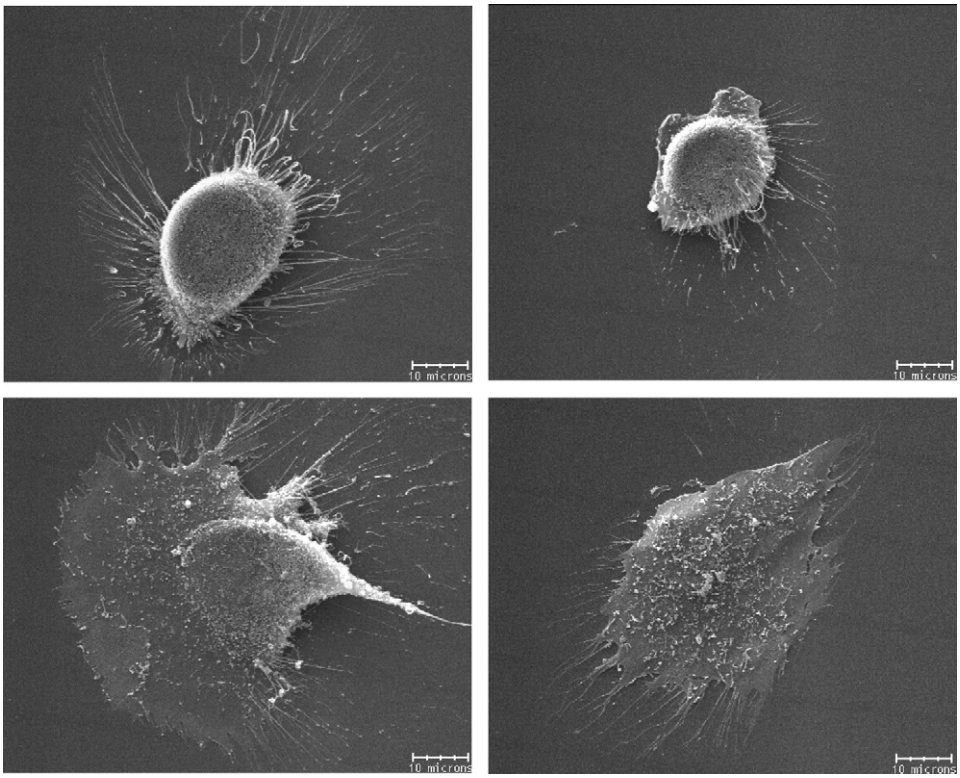

Fig. 6. Variation in hFOB shape on plasma-treated glass (PTG) after 4 h culture as assessed by SEM showing widely varying morphological response to apparently cytotoxic SiO_x glass. Scale bar = 10 μm.

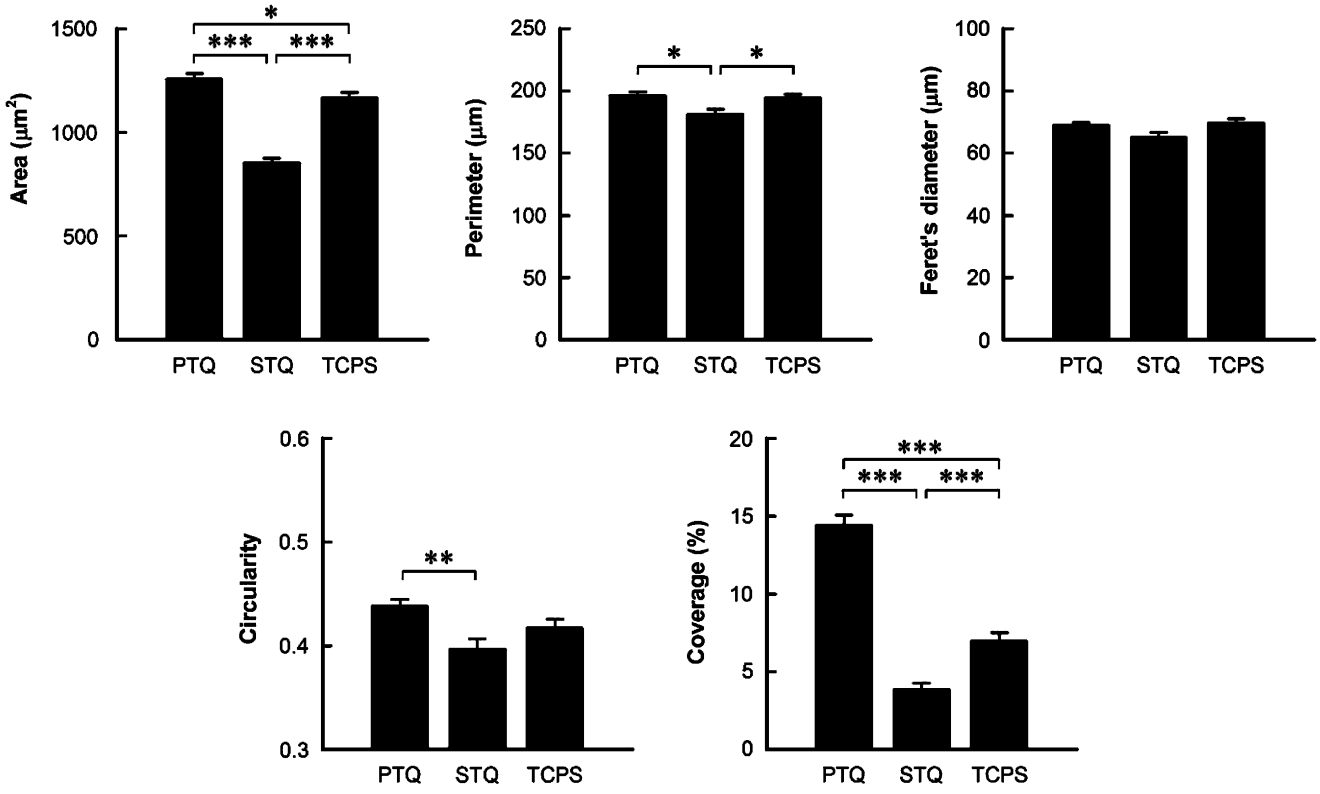

Fig. 7. Dimensional analysis by image analysis (Image J, NIH) of Coomassie-blue-stained hFOB cultured on hydrophilic surfaces (PTQ = plasma-treated quartz, TCPS = tissue-culture grade polystyrene) and hydrophobic surfaces (STQ = silane-treated quartz) for 24 h. Statistical significance indicated by *($p<0.05$), **($p<0.01$) and ***($p<0.001$).

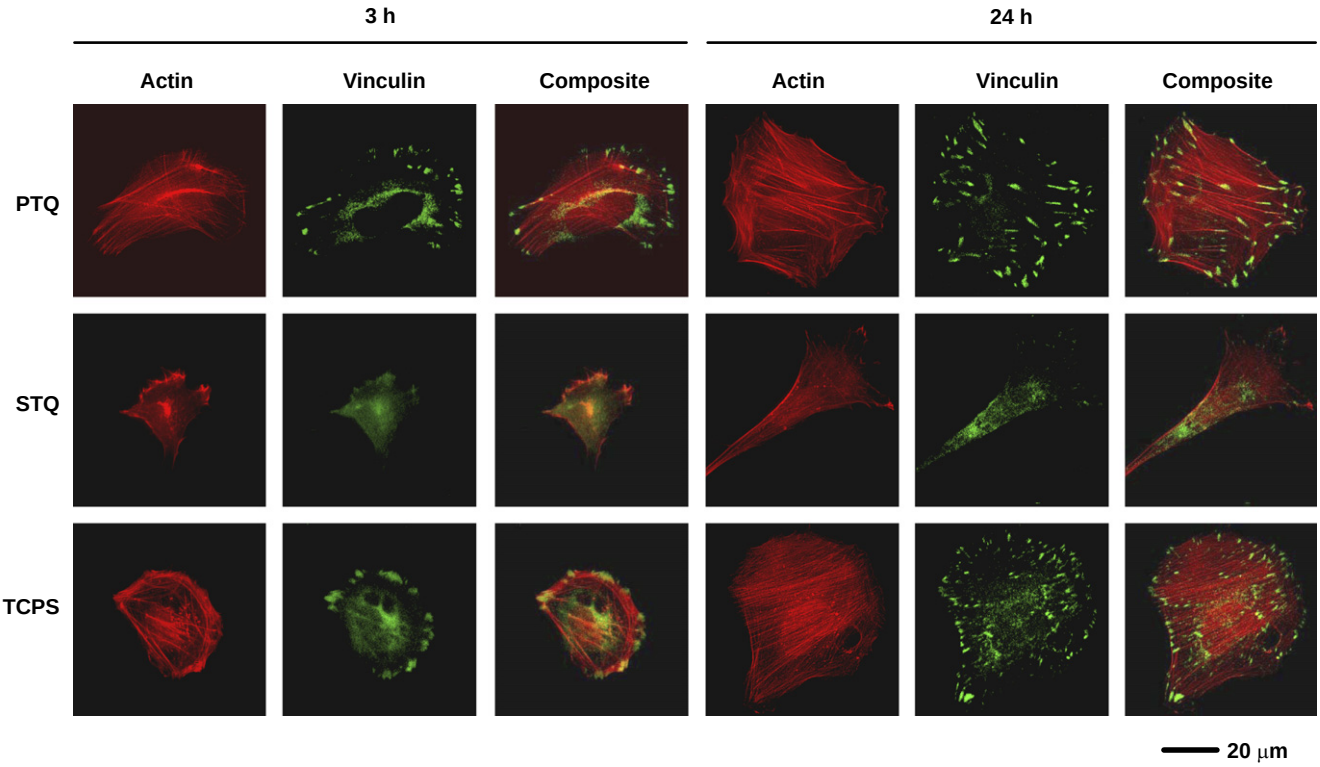

Fig. 8. Actin, vinculin, and composite immunofluorescent images (400 ×) of hFOB cultured for 3 and 24 h on hydrophilic substratum (PTQ = plasma-treated quartz, TCPS = tissue-culture grade polystyrene), and hydrophobic surfaces (STQ = silane-treated quartz).

more evident. hFOB on PTQ and TCPS displayed a well-spread and interconnected morphology with well-developed actin stress fibers and vinculin plaques, whereas cells on STQ became more spindle-like shape with less-developed actin and vinculin structures. Perhaps, the most pronounced effect was co-localization of actin fiber ends and vinculin adhesion structures on TCPS and PTQ that were conspicuously absent in hFOB culture on STQ. In one sense, these results are not surprising because it is well known that cell adhesion and spreading is accomplished by significant changes in cytoskeleton and maturation of adhesion plaques. However, there are relatively few studies that compare gross morphology to cytoskeletal changes over time on substrata with varying surface energy. In fact, reports by Lim et al. are to our knowledge the only comprehensive studies for hFOB in the literature at this writing.

3.3. Integrin and extracellular matrix protein expression by hFOB on different surfaces

Lim et al. [61] compared integrin (α_2, α_3, α_4, α_5, α_v, β_1, β_3) and vinculin protein expression by hFOB cultured on hydrophilic and hydrophobic surfaces (PTQ/STQ and PTG/STG: hydrophilic/hydrophobic contrast) for 3 and 6 days. Steady-state levels of osteopontin (OP) and type I collagen (Col I) mRNA were also quantified, providing a sense of ECM protein production. In brief summary, Lim found that hFOB cultured on hydrophobic surfaces expressed significantly lower levels of α_v and β_3 subunits than on hydrophilic surfaces and that this difference decreased with time in culture. These results are generally consistent with expectations outlined in the previous section, including the proposed time–cell–substratum–compatibility–superposition principle.

To amplify on these trends relative to TCPS as reference surface, Lim's quantitative data have been normalized to TCPS and reported in Table 1 in the form of a simple +/−/0 rating emphasizing significant trends ((+) = higher than TCPS, (−) = lower than TCPS, (0) = not different than TCPS). Inspection of Table 1 reveals that the most significant differences from hFOB behavior on TCPS occurred by day 3 ($p<0.01$) at which time integrin α_v expression on STG and STQ was significantly lower and OP mRNA levels on STQ were significantly higher. By day 6, however, integrin α_v and OP expression was only slightly different on STQ ($p<0.05$) and were not different on STG. β_3 was slightly different on STQ than TCPS on both day 3 and 6 at the $p<0.05$ level. Vinculin was down-regulated at STQ on day 3 but recovered by day 6. The other integrin subunits (α_2, α_3, α_4, α_5, and β_1) and Col I were not significantly different on glass or quartz relative to TCPS. Integrin and ECM protein expression data correlated with SEM and other morphological analyses presented in the preceding section, confirming that hFOB had substantially, but not fully, recovered from poorly cytocompatible hydrophobic surface characteristics within 6 days. In particular, we note that a significant down-regulation of

Table 1
Integrin, vinculin, osteopontin, and type I collagen expression in hFOB on different glass and quartz surfaces (relative to TCPS)

Factors	PTG		PTQ		STG		STQ	
	3 days	6 days	3 days	6 days	3 days	6 days	3 days	6 days
α_2	0	0	0	0	0	0	0	0
α_3	0	0	0	0	0	0	0	0
α_4	0	0	0	0	0	0	0	0
α_5	0	0	0	0	0	0	0	0
α_v	− (*)	0	0	0	−− (**)	0	−− (**)	− (*)
β_1	0	0	0	0	0	0	0	0
β_3	0	0	0	− (*)	0	0	− (*)	− (*)
Vin	0	0	0	0	0	0	− (*)	0
OP	− (*)	0	0	+ (*)	0	0	+ + (**)	+ (*)
Col I	0	0	0	0	0	0	0	0

Notes: Vin = vinculin; OP = osteopontin; Col I = type I collagen; (0) = not significantly different than TCPS; (−) = significantly lower than TCPS; (+) = significantly higher than TCPS; (−−) = much lower than TCPS; (+ +) = much higher than TCPS; 0/−, 0/+ = modestly lower or higher. *$p<0.05$; **$p<0.01$, respectively. Integrin and Vin was measured by immunoblotting. OP and Col I measured by RT PCR.

α_v integrin (which was uncorrelated with β_3) and up-regulation of OP correlated with retention of spindle-shaped cell morphology on hydrophobic surfaces as compared to on hydrophilic counterparts.

Stepping back from these details momentarily (which are already highly simplified relative to Lim's quantitative analysis), Table 1 suggests that hFOB discrimination between hydrophobic (STG and STQ) and hydrophilic surfaces (PTG and PTQ) was substantially over within 3 days if TCPS is used as the standard of reference. Nearly all of the entries are null or only slightly different in a statistical sense. By day 3, and certainly by day 6, hFOB on both hydrophobic and hydrophilic surfaces were confluent with no difference in Col I synthesis among surfaces. Based on the speculation of Section 2.4, it is reasonable to suggest that analysis at earlier culture intervals would be required to sense differences in cell–substratum–compatibility hFOB experienced on the surfaces, at least for the factors listed in Table 1. In other words, effects of the life and death struggle to populate poorly compatible hydrophobic surfaces were all but erased within 3 days of cell–surface contact during which time hFOB substantially remodeled STG and STQ surfaces.

3.4. Long-term viability of hFOB in culture

The primary focus of this review has been the phenotypic progression of hFOB on different substrata over relatively short culture intervals. However, growth of isolated osteoblasts into a mature osteogenic-cell monolayer that significantly mineralizes the surrounding matrix is a slow process, at least for hFOB that generally requires a week or more of continuous culture to accrue significant production of mineral nodules. Also, for the purpose of complete cell–substratum–compatibility testing of orthopedic biomaterials *in vitro*, it may be very desirable to culture osteoblasts in contact with candidate materials for extended periods measured in weeks or months, not days.

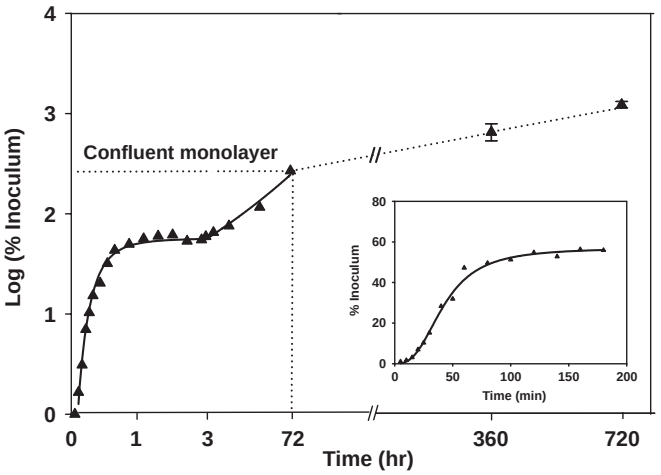

Fig. 9. Short- and long-term growth dynamics of hFOB on tissue-culture grade polystyrene (TCPS) spanning 30 days in continuous culture without subculture. Inset expands short-term attachment rates using a linear ordinate.

Thus, it is of interest to end this review with a brief examination of the viability of hFOB in long-term culture.

Dhurjati et al. [112] recently compared hFOB culture in TCPS for up to 30 days to that obtained in a specialized bioreactor. TCPS cultures were maintained with medium exchanges every 2 days but without subculture. The bioreactor design was based on the 'simultaneous growth and dialysis' method pioneered by Rose in the early 1960s [113,114] and avoided both subculture and periodic media exchanges, so that the pericellular environment was extremely stable within the bioreactor. Fig. 9 quantifies cell attachment, proliferation, and post-confluent population expansion phases (inset expands time axis and expresses % inoculum on a linear axis; compare to Fig. 2). Table 2 compares 15- and 30-day culture characteristics, including alizarin red staining that suggests cultures were mineralizing (although no mineral nodules were evident by

Table 2
Long-term hFOB cell growth in tissue-culture grade Polystyrene (TCPS)

Culture time	15 days	30 days
Alkaline phosphatase activity (nmol/mg pr./min)	4.39±0.26	4.47±0.38
Alizarin red (μmol)	2.89±0.04	3.03±0.02

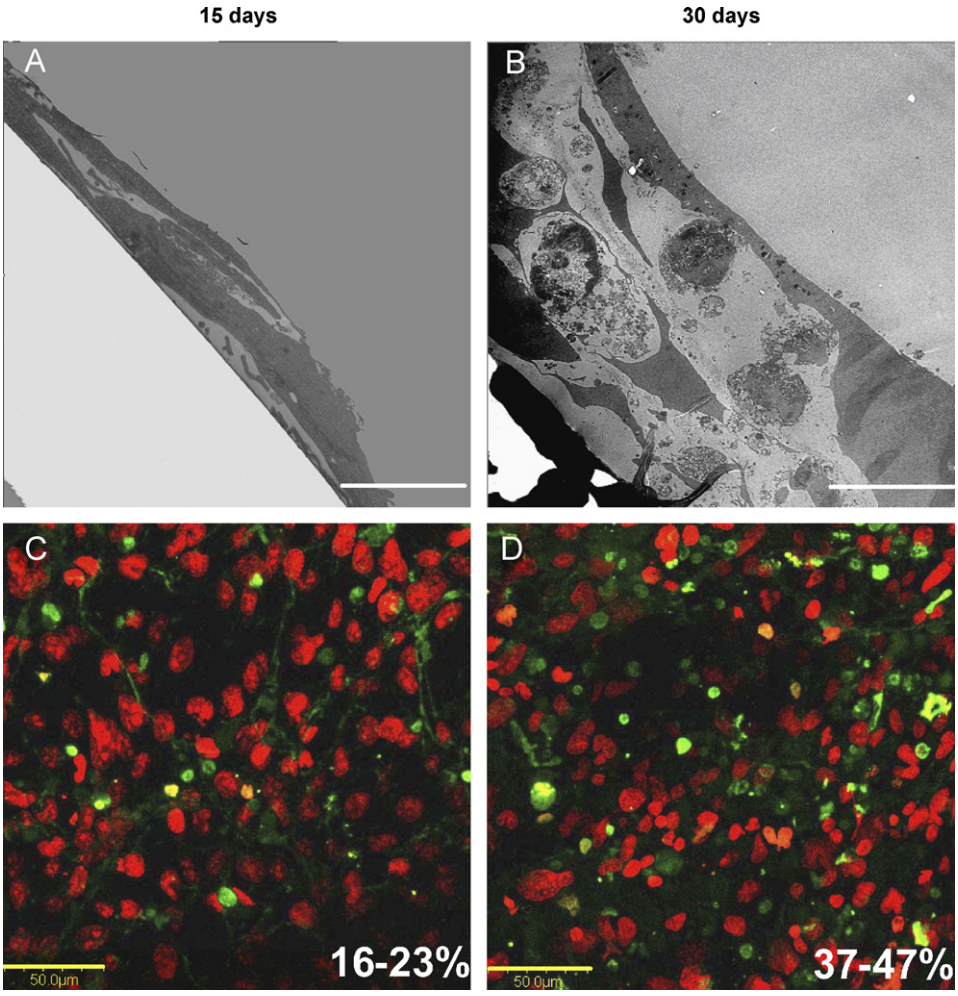

Fig. 10. Variation in long-term hFOB morphology on tissue-culture grade polystyrene (TCPS) assessed by cross-sectional TEM (Panels A: scale bar = 5 μm; B: scale bar = 10 μm) showing formation of multiple cell layers. Note that apoptotic bodies were clearly evident after 30 days of culture. Apoptotic cells (green) among normal cells (red, Sytox Orange) visualized using confocal microscopy confirm an increase in apoptosis with culture age (Panels C, D: Scale bar = 50 μm). Percent apoptotic bodies noted in lower right of Panels C, D were estimated by image analysis (see Ref. [112] for experimental details).

SEM and von Kossa staining was negative). Somewhat surprisingly, TCPS cultures remained robust in appearance until about 30 days when cell rounding and debris formation indicated viability issues. TEM and apoptosis assays (see Fig. 10) confirmed loss of culture integrity. Evidently, hFOB cannot be maintained in standard TCPS without subculture for longer than about 30 days. By contrast, Dhurjati reports indefinite culture intervals longer than 4 months (10 months for MC3T3-E1 in unpublished work), suggesting that long-term maintenance of an osteogenic tissue is possible in a relatively simple bioreactor setup.

4. Concluding remarks

Time-dependent phenotypic response of a model osteoblast (hFOB 1.19, ATCC, CRL-11372) to substrata with varying surface chemistry and topography has been reviewed in the context of cell-adhesion theory. The general sequence of events—contact, attachment, spreading, and proliferation—appears to be very similar among all surfaces, independent of surface chemistry. However, this sequence of events is delayed and attenuated on poorly cytocompatible hydrophobic substrata. Poorly cytocompatible surfaces exhibit characteristically low attachment

efficiency and long induction periods during which cells are apparently engaged in a life-or-death struggle to improve the pericellular environment by excretion of matrix proteins. A kind of time–cell–substratum–compatibility–superposition principle seems to be in play here in which similar bioadhesive outcomes can be ultimately achieved on all surfaces, but the time required to arrive at this outcome increases with decreasing cell–substratum–compatibility.

Modern genomic and proteomic tools offer unprecedented opportunity to directly measure changes in the cellular machinery that lead to the observed cell response to different materials. This information is key to bridging the gap between a purely physical–chemical and a purely biological understanding of cell adhesion in a way that promises to yield structure–property relationships so critical to the prospective engineering of biomaterials. For this purpose, timing is critical. Genomic/proteomic tools must be used during a stage of cell adhesion when cell–surface interactions most profoundly affect cell physiology. Applied too early, little information will be gained because cells have not yet sensed the interfacial environment in which they find themselves immersed. Applied too late, little information will be gained because cells have had time to remodel the pericellular environment. We intuit from the information reviewed in this paper that the most sensitive stage of cell adhesion for application of genomic/proteomic tools is within spreading and proliferation phases. Thus, the implication for cell-adhesion research is that genomic and proteomic tools should be applied early in the adhesion/spreading process before cells have an opportunity to significantly remodel the cell–substratum interface, effectively erasing cause and effect relationships between cell–substratum–compatibility and substratum properties.

Acknowledgments

This work was supported, in part, by a grant from the Pennsylvania Department of Health. The Pennsylvania Department of Health specifically disclaims responsibility for any analyses, interpretations, or conclusions. This work was also supported by The Pennsylvania State Tobacco Settlement Formula Fund, National Institutes of Health Grant AG13087-10, US Army Medical Research and Materials Command Breast Cancer Research Program WX81XWH-06-10432, and the Susan G. Komen Breast Cancer Foundation BCTR 0601944. Authors appreciate additional support from the Huck Institutes of Life Sciences, Materials Research Institute, and Departments of Bioengineering and Materials Science and Engineering of the Pennsylvania State University.

References

[1] Baxter LC, Frauchiger V, Textor M, Gwynn Ia, Richards RG. Fibroblast and osteoblast adhesion and morphology on calcium phosphate surfaces. Eur Cells Mater 2002;4:1–17.

[2] Grinnell F. Cellular Adhesiveness and extracellular substrata. In: Bourne GH, Danielli JF, Jeon KW, editors. International review of cytology. New York: Academic Press; 1978. p. 67–145.

[3] Altankov G, Grinnell F, Groth T. Studies on the biocompatibility of materials: fibroblast reorganization of substratum-bound fibronectin on surfaces varying in wettability. J Biomed Mater Res 1996;30:385–91.

[4] Pethica BA. The physical chemistry of cell adhesion. Exp Cell Res Suppl 1961(8):123–40.

[5] Rutter PR. The physical chemistry of the adhesion of bacteria and other cells. In: Curtis ASG, Pitts JD, editors. Cell adhesion and motility. London: Cambridge University Press; 1980. p. 103–35.

[6] Bongrand P, Capo C, Depieds R. Physics of cell adhesion. Prog Surf Sci 1982;12:217–35.

[7] Pethica BA. Microbial and cell adhesion. In: Berkeley RCW, Lynch JM, Melling J, Rutter PR, Vincent B, editors. Microbial adhesion to surfaces. London: Ellis Horwood Limited; 1983. p. 19–45.

[8] Bell G, Dembo M, Bongrand P. Cell adhesion: competition between nonspecific repulsion and specific bonding. Biophys J 1984;45:1051–64.

[9] Barngrover D. Substrata for anchorage-dependent cells. In: Thilly WG, editor. Mammalian cell technology. Boston: Butterworths; 1986. p. 131–49.

[10] Horbett TA, Klumb LA. Cell culturing: surface aspects and considerations. In: Brash JL, Wojciechowski PW, editors. Interfacial phenomena and bioproducts. New York: Marcel Dekker; 1996. p. 351–445.

[11] Hammer DA, Tirrell M. Biological adhesion at interfaces. Ann Rev Mater Sci 1996;26:651–91.

[12] Adao MH, Fernandes AC, Saramago B, Cazabat AM. Influence of preparation method on the surface topography and wetting properties of polystyrene films. Colloids Surf A: Physicochem Eng Aspects 1998;132:181–92.

[13] Dillow AK, Tirrell M. Targeted cellular adhesion at biomaterial interfaces. Curr Opinion Solid State Mater Sci 1998;3:252–9.

[14] Donahue HJ, Siedlecki CA, Vogler E. Osteoblastic and osteocytic biology and bone tissue engineering. In: Hollinger JO, Einhorn TA, Doll B, Sfeir C, editors. Bone tissue engineering. Boca Raton: CRC Press; 2004. p. 44–54.

[15] Hench LL. Biomaterials: a forecast for the future. Biomaterials 1998;19:1419–23.

[16] Delmas PD, Anderson M. Launch of the bone and joint decade: 2000–2010. Osteoporosis Int 2000;11:95–7.

[17] Praemer A, Rice DF. Musculoskeletal conditions in the United States. Am Acad Orthopeadic Surg 1999.

[18] Piehler HP. The future of medicine: biomaterials. MRS Bull 2000(August):67–70.

[19] Kiberstis P, Smith O, Norman C. Bone Health in the balance. Science. 2000 September 1, 2000; 289(5484): 1497.

[20] Rodan GA, Martin TJ. Therapeutic approaches to bone diseases. Science. 2000 September 1, 2000; 289(5484): 1508–14.

[21] Service RF. Tissue engineers build new bone. Science. 2000 September 1, 2000; 289(5484): 1498–500.

[22] Keeting PE, Scott RE, Colvard DS, Anderson MA, Outsler MJ, Spelsberg TC, et al. Development and characterization of a rapidly proliferating, well-differentiated cell line derived from normal adult human osteoblast-like cells transfected with SV40 large T antigen. J Bone Miner Res 1992;7(2):127–36.

[23] Clover J, Gowen M. Are MG63 and HOS TE85 human osteosarcoma cell lines representative models of the osteoblastic phenotype? Bone 1994;15:585–91.

[24] Harris SA, Enger RJ, Riggs BL, Spelsberg TC. Development and characterization of a conditionally immortalized human fetal osteoblastic cell line. J Bone Miner Res 1995;10:178–86.

[25] Subramaniam M, Jalal SM, Rickard DJ, Harris SA, Bolander ME, Spelsberg TC. Further characterization of human fetal osteoblastic hFOB 1.19 and hFOB/ERa cells: bone formation in vivo and karyotype analysis using multicolor fluorescent in situ hybridization. J Cell Biochem 2002;87:9–15.

[26] Mudd S, Mudd EBH. Certain interfacial tension relations and the behavior of bacteria in films. J Exp Med 1924;40:647–60.
[27] Mudd S, Mudd E. The penetration of bacteria through capillary spaces: IV. A kinetic mechanism in interfaces. J Exp Med 1924;40: 633–45.
[28] Gerson DF. Interfacial free energies of cells and polymers in aqueous media. In: Mittal KL, editor. Int Symp Physicochem Aspects Polym Surf. New York: Plenum Press; 1981. p. 229–40.
[29] Torney DC, Dembo M, Bell GI. Thermodynamics of cell adhesion II. Freely mobile repellers. Biophys J 1986;49:501–7.
[30] Facchini PJ, Neumann AW, DiCosmo F. Thermodynamic aspects of cell adhesion to polymer surfaces. Appl Microbiol Biotechnol 1988;29:346–55.
[31] Vogler EA. Thermodynamics of short-term cell adhesion in vitro. Biophys J 1988;53:759–69.
[32] Norde W, Lyklema J. Protein adsorption and bacterial adhesion to solid surfaces: a colloid-chemical approach. Colloids Surf 1989;38: 1–13.
[33] Vogler EA. A thermodynamic model of short-term cell adhesion in vitro. Colloids Surf 1989;42:233–54.
[34] Rappaport C. Some aspects of the growth of mammalian cells on glass surfaces. In: Hair ML, editor. The chemistry of biosurfaces. New York: Marcel Dekker, Inc.; 1972. p. 449–87.
[35] Matsuda T, Litt MH. Modification and characterization of polystyrene surfaces used in cell culture. J Polym Sci 1974;12:489–97.
[36] Klemperer HG, Knox P. Attachment and growth of BHK cells and liver cells on polystyrene: effect of surface groups introduced by treatment with chromic acid. Lab Pract 1977;26:179–80.
[37] Benedict RW, Williams MC. Bonding erythrocytes to plastic substrates by glow-discharge activation. Biomat, Med, Art Org 1979;7(4):477–93.
[38] Vogler EA. Interfacial chemistry in biomaterials science. In: Berg J, editor. Wettability. New York: Marcel Dekker; 1993. p. 184–250.
[39] Curtis ASG. Adhesion of cells to polystyrene surfaces. J Cell Bio 1983;97:1500–6.
[40] Ramsey WS, Hertl W, Nowlan ED, Binkowski NJ. Surface treatments and cell attachment. In Vitro 1984;20(10):802–8.
[41] Curtis A, Wilkinson C. Ambiguities in the evidence about cell adhesion problems with activation events and with the structure of the cell-contact. Studia Biophys 1988;127(1–3):75–82.
[42] Owens NF, Gingell D, Trommler A. Cell adhesion to hydroxyl groups of a monolayer film. J Cell Sci 1988;91:269–79.
[43] Margel S, Vogler EA, Firment L, Watt T, Haynie S, Sogah DY. Peptide, protein, and cellular interactions with self-assembled monolayer model surfaces. J Biomed Mater Res 1993;27:1463–76.
[44] Vogler EA. On the biomedical relevance of surface spectroscopy. J Electron Spectrosc Relat Phenom 1996;81:237–47.
[45] Vogler EA, Bussian RW. Short-term cell-attachment rates: a surface sensitive test of cell-substrate compatibility. J Biomed Mater Res 1987;21:1197–211.
[46] Vogler EA. Structure and reactivity of water at biomaterial surfaces. Adv Colloid Interf Sci 1998;74(1-3):69–117.
[47] Vogler EA. Water and the acute biological response to surfaces. J Biomater Sci Polym Ed 1999;10(10):1015–45.
[48] Vogler EA. How water wets biomaterials. In: Morra M, editor. Water in biomaterials surface science. New York: Wiley; 2001. p. 269–90.
[49] Duguid JP. Fimbriae and adhesive properties in *Klebsiella* strains. J Gen Microbiol 1959;21:271–86.
[50] Duguid JP, Old DC. Adhesive properties of Enterobacteriaceae. In: Beachey EH, editor. Bacterial adherence. London: Chapman and Hall; 1980. p. 185–217.
[51] Beachey EH. Bacterial adherence: adhesin–receptor interactions mediating the attachment of bacteria to mucosal surfaces. J Infect Dis 1981;143(3):325–45.
[52] Andrade JD. Principles of protein adsorption. In: Andrade JD, editor. Surf Interf Aspects Biomed Polym: Protein Adsorption. New York: Plenum Press; 1985. p. 1–80.
[53] Ramsden JJ. Puzzles and paradoxes in protein adsorption. Chem Soc Rev 1995;24:73–8.
[54] Weiss L. The adhesion of cells. In: Bourne GH, Danielli JF, editors. International review of cytology. New York: Academic Press Inc.; 1960. p. 187–225.
[55] Grinnell F. The serum dependence of baby hamster kidney cell attachment to a substratum. Exp Cell Res 1976;97:265–74.
[56] Yamada KM, Kennedy DW. Dualistic nature of adhesive protein function: fibronectin and its biologically active peptide fragments can autoinhibit fibronectin function. Cell Biol 1984;99:29–36.
[57] Andrade JD, Hlady V. Protein adsorption and materials biocompatibility: a tutorial review and suggested mechanisms. Adv Polym Sci 1986;79:3–63.
[58] Lee JH, Khang G, Lee JW, Lee HB. Platelet adhesion onto chargeable functional group gradient surfaces. J Biomed Mater Res 1998;40:180–6.
[59] Teare DOH, Emmison N, Ton-That C, Bradley RH. Effects of serum on the kinetics of CHO attachment ot Ultravioliet–ozone modified polystyrene surfaces. J Colloid Interf Sci 2001;234: 84–9.
[60] Lim JY, Liu X, Vogler EA, Donahue HJ. Systematic variation in osteoblast adhesion and phenotype with substratum surface characteristics. J Biomed Mater Res 2004;68A:504–12.
[61] Lim JY, Taylor AF, Li Z, Vogler EA, Donahue HJ. Integrin expression and osteopontin regulation in human fetal osteoblastic cells mediated by substratum surface characteristics. Tissue Eng 2005;11(1–2):19–29.
[62] Marmur A, Gill WN, Ruckenstein E. Kinetics of cell deposition under the action of an external field. Bull Math Biol 1976;38:713–21.
[63] Ruckenstein E, Marmur A, Gill WN. Coverage dependent rate of cell deposition. J Theor Biol 1976;58:439–54.
[64] Ruckenstein E, Marmur A, Radower SR. Sedimentation and adhesion of platelets onto a horizontal glass surface. Thrombos Haemostas 1976;36:334–42.
[65] Srinivasan R, Ruckenstein E. Kinetically caused saturation in the deposition of particles or cells. J Colloid Interf Sci 1981;79(2): 390–8.
[66] Ruckenstein E, Srinivasan R. Comments on cell adhesion to biomaterial surfaces: the origin of saturation in platelet deposition—is it kinetic or thermodynamic. J Biomed Mater Res 1982; 16:169–72.
[67] Smith U, Ryan JW. Electron microscopy of endothelial cells collected on cellulose acetate paper. Tissue Cell 1973;5(2):333–6.
[68] Manduca P, Sanguineti C, Pistone M, Boccignone E, Sanguineti F, Santolini F, et al. Differential expression of alkaline phosphatase in clones of human osteoblast-like cells. J Bone Miner Res 1993; 8(3):219–300.
[69] Morais S, Dias N, Sousa JP, Fernandes MH, Carvalho GS. *In vitro* osteoblastic differentiation of human bone marrow cells in the presence of metal ions. J Biomed Mater Res 1999;44:176–90.
[70] Shah AK, Sinha RK, Hickok NJ, Tuan RS. High-resolution morphometric analysis of human osteoblastic cell adhesion on clinically relevant orthopedic alloys. Bone 1999;24:499–506.
[71] Salih V, Georgiou G, Knowles JC, Olsen I. Glass reinforced hydroxyapatite for hard tissue surgery—part II: *in vitro* evaluation of bone cell growth and function. Biomaterials 2001;22:2817–24.
[72] Cerroni L, Filocamo R, Fabbri M, Piconi C, Caropreso S, Condo SG. Growth of osteoblast-like cells on porous hydroxyapatite ceramics: an in vitro study. Biomol Eng 2002;19:119–24.
[73] Dettin M, Conconi MT, Gambaretto R, Pasquato A, Folin M, Bello CD, et al. Novel osteoblast-adhesive peptides for dental/orthopedic biomaterials. J Biomed Mater Res 2002;60:466–71.
[74] Hendrich C, Noth U, Stahl U, Merklein F, Rader CP, Schiitze N, et al. Testing of skeletal implant surfaces with human fetal osteoblasts. Clin Orthopedics Relat Res 2002;394:278–89.
[75] Sharefkin JB, Lather C, Smith M, Rich NM. Endothelial cell labeling with indium-111-oxine as a marker of cell attachment to bioprosthetic surfaces. J Biomed Mater Res 1983;17:345–57.

[76] Dee KC, Andersen TT, Bizios R. Design and function of novel osteoblast-adhesive peptide for chemical modification of biomaterials. J Biomed Mater Res 1998;40:371–7.
[77] Dalby MJ, Kayser MV, Bonfield W, Silvio LD. Initial attachment of osteoblasts to an optimised HAPEX topography. Biomaterials 2002;23:681–90.
[78] Salgado AJ, Figueiredo JE, Coutinho OP, Reis RL. Biological response to pre-mineralized starch based scaffolds for bone tissue engineering. J Mater Sci: Mater Med 2005;16:267–75.
[79] Ahmad M, Gawronski D, Blum J, Goldberg J, Gronowicz G. Differential response of human osteoblast-like cells to commercially pure (cp) titanium grades 1 and 4. J Biomed Mater Res 1999;46: 121–31.
[80] Wachem PBv, Beugeling T, Feijen J, Bantjes A, Detmers JP, Aken WGv. Interaction of cultured human endothelial cells with polymeric surfaces of different wettability. Biomaterials 1985;6: 403–8.
[81] Grinnell F. Concanavalin a increases the strength of baby hamster kidney cell attachment to substratum. J Cell Biol 1973;58:602–7.
[82] Sharefkin JB, Watkins MT. Methods for the measurement of cell attachment to bioprosthetic surfaces. In: Williams DF, editor. Techniques of biocompatibility testing. Boca Raton, FL: CRC Press, Inc.; 1986. p. 95–107.
[83] Webster TJ, Ergun C, Doremus RH, Siegel RW, Bizios R. Specific proteins mediate enhanced osteoblast adhesion on nanophase ceramics. J Biomed Mater Res 2000;51:475–83.
[84] Hunter A, Archer CW, Walker PS, Blunn GW. Attachment and proliferation of osteoblasts and fibroblasts on biomaterials for orthopaedic use. Biomaterials 1995;16:287–95.
[85] Ruan J-M, Grant HM. Biocompatibility evaluation *in vitro*. Part I: morphology expression and proliferation of human and rat osteoblasts on the biomaterials. J Cent South Univ Technol 2001; 8(1):1–8.
[86] Howlett CR, Evans MDM, Walsh WR, Johnson G, Steele JG. Mechanism of initial attachment of cells derived from human bone to commonly used prosthetic materials during cell culture. Biomaterials 1994;15(3):213–22.
[87] Krause A, Cowles EA, Gronowicz G. Integrin-mediated signaling in osteoblasts on titanium implant materials. J Biomed Mater Res 2000;52:738–47.
[88] Kim H-K, Jang J-W. Surface modification of implant materials and its effect on attachment and proliferation of bone cells. J Mater Sci: Mater Med 2004;15:825–30.
[89] Rea SM, Brooks RA, Schneider A, Best SM, Bonfield W. Osteoblast-like cell response to bioactive composites–surface–topography and composition effects. J Biomed Mater Res 2004;70B: 250–61.
[90] van der Valk P, van Pelt AWJ, Busscher HJ, de Jong HP, Wildevuur CRH, Arends J. Interaction of fibroblasts and polymer surfaces: relationship between surface free energy and fibroblast spreading. J Biomed Mater Res 1983;17:807–17.
[91] Lydon MJ, Minett TW, Tighe BJ. Cellular interactions with synthetic polymer surfaces in culture. Biomaterials 1985;396–402: 396–402.
[92] Takayama H, Tanigawa T, Takagi A, Hatada K. Polymers of methacrylate available for obtaining varieties of cell–substratum adhesivity. Biomed Res 1986;7(1):11–8.
[93] Gerson DF. Cell surface energy, contact angles and phase partition I. Lymphocytic cell lines in biphasic aqueous mixtures. Biochim Biophys Acta 1980;602:269–80.
[94] Corry WD, Defendi V. Centrifugal assessment of cell adhesion. J Biochem Biophys Meth 1981;4:29–38.
[95] Hertl W, Ramsey WS, Nowlan ED. Assessment of cell-substrate adhesion by a centrifugal method. In Vitro 1984;20(10):796–801.
[96] Crouch CF, Fowler HW, Spier RE. The adhesion of animal cells to surfaces: the measurement of critical surface shear stress permitting attachment or causing detachment. J Chem Technol Biotechnol 1985;35B:273–81.
[97] Lampin M, Warocquier-Clerout R, Legris C, Degrange M, Sigot-Luizard MF. Correlation between substratum roughness and wettability, cell adhesion and cell migration. J Biomed Mater Res 1997;36:99–108.
[98] Usson Y, Guignandon A, Laroche N, Lafage-Proust M-H, Vico L. Quantitation of cell-matrix adhesion using confocal image analysis of focal contact associated proteins and interference reflection microscopy. Cytometry 1997;28:298–304.
[99] van Kooten TG, Klein CL, Wagner M, Kirkpatrick CJ. Focal adhesion and assessment of cytotoxicity. J Biomed Mater Res 1999;46:33–43.
[100] Zamir E, Katz B-Z, Aota S-i, Yamada KM, Geiger B, Kam Z. Molecular diversity of cell-matrix adhesions. J Cell Sci 1999;112: 1655–69.
[101] Dalby MJ, Silvio LD, Harper EJ, Bonfield W. In vitro adhesion and biocompatibility of osteoblast-like cells to poly(methylmethacrylate) and poly(ethylmethacrylate) bone cements. J Mater Sci: Mater Med 2002;13:311–4.
[102] Kumari TV, Vasudev U, Kumar A, Menon B. Cell surface interactions in the study of biocompatibility. Trends Biomater Artif Organs 2002;15(2):37–41.
[103] Zerhouni E. The NIH Roadmap. Science 2003;302:63–702.
[104] Freitas Jr RA. What is nanomedicine? Nanomed: Nanotechnol, Biol, Med 2005;1:2–9.
[105] Hughes GA. Nanostructure-mediated drug delivery. Nanomed: Nanotechnol, Biol, Med 2005;1:22–30.
[106] Vogler EA. On the origins of water wetting terminology. In: Morra M, editor. Water in Biomaterials surface science. New York: Wiley; 2001. p. 150–82.
[107] Kruse PF, Patterson MK. Tissue culture: methods and applications. New York: Academic Press; 1973.
[108] Freshney RI. Culture of animal cells: a manual of basic technique. New York: Alan R. Liss, Inc.; 1983.
[109] Hao L, Lawrence J, Li L. Manipulation of the osteoblast response to a Ti-6Al-4V titanium alloy using a high power diode laser. Appl Surf Sci 2005;247:602–6.
[110] Lim JY, Hansen JC, Siedlecki CA, Hengstebeck RW, Cheng J, Winograd N, et al. Osteoblast adhesion on poly(L-lactic acid)/polystyrene demixed thin film blends: effect of nanotopography, surface chemistry, and wettability. Biomacromolecules 2005;6:3319–27.
[111] Lim JY, Hansen JC, Siedlecki CA, Runt J, Donahue HJ. Human foetal osteoblastic cell response to polymer-demixed nanotopographic interfaces. J R Soc Interface 2005;2:97–108.
[112] Dhurjati R, Liu X, Gay CV, Mastro AM, Vogler EA. Extended-term culture of bone cells in a compartmentalized bioreactor. Tissue Eng 2006;12:3045–54.
[113] Rose GG. Cytopathophysiology of tissue cultures growing under cellophane membranes. In: Richter GW, Epstein MA, editors. Int Rev Exp Pathol. New York: Academic Press; 1966. p. 111–78.
[114] Rose GG, Pomerat CM, Shindler TO, Trunnell JB. A cellophane-strip technique for culturing tissue in multipurpose culture chambers. J Cell Biol 1958;4(6):761–4.

Clin Exp Metastasis
DOI 10.1007/s10585-008-9185-z

RESEARCH PAPER

Metastatic breast cancer cells colonize and degrade three-dimensional osteoblastic tissue in vitro

Ravi Dhurjati · Venkatesh Krishnan · Laurie A. Shuman · Andrea M. Mastro · Erwin A. Vogler

Received: 20 March 2008 / Accepted: 20 May 2008

Abstract Metastatic breast cancer cells (BCs) colonize a mineralized three-dimensional (3D) osteoblastic tissue (OT) grown from isolated pre-osteoblasts for up to 5 months in a specialized bioreactor. Sequential stages of BC interaction with OT include BC adhesion, penetration, colony formation, and OT reorganization into "Indian files" paralleling BC colonies, heretofore observed only in authentic pathological cancer tissue. BCs permeabilize OT by degrading the extracellular collagenous matrix (ECM) in which the osteoblasts are embedded. OT maturity (characterized by culture age and cell phenotype) profoundly affects the patterns of BC colonization. BCs rapidly form colonies on immature OT (higher cell/ECM ratio, osteoblastic phenotype) but fail to completely penetrate OT. By contrast, BCs efficiently penetrate mature OT (lower cell/ECM ratio, osteocytic phenotype) and reorganize OT. BC colonization provokes a strong osteoblast inflammatory response marked by increased expression of the pro-inflammatory cytokine IL-6. Furthermore, BCs inhibit osteoblastic bone formation by down-regulating synthesis of collagen and osteocalcin. Results strongly suggest that breast cancer disrupts the process of osteoblastic bone formation, in addition to upregulating osteoclastic bone resorption as widely reported. These observations may help explain why administration of bisphosphonates to humans with osteolytic metastases slows lesion progression by inhibiting osteoclasts but does not bring about osteoblast-mediated healing.

Keywords Bone metastases · Breast cancer · Colonization · Inflammation · Invasion · Osteoblast · Three-dimensional cell culture model

Ravi Dhurjati and Venkatesh Krishnan contributed equally to this work.

This work is a contribution from the Osteobiology Research Group, The Pennsylvania State University.

R. Dhurjati · E. A. Vogler
Department of Materials Science and Engineering, The Pennsylvania State University, University Park, PA 16802, USA

V. Krishnan · L. A. Shuman · A. M. Mastro
Department of Biochemistry and Molecular Biology, The Pennsylvania State University, University Park, PA 16802, USA

E. A. Vogler
Materials Research Institute and the Huck Institutes of Life Sciences, The Pennsylvania State University, University Park, PA 16802, USA

E. A. Vogler (✉)
Department of Bioengineering, The Pennsylvania State University, University Park, PA 16802, USA
e-mail: eav3@psu.edu

Introduction

Skeleton is a favored site for the metastatic spread of breast, prostrate, lung, and multiple myeloma cancers [1]. Metastatic cancer in bone is particularly pernicious because, once bone colonization occurs, the cure rate is almost zero [1–3]. Cancers in bone progress with significant morbidity related to bone loss (lytic cancer) or gain (blastic cancer), hypercalcemia, pathological fractures, and spinal compression [3]. Specific aspects of cancer cell growth in bone such as dormancy [4, 5] contribute to a protracted disease progression with intervals of remission that can sometimes last up to decades [6]. Metastatic colonization of bone is the culmination of a sequence of steps beginning with migration of cancer cells to bone, survival and adaptation to the bone environment, proliferation to form micrometastases, and finally development of vascularized

tumors [7]. Successful progression through these different stages requires reciprocal interactions between cancer cells and the bone microenvironment [8]. Of the cancer cells that reach bone, only a small percentage of cells develop into clinically detectable tumors; the remaining either die, persist as solitary dormant cells, or develop into pre-angiogenic micrometastases that fail to develop into overt tumors [7, 9].

The specific cellular and molecular mechanisms responsible for the variable fate of cancer cells in bone are incompletely understood [7]. Investigations of metastasis suppressor genes [10] and cell trafficking studies using intravital videomicroscopy [11, 12] have revealed that early stage, pre-angiogenic interactions between the cancer cells and the bone environment are crucial regulators of cancer cell growth and disease progression. Evidence from these two independent lines of investigation suggest that early stages of metastatic colonization constitute a rate-limiting step in disease progression that can be an effective target for therapeutic intervention [13]. Consequently, a full appreciation of the mechanistic basis of metastatic colonization can greatly enhance discovery of drugs aimed at the arrest of cancer cell growth that will limit disease progression to a minimal residual, asymptomatic stage [14].

One difficulty encountered in drug development is that early stage detection of cancer cell colonization is difficult, both in the clinic and laboratory, because of the refractory nature of whole bone and lack of relevant in vitro models, respectively. Excised tissue [15] faithfully captures end stages of cancer in bone associated with fully-developed tumors, but the critical initial stages of disease remain largely inaccessible in this surrogate. Effective in vitro bone models must strike a balance between experimental efficiency and retention of biological complexity. In particular, the model must recapitulate the in vivo bone microenvironment to the greatest extent possible. Three-dimensional (3D) tissue models have become a focus of recent investigation for this reason [16]. Herein, we report use of a multiple-cell layer (3D) mineralizing osteoblastic tissue (OT) grown from isolated osteoblasts in a specialized bioreactor as an effective surrogate for studies of cancer colonization of bone. By challenging OT with metastatic breast cancer cells (BCs) known to invade the skeleton, important hallmarks of the metastatic process including cancer cell/tissue adhesion, tissue penetration, and ultimate degradation of the osteoblast-derived extracellular matrix were directly observed in vitro.

Materials and methods

Bioreactor design and implementation

Bioreactors based on the principle of simultaneous-growth-and-dialysis [17, 18] were implemented using a two-compartment bioreactor design described previously [19, 20]. One of the compartments was a cell growth chamber (5 ml total volume) that was separated from a 30-ml medium reservoir compartment by a dialysis-membrane (6–8 KDa cutoff). Cells were inoculated into the growth chamber in complete medium including serum. The reservoir was filled with basal medium consisting of nutrients such as glucose and amino acids but no proteins. The entire vessel was ventilated through transparent, gas-permeable but liquid-impermeable films that offered optimum cell adhesion and delivered requisite oxygen tension to the cells. The bioreactor was specifically designed to enable non-invasive, live-cell analysis with an inverted (phase-contrast, fluorescence, or confocal) microscope. Completely assembled units used in this work had a cell growth space of 25 cm^2 total area emulating a standard T25 flask. Bioreactors were sterilized by gamma radiation at the Breazeale Nuclear Reactor on the campus of The Pennsylvania State University.

During culture, cells were bathed in pH-equilibrated and oxygenated medium that continuously dialyzed from the medium reservoir. At the same time, metabolic waste products such as lactic acid dialyzed out of the growth compartment, maintaining low pericellular concentrations. The medium reservoir was periodically replenished to provide additional nutrients and remove accumulated waste products without disturbing the cell growth chamber. Serum constituents or macromolecules synthesized by cells with molecular weights in excess of the dialysis membrane cutoff (8–10 kDa) were retained and concentrated within the growth compartment. This simple-to-use bioreactor design was integrated into conventional tissue culture protocols. The system conferred an extraordinarily stable pericellular environment that improved cell recovery from "culture shock" [21], and resulted in development of OT with a normal phenotype over extended, uninterrupted culture intervals tested for as long as 10 months with no sign of necrosis [19, 20]. In the course of defining the experimental bioreactor system, we have cultured MC3T3-E1 for various times from 1 week to 10 months. Cocultures with BCs were carried out at three ratios of cancer cells to osteoblasts (1:10, 1:100, and 1:1,000). Tissue with up to 5 months maturity was utilized in this work. Data from other times of culture is shown as indicated for individual experiments.

Cells and cell culture

Murine calvarial pre-osteoblasts (MC3T3-E1) were a gift from Dr. Norman Karin at the Pacific Northwest National Laboratories (ATCC CRL-2593 presumptive equivalent). MC3T3-E1 were inoculated into the growth chamber of the bioreactors at a sub-confluent density (10^4 cells/cm^2) and

cultured in alpha minimum-essential medium (α-MEM) (Mediatech, Herdon, VA) supplemented with 10% neonatal FBS (Cansera, Roxdale, Ontario) and 100 U/ml penicillin and 100 μg/ml streptomycin (Sigma Aldrich, St. Louis, MO). The medium reservoir of the bioreactor was filled with α-MEM supplemented with 100 U/ml penicillin and 100 μg/ml streptomycin but no serum. Once the cells reached confluence, usually 4–5 days, the medium in the growth chamber was replaced with differentiation medium containing the additional ingredients of 50 μg/ml ascorbic acid and 10 mM β-glycerophosphate (Sigma Aldrich, St. Louis, MO). This change to differentiation medium was the only time during the course of the experiment that medium in the cell chamber was replaced. Subsequent medium changes involved only the basal medium within the medium reservoir that was refreshed every 30 days. Bioreactors were maintained in a water-jacketed 5% CO_2 incubator (Model 3110, Thermo Fisher Scientific, Waltham, MA) held at 37°C. In this way, MC3T3-E1 cultures have been maintained continuously in the bioreactor without subculture for extended intervals up to 10 months, generating a multiple-cell layer tissue with controllable age (maturity), herein referred to as OT.

Human metastatic BCs (MDA-MB-231, ATCC-HTB 26 presumptive equivalent) genetically engineered to produce green fluorescent protein (GFP), were a gift from Dr. Danny Welch, University of Alabama at Birmingham, and herein referred to as BCs. Derived from a pleural effusion [22], MDA-MB-231^{GFP} cells are known to invade the murine skeleton [23].

MDA-MB-231^{GFP} cells were cultured in standard tissue culture dishes in Dulbecco's Modified Eagle's Medium (DMEM) (Mediatech, Herdon, VA) containing 5% neonatal bovine serum and 100 U/ml penicillin and 100 μg/ml streptomycin for 3–4 days before coculture with bioreactor-derived OT.

Reverse transcription polymerase chain reaction

Relative quantitative PCR was performed on RNA isolated from MC3T3-E1 cells cultured in the bioreactor for various intervals (7, 22, 30 or 60 days) to determine expression levels of osteopontin, osteonectin, type I collagen, osteocalcin, MMP-13, E11, and β-actin. Total RNA was isolated from the cells using the RNeasy kit (Qiagen, Valencia, CA) with on-column DNase treatment. Five hundred nanograms of total RNA was reverse transcribed from an oligo dT primer using the RETROscript kit (Ambion, Austin, TX). Two microliters of the cDNA were used in PCR reactions that had been previously optimized by varying the cycle number to determine the linear range of amplification. PCR reactions for each of the proteins of interest were performed using the primer pairs, annealing temperatures and cycle numbers listed in Table 1. PCR products were separated by electrophoresis on a 2% agarose gel in Tris-borate EDTA buffer and stained with ethidium bromide. Gel documentation was performed on the Kodak Gel Logic 100 Imaging System (Eastman Kodak, Rochester, NY) and band volume quantitation was done by ImageQuant software (Molecular Dynamics, Sunnyvale, CA). Expression levels were normalized by determining the ratio of the band volume for each message relative to the band volume for β-actin for the same cDNA.

Bioreactor cocultures

BCs were inoculated into bioreactor cell growth chambers containing OT at maturities between 15 and 145 days of

Table 1 Primer sequences and experimental conditions for RT-PCR

Gene	Primers (F = Forward; R = Reverse)	Annealing temperature (°C)	Cycles	Amplicon size (bp)
Osteocalcin	F: 5′-CAA GTC CCA CAC AGC AGC TT-3′	55	23	370
	R: 5′-AAA GCC GAG CTG CCA GAG TT-3′			
Osteonectin	F: 5′-CTG CCT GCC TGT GCC GAG AGT TCC-3′	55	17	653
	R: 5′-CCA GCC TCC AGG CGC TTC TCA TTC-3′			
Type I collagen	F: 5′-TCT CCA CTC TTC TAG TTC CT-3′	55	16	269
	R: 5′-TTG GGT CAT TTC CAC ATG-3′			
MMP-13	F: 5′-GAT GAC CTG TCT GAG GAA G-3′	58	21	357
	R: 5′-ATC AGA CCA GAC CTT GAA G-3′			
E11	F: 5′-TCCAACGAGACCAAGATGTG-3′	60	24	539
	R: 5′-AGCTCTTTAGGGCGAGAACCT-3′			
Osteopontin	F: 5′-ACA CTT TCA CTC CAA TCG TCC-3′	58	16	240
	R: 5′-TGC CCT TTC CGT TGT TGT CC-3′			
β-Actin	F: 5′-CGT GGG CCG CCC TAG GCA-3′	62	20	242
	R: 5′-TTG GCC TTA GGG TTC AGG-3′			

culture at an estimated 1:10, 1:100, or 1:1,000 breast cancer-to-osteoblast cell ratio; corresponding to 10^5, 10^4, or 10^3 BCs/bioreactor, respectively. BC challenged bioreactors were monitored microscopically for 7 days. On day 7, bioreactors were dismantled and substratum film with adherent tissue was carefully cut into pieces for various assays, avoiding loss of OT that was conspicuously degraded by BC challenge. Medium from the cell growth space of the bioreactor was collected and used for various analyses. Tissue was fixed in 2.5% glutaraldehyde (in cacodylate buffer) and stained for actin filaments with Alexa Fluor 568 phalloidin stain (Invitrogen, Carlsbad, CA). Osteoblasts were optionally stained with Cell Tracker Orange™ (Invitrogen, Carlsbad, CA) for live in situ confocal imaging to monitor cell growth dynamics, prior to staining with actin stain.

Conditioned media experiments

BCs were grown to 90% confluency in standard tissue culture plates and growth medium was removed. Adherent BCs were rinsed with PBS and the original growth medium replaced with fresh α-MEM (20 ml in a T-150 flask, $\sim 1.3 \times 10^5$ cells/cm^2). Cultures were incubated for an additional 24 h, the medium collected and centrifuged ($300\times$ *g* for 10 min) to remove cellular debris resulting in "BC-conditioned medium". At desired OT maturity, medium in the growth chamber of the bioreactor was completely replaced with a mixture of 50% breast cancer conditioned medium and 50% differentiation medium as previously described [24]. Osteoblast tissue in the bioreactor was exposed to BC-conditioned medium for 2 weeks.

Confocal microscopy

In situ laser-scanning confocal microscopy of cocultures in the bioreactor was performed using Olympus FV-300 laser-scanning microscope (Olympus America Inc., Center Valley, PA). Sections were observed with a 40X Olympus UPlanF1 objective with an 0.85 numerical aperture. Cell Tracker Orange ™ was excited using a 543 nm line from a helium-neon laser and collected through a 565 nm long-pass filter. GFP was excited using a 488-nm argon laser and collected through 510 nm long-pass and 530 nm short-pass filters. A 570 nm dichroic long-pass filter was used to split the emission. Serial optical sections were taken at 1 μm intervals throughout the tissue. Confocal images were processed using image processing software (Fluoview 300, Version 4.3b, Olympus, Center Valley, PA). 3D optical reconstructions of 2D serial sections were obtained using AutoQuant, AutoDeblur and AutoVisualize software (Version 9.3, Media Cybernetics, Bethesda, MD). Number of cell layers within the tissue was determined visually by counting and by following the sub-volumes of cells in the 3D-reconstructed Z-stack images.

Biochemical and immunochemical assays

Soluble collagen (indicative of collagen synthesis) was quantified using Sircol Assay (Biocolor, Carrickfergus, UK). Prior to running the assay following manufacturer's protocol, the collagen was extracted/precipitated from cell culture supernatants by addition of 4 M NaCl. Supernatants were centrifuged and the resulting collagen pellet was re-suspended in 0.5 M acetic acid. Levels of osteocalcin and IL-6 secreted into the medium were quantified using multiplex ELISA kit (LINCOplex™ Mouse Bone Panel 2B, Millipore, Billerica, MA). Alkaline phosphatase activity was quantitated using the QuantiChrom™ Alkaline Phosphatase Assay Kit (DALP-250), BioAssay Systems, Hayward, CA according to manufacturers protocol. Briefly, cells were lysed in a solution of 100 mM glycine, 0.1% Triton-X 100, 1 mM $MgCl_2$, pH 10, and the lysate was added to 96-well plates coated with tartrazine standard working solution containing the pNPP substrate. The 96-well plate was gently tapped to mix all components, and immediately read at 405 nm. The plate was read again after 4 minutes at 405 nm and the optical densities from the two readings were used to calculate the alkaline phosphatase enzyme activity. Each sample was tested three times.

Results

Osteoblast tissue model

Murine MC3T3E-1 pre-osteoblasts maintained in the bioreactor developed into a 3D osteoblast tissue (OT, Panel A of Fig. 1) comprised of 6–8 layers of differentiated cells (Panels B, top layer; Panel C, bottom layer) that stained positive for alkaline phosphatase activity and for mineralization by von Kossa (not shown). Continuous culture in the bioreactor resulted in transformation of spindle shaped pre-osteoblasts (Fig. 2, Panel A) to cuboidal osteoblasts (Panel B) that secreted and mineralized an extensive, collagenous extracellular matrix (Panel C) that completely enveloped the cells (Panel D). Examination of numerous histological and ultra-structural (not shown), and confocal sections of tissue from bioreactor cultures at different times revealed reproducible and continuous transformation of tissue in which cells were initially closely packed (high cell/ECM ratio; Fig. 2 Panel A) to a more mature phenotype characterized by lower cell density (low cell/ECM ratio; Fig. 2 Panels C, D) with intercellular contacts maintained by a network of cellular processes [20]. Growth and maturation of OT in the bioreactor thus recapitulated

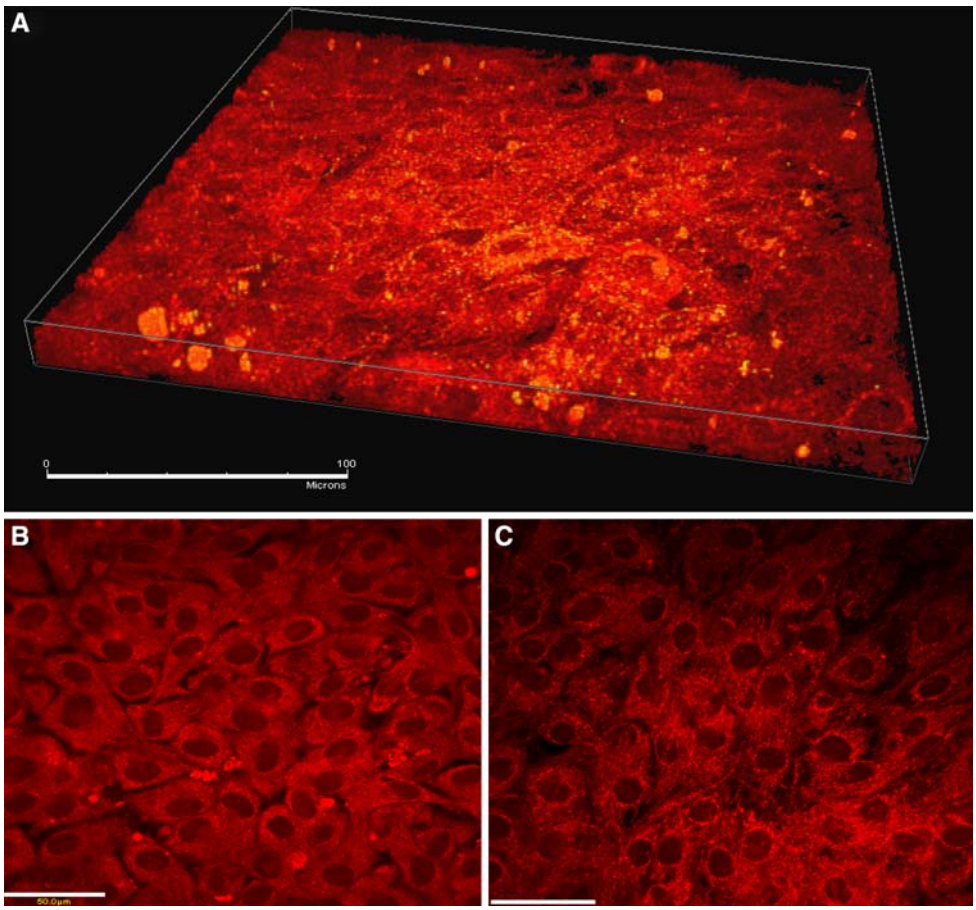

Fig. 1 Phalloidin-stained MC3T3-E1 osteoblast-derived tissue (OT) after 22 days of continuous culture in the bioreactor. MC3T3-E1 pre-osteoblasts grow into a 3D OT comprised of 6–8 cell layers enmeshed in a collagenous matrix (see also Figs. 2, 5). Panel A is a 3D reconstruction of serial confocal optical sections (magnification = 40×, scale bar = 100 μm). A morphological gradient in the tissue was evident wherein top layer of cells (Panel B) were conspicuously more cuboidal than bottom layer of cells (Panel C) which exhibited filamentous inter-cell connections reminiscent of osteocyte morphology

the normal sequence of bone development characterized by stages of proliferation, matrix maturation, and mineralization. This phenotypic progression was also reflected in the characteristic expression of genes such as Type I collagen, osteonectin, osteocalcin and osteopontin (Fig. 2, Panel E) [25]. Up-regulation of matrix-metallo protease (MMP)-13 (indicative of extracellular matrix remodeling) and the protein E11 (indicative of osteocytic transformation) occurred in mature cultures (Fig. 2, Panel E).

Breast cancer cell challenge to osteoblast tissue

Interaction of cancer cells with OT were followed by fluorescence microscopy after injecting MDA-MB-231^{GFP} human BCs directly onto 5-month OT stained with Cell Tracker Orange^{TM} to clearly differentiate osteoblasts from cancer cells. BCs adhered to OT (Fig. 3 Panel A) in the first 24 h. By the second day, the BC cells penetrated tissue (Panel B), apparently through the agency of cellular processes extended by BCs (see Fig. 3). Within 3 days of coculture, BCs proliferated and organized into lines of cells (Panels C). Close inspection of 2D optical sections (Fig. 4, Panel A, Day 3) and 3D reconstructions (Fig. 4, Panel D) revealed concomitant re-organization of OT. Before cancer cell challenge, osteoblasts exhibited a cuboidal morphology. Over 3 days of BC coculture, osteoblasts took on a definitively elongated appearance and aligned with cancer cells which also became spindle shaped. In particular, osteoblasts paralleled the BC cells, as though marshaled into an order that seemed to permeabilize OT structure. The BC alignment in the bioreactor was reminiscent of the classical "Indian filing" pattern that is one of the defining characteristics of breast cancer invasion [26–28].

Breast cancer cell conditioned medium effects on osteoblast tissue

Prior work determined that exposure of MC3T3-E1 cells to conditioned medium (CM) from MDA-MB-231 cells caused a change in osteoblast morphology and adherence to the substrate under standard tissue culture conditions [29]. In order to determine if this effect occurred with 3D OT, 16 day OT in the bioreactor was maintained in CM for 2 weeks (see Materials and methods). Exposure of OT to BC-conditioned medium induced significant cytoskeletal reorganization in response to factors secreted by BCs, as revealed by actin stress-fiber reorganization (Fig. 3, compare control Panel D to test Panel E). Control OT were

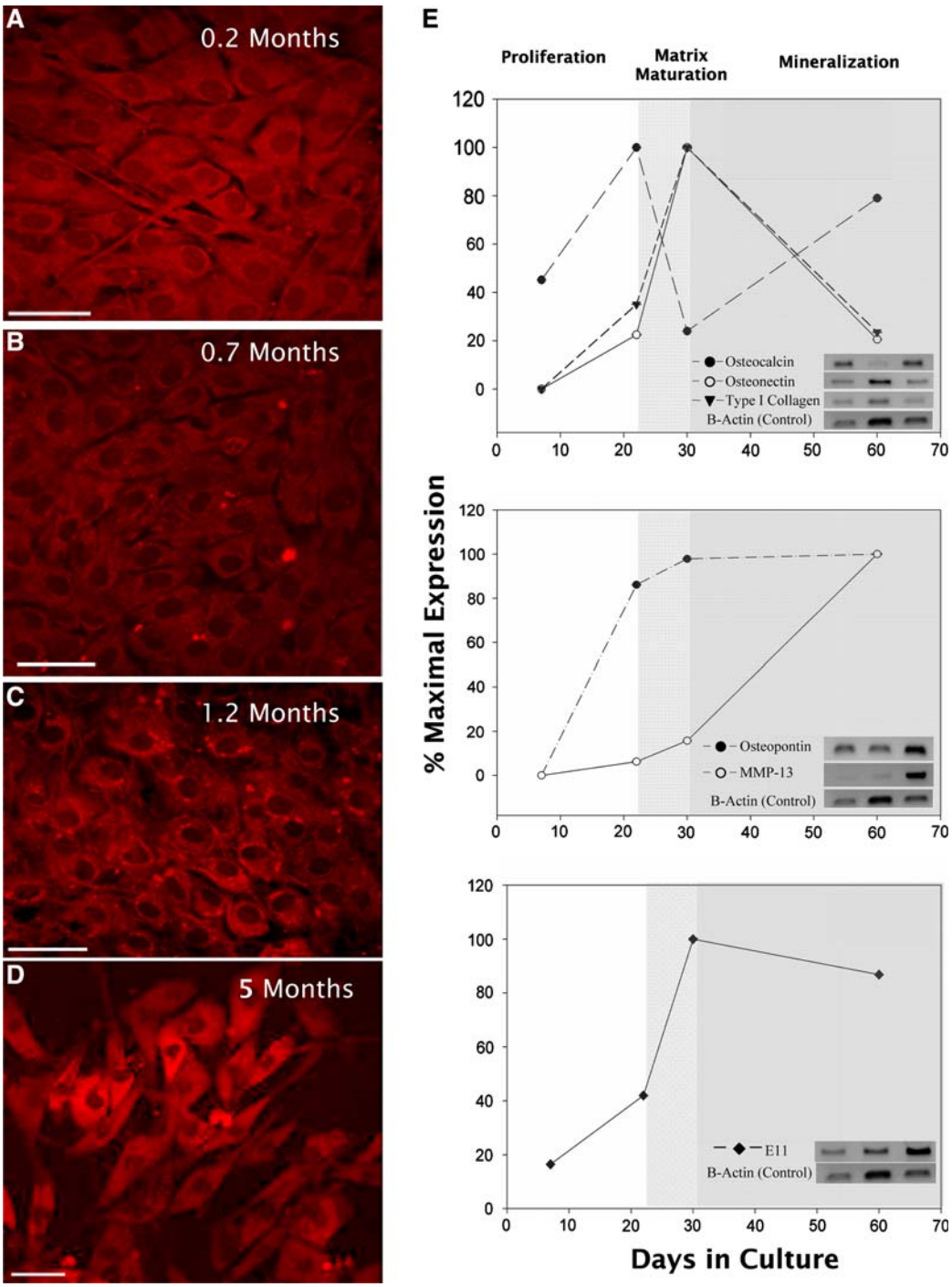

Fig. 2 Maturation of MC3T3-E1 derived OT within the bioreactor (see also Figs. 1, 5). Panels (A–D) are confocal images of actin-stained cells over several months of continuous culture (scale bar = 50 μm, annotations give culture age). Spindle shaped pre-osteoblasts (Panel A) progressively transformed into cuboidal osteoblasts (Panel B) that became enmeshed in a collagenous matrix (Panel C appearing black) that eventually buried cells exhibiting an osteocytic-like morphology (Panel D). Relative quantitative PCR was performed on RNA isolated from MC3T3-E1 cells cultured in the bioreactor for various intervals (7, 22, 30 or 60 days) to determine expression levels of osteopontin, osteonectin, type I collagen, osteocalcin, MMP-13, E11 and β-actin (Panel E). Insets show ethidium bromide stained bands for the genes indicated for 22, 30 and 60 days. The gene expression for the 7 day cultures was very faint, and is not shown. Samples from replicate bioreactors at days 22 and 30 were also tested with similar results. Expression levels were normalized by determining the ratio of the band volume for each message relative to the band volume for β-actin for the same cDNA. The data are expressed as percent of maximum expression following the work of Lian et al. [25]. Changes in gene expression were consistent with progression of the osteoblast phenotype through the stages of proliferation, matrix maturation and mineralization as indicated by the shaded vertical bars in Panel E. Two bioreactors were tested but data from only one of each age are shown

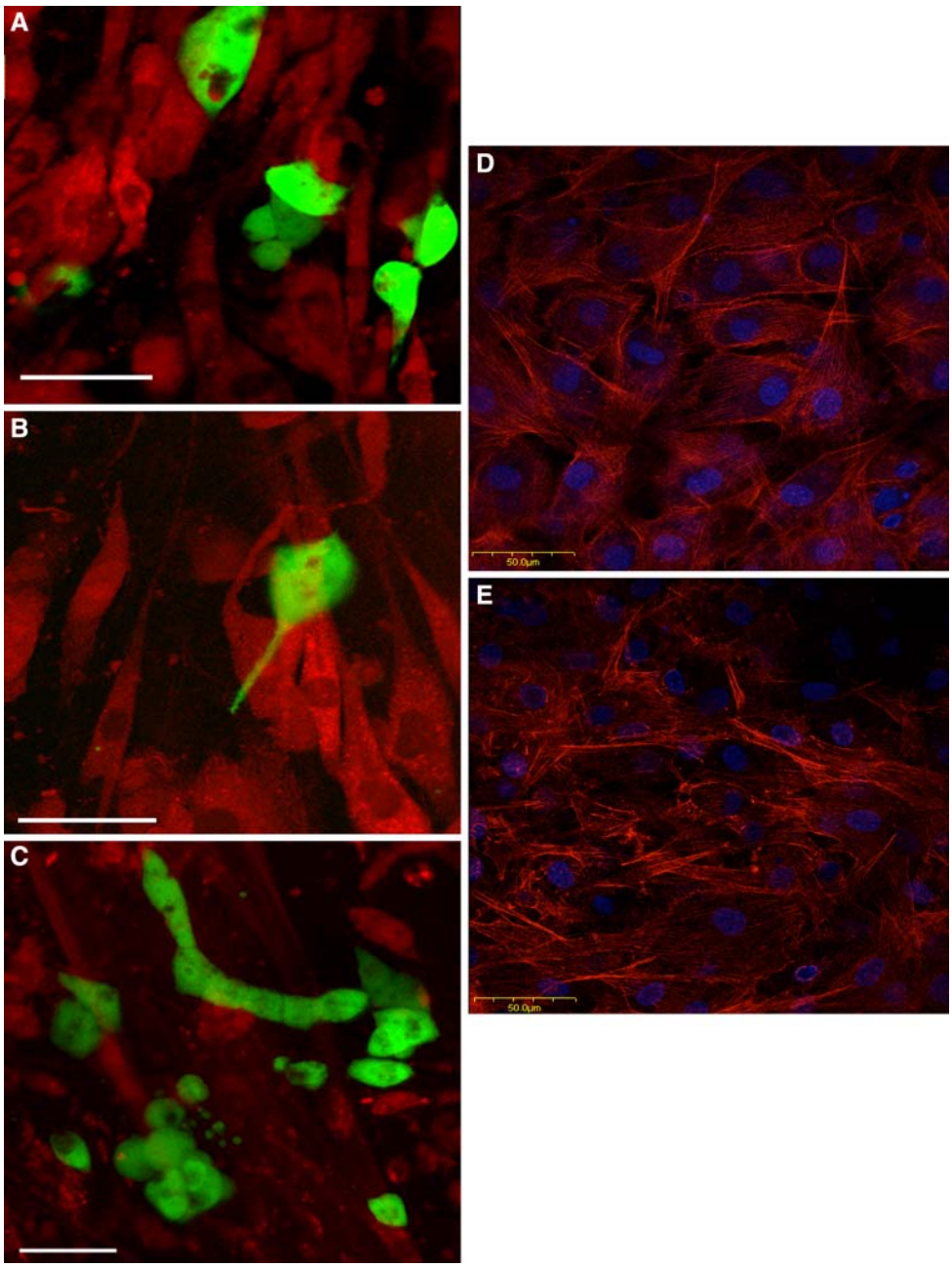

Fig. 3 MDA-MB-231^{GFP} breast cancer cell invasion of MC3T3-E1 derived OT grown for 5 months within the bioreactor. OT (stained with Cell Tracker Orange^{TM}) was cocultured with MDA-MB-231 breast cancer cells (BCs) genetically engineered to produce GFP. Confocal images (scale bar = 50 µm, magnification = 40×) were collected over 3 days (Panels A–C). These representative images are interpreted as stages of BC adhesion (Panel A, day one), penetration (Panel B, day two), and replication/ organization into characteristic filing patterns (Panel C, day three), respectively (see also Fig. 4). Phalloidin-stained OT grown for 16 days in the bioreactor (Panel D) was compared to similar tissue exposed to MDA-MB-231 conditioned medium for 2 weeks (Panel E, scale bar = 50 µm, magnification = 40×). Note that exposure to conditioned media disrupted actin fiber organization in OT. Draq5 (Biostatus, Shepshed, UK) stained nuclei (blue) reveal concomitant nuclear shrinkage. Breast cancer conditioned medium was prepared as reported previously [24]

characterized by smooth, long actin stress fibers (Panel D), whereas, F-actin stress fibers were clumped and punctate in OT exposed to conditioned medium (Panel E). These cytoskeletal changes correlated with the observation that OT from coculture experiments was consistently more fragile than OT not exposed to cancer cells. In fact, very careful processing was required to prevent wholesale cell sloughing during the wash steps involved in preparation of specimens for histology and electron microscopy. It was plainly evident from these latter observations that OT structure and adhesion to the bioreactor substratum film was significantly eroded by BC exposure. Details of BC interaction with OT were followed using the confocal microscopy study outlined in the legend to Fig. 4 and as detailed in the section Discussion.

Effect of osteoblast tissue maturity on breast cancer cell interactions

The interaction of BC cells with OT depended on the stage of OT maturity. As the OT matured, there was decrease in the number of cell layers with increasing culture time (Fig. 5, left-hand axis of graphic portion) that translated into a linear-like decrease in cell layer/tissue-thickness ratio (Fig. 5, right-hand axis). Qualitative aspects of BC interactions were correlated with OT characteristics (Fig. 5,

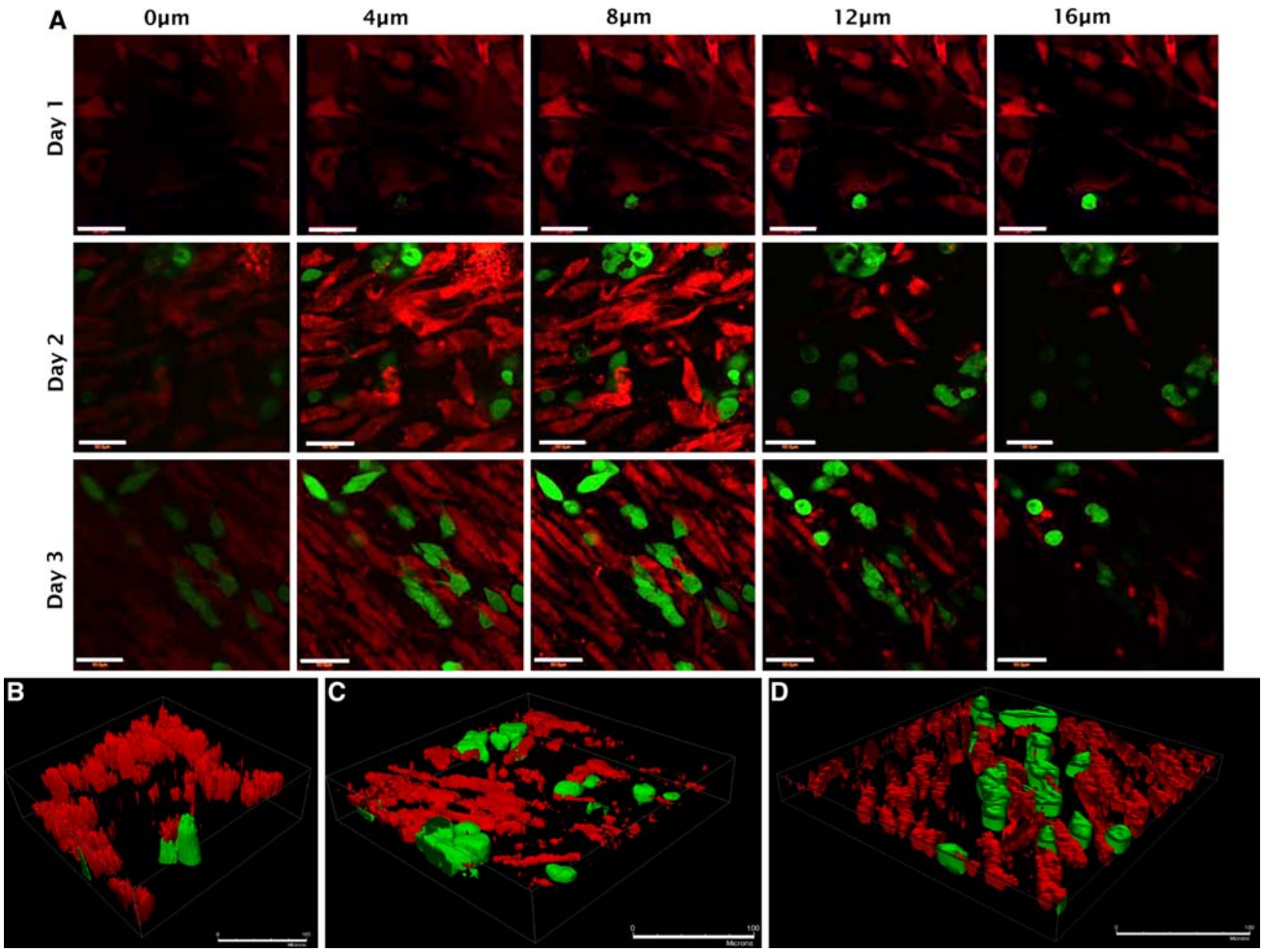

Fig. 4 MDA-MB-231 breast cancer cell (BC) invasion of MC3T3-E1 derived OT grown for 5 months the bioreactor (see also Figs. 1, 3). BCs were added to a 5 month OT culture as described as in the legend to Fig. 3. Optical sections (40×, scale bar = 50 μm) at various depths within OT at successive days in culture were collected by laser scanning confocal microscopy. It appeared that BCs fully penetrated OT only in a few locations within day 1 of coculture. Penetration increased over days 2 and 3. Linear-like organization of breast cancer cells and osteoblasts within the tissue was evident beginning at day 2 but more obvious at day 3. Optical reconstructions of serial sections over 3 days (Panels B–D respectively, 40×) revealed significant re-organization and permeablization of OT

table portion), suggesting that declining rates of BC colonization and increasing efficiency of tissue penetration, filing, and colony formation were related to OT maturity.

The effect of BCs on OT was further assessed by measuring the changes in levels of secreted factors representing primary osteoblast functions of extracellular matrix production (secreted collagen) and mineralization (osteocalcin). Introduction of BCs led to reduced production of new collagen (Fig. 6, Panel A) and to less secretion of osteocalcin (Fig. 6, Panel B) at all tested OT maturities. Alkaline phosphatase activity deceased as the cultures aged (Fig. 6, Panel C). This effect has been reported previously [30]. Nevertheless, at each time tested, the alkaline phosphatase in the presence of the cancer cells was less than in the OT alone. Furthermore, BCs stimulated increased production of IL-6, indicative of an inflammatory stress response (Fig. 6, Panel D) [24].

Discussion

Osteoblastic tissue model

A relatively simple bioreactor was used to grow a 3D OT from murine MC3T3E-1 pre-osteoblasts for culture periods up to 5 months. This extended culture interval allowed maturation of OT through successive stages of phenotypic development, up-to-and-including osteocyte-like cells. A morphologically stratified tissue developed within the first month of culture (Fig. 1; compare top layer Panel B to bottom layer Panel C). Over successive months of culture, cuboidal osteoblastic cells underwent continued morphological changes (Fig. 2) accompanied by characteristic expression of genes such as Type I collagen, osteonectin, osteocalcin and osteopontin; as well as up-regulation of

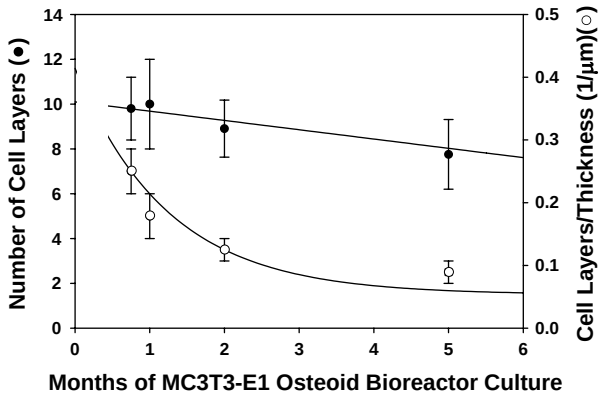

Experimental Parameter @ BC:OB=1:10	Months of Bioreactor Culture			
	0.75	1	2	5
BC Colonization	(+++)	(++)	(+)	(+)
Tissue Penetration	(-)	(+/-)	(+)	(+)
BC Filing	(-)	(+)	(++)	(++)
Tumor Formation	(-)	(+)	(++)	(++)

Fig. 5 Qualitative aspects of MDA-MB-231 metastatic breast cancer cell (BC) interaction correlate with MC3T3-E1 derived OT maturity. An exponential-like decrease in the number of cell layers with time (left-hand axis, graph) translated into a linear-like decrease in cell layer/tissue-thickness ratio (right-hand axis, graph). This observation was consistent with the process of bone-tissue maturation that resulted in transformation of proliferating pre-osteoblasts into non-dividing osteoblasts that become engulfed in mineralized matrix and mature into osteocytes through a process of phenotypic transformation marked by increased osteoblast apoptosis [31]. The data presented in the summary table suggested that declining rates of BC colonization and increasing efficiency of tissue penetration, cell organization into chains, and colony formation were related to OT maturity

MMP-13 (suggestive of active matrix turnover) and protein E11 (indicative of osteocytic transformation). The number of cell layers comprising OT and tissue-thickness decreased with culture time (Fig. 5) in a manner consistent with the increased osteoblast apoptosis observed in the formation of natural bone [31]. These observations were collectively interpreted to mean that continuous culture of MC3T3-E1 cells in the bioreactor recapitulated growth and phenotypic development of native bone-tissue in vivo, excluding osteoclast-mediated remodeling. Osteoclasts were purposely excluded from the bioreactor-based model so that osteoblast biology could be clearly observed.

Breast cancer cell challenge to osteoblast tissue

Confocal microscopy indicated that MDA-MB-231 human BCs adhered to and penetrated OT (Figs. 3, 4). BCs penetrated OT by extending long cellular protrusions that were enriched in filamentous actin and formed chains of cells similar to "Indian files" described for infiltrating lobular or metaplastic breast carcinomas [26, 27]. Migration of cancer cells along tracks of remodeled ECM produced by preceding invading cell(s) results in characteristic cell alignment patterns [28]. Invasion by chains of tumor cells linked together by cell–cell contacts is considered to be an effective penetration mechanism conferring high metastatic capacity and commensurately poor prognosis [26, 28]. Observation of BC invasion "Indian files" in the OT model suggests a considerable degree of physiological relevance.

BC attachment and penetration varied significantly with OT maturity (Fig. 5). BCs failed to penetrate immature OT (less than 30 days in culture); instead forming colonies substantially on, not in, OT. Significant penetration, remodeling, and characteristic cancer cell alignment patterns were observed only in relatively mature OT. We speculate that BC penetration is inhibited by close contacts among osteoblasts comprising immature OT and becomes more efficient as the cell/ECM ratio decreases, creating a more permeable tissue. The first penetrating BC remodels the extracellular matrix in a way that creates a path for other BCs [32], leading to the chains of cells as discussed above. This progressive process marshals OT into a pattern that paralleled the lines of breast cancer cells.

Unlike conventional cell culture wherein continuous or scheduled medium exchanges lead to loss of cell secreted growth factors and cytokines, the compartmentalized bioreactor retains all factors secreted into the cell growth compartment that have molecular weight greater than 6–8 KDa dialysis-membrane cutoff (see Materials and methods). We believe this attribute is critical to simulating the bone microenvironment because osteoblasts are known to secrete a number of growth factors and cytokines in a spatially and temporally ordered sequence that is closely aligned with the specific stages in osteoblast development [25]. Likewise, BC coculture introduces growth factors and cytokines that would presumably concentrate in the microenvironment in physiological conditions. For these reasons, we maintain that the OT model is a relevant model for cancer colonization of bone.

Osteoblast inflammatory response

Inflammation is linked closely with the progression of many cancers [33]. Osteoblasts are able to mount an inflammatory response independent of immune cells [34]. Inflammation appears to play a critical role in bone loss in osteomyelitis due to bacterial infection in the bone [34] and in debris-mediated bone loss associated with titanium implants [35]. Previous studies in conventional culture have shown that exposure to BC-conditioned medium produced a profound osteoblastic inflammatory stress

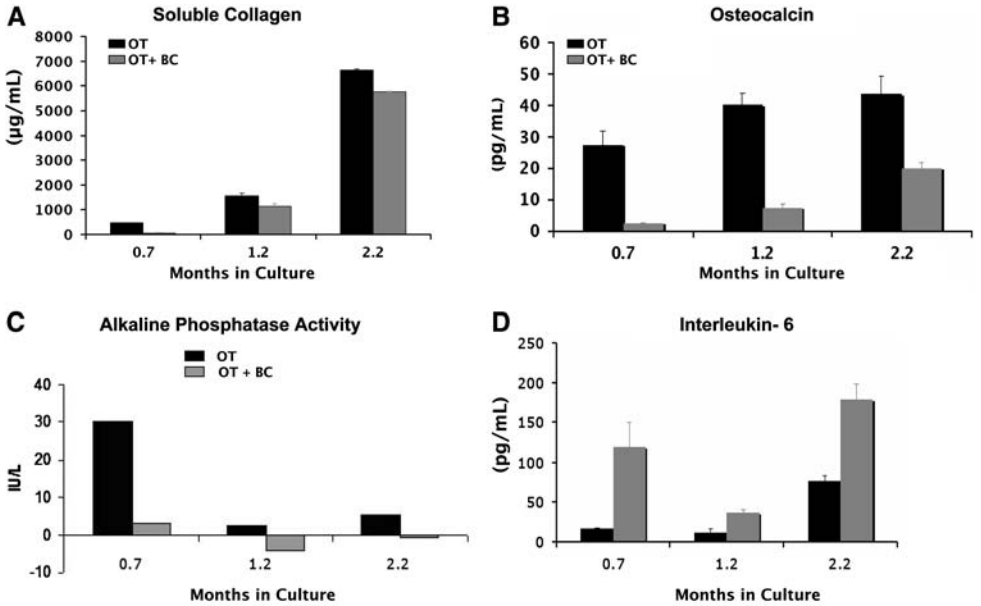

Fig. 6 Osteoblasts cocultured with MDA-MB-231 metastatic breast cancer cells (BC) showed a reduction in the production of osteoblast maturation proteins and an increase in IL-6. MC3T3-E1 derived osteoblast tissue (OT) were grown in the bioreactor for 0.7, 1.2, and 2.2 months before breast cancer cells (BC) were injected onto OT at a 1:10 BC-to-osteoblast cell ratio and cocultured for 7 days. OT with no added BC served as controls. Levels of soluble collagen secreted by osteoblasts into the medium in the presence and absence of breast cancer cells were quantified using Sircol^{TM} Assay (Biocolor) ($n \geq 2$) (Panel A). Levels of osteocalcin (OCN) secreted into the medium in the presence and absence of breast cancer cells were quantified using multiplex ELISA assay (LINCOplex^{TM} Mouse Bone Panel 2B, Millipore). Shown are averages of duplicate sample determination. (Panel B). Alkaline phosphatase activity was quantitated using the QuantiChrom^{TM} Alkaline Phosphatase Assay Kit (DALP-250), Bio-Assay Systems, Hayward, CA as indicated in the methods section. Each sample was tested three times (Panel C). Levels of murine IL-6 released into the culture media were determined with a multiplex ELISA assay (LINCOplex^{TM} Mouse Bone Panel 2B, Millipore). Shown are averages of duplicate sample determinations (Panel D)

response that included increased expression of the inflammatory cytokines, IL-6, IL-8 and MCP-1 [36]. These cytokines are known to attract and activate osteoclasts, and are likely to contribute to the tumor-host microenvironment in vivo. In particular, IL-6 a pleiotropic cytokine [37], has been implicated in pathogenesis of osteolysis associated with Paget's disease [38], Gorham-Stout syndrome [39], and multiple myeloma [40]. IL-6 levels in breast cancer patients have been found to correlate to the clinical stage of the disease [41, 42] as well to the rate of recurrence [43]. High IL-6 serum levels in breast cancer patients were found to be an unfavorable prognosis indicator [44–46]. We thus interpret pronounced IL-6 production by OT in coculture experiments (Fig. 6, Panel D) as a strong osteoblast inflammatory provoked by the presence of BCs. The concomitant decrease in collagen and osteocalcin secreted by OT cocultured with BCs confirms that BC suppress osteoblast function in a manner consistent with inflammation-induced bone loss observed in bone pathologies.

Breast cancer induced bone loss

Cancer-related bone loss appears to occur through multiple pathways. Evidence for osteoclast-mediated resorption is indeed very strong [47]. In addition, destruction of devitalized bone directly by cancer cells has also been reported [48], especially late in metastasis when bone-degradation rate is highest and osteoclast cell numbers are in decline [49]. These lines of evidence support the idea that osteoclasts are not solely responsible for excessive bone-degradation and that cancer cells may directly contribute to bone loss. Degradation of the osteoblast tissue by coculture with BCs observed in the bioreactor model (that purposely excludes osteoclasts) strongly suggests that yet another mechanism of bone loss is related to disruption of the bone-accretion process by destruction of osteoblastic tissue. There is clinical and experimental literature to support this concept. For example, quantitative histomorphometric analyses of bone biopsies from patients with hypercalcemia due to bone metastasis indicated a dramatic decrease in osteoblast activity [50]. Histomorphometric analysis of rodents inoculated with lytic human BCs (MDA-MB-231) indicated that, even though administration of risedronate (a bisphosphonate) reduced the number of osteoclasts, slowed bone lysis, and significantly reduced tumor burden, there was no evidence of new bone deposition or repair [51]. Similarly, administration of bisphosphonates to humans with osteolytic metastasis slowed lesion progression but

did not bring about healing [52]. Our previous work in vivo and in vitro also indicate that metastatic BCs suppress osteoblast adhesion and differentiation and increase osteoblast apoptosis [29, 49, 53]. All taken together, these observations strongly suggest that normal osteoblast function (i.e., deposition and mineralization of matrix) is not only impaired in the presence of BCs but, in fact, OT is degraded by breast cancer invasion, possibly by enlisting a cooperative inflammatory response by osteoblasts themselves. Further understanding of the cellular and molecular basis for breast cancer colonization of bone and discovery of therapeutic interventions will be greatly expedited by the use of 3D tissue models such as the one demonstrated in this study.

Acknowledgments This work was supported by U.S. Army Medical Research and Material Command Breast Cancer Research Program WX81XWH-06-1-0432, and the Susan G. Komen Breast Cancer Foundation BCTR 0601044, National Foundation for Cancer Research, Center for Metastasis Research, The University of Alabama-Birmingham. Authors appreciate the expert technical assistance of Ms. Donna Sosnoki and the assistance of the Cytometry Facility and the Electron Microscopy Facility at the Huck Institutes of Life Sciences, Penn State University.

References

1. Rubens RD, Mundy GR (2000) Cancer and the skeleton. Martin Dunitz, London
2. Rubens RD (1998) Bone metastases—the clinical problem. Eur J Cancer 34:210–213. doi:10.1016/S0959-8049(97)10128-9
3. Nielsen OS, Munro AJ, Tannock IF (1991) Bone metastases: pathophysiology and management policy. J Clin Oncol 9(3): 509–524
4. Aguirre-Ghiso JA (2007) Models, mechanisms and clinical evidence for cancer dormancy. Nat Rev Cancer 7(11):834–846. doi: 10.1038/nrc2256
5. Demicheli R (2001) Tumour dormancy: findings and hypotheses from clinical research on breast cancer. Semin Cancer Biol 11:297–306. doi:10.1006/scbi.2001.0385
6. Kvalheim G, Naume B, Nesland JM (1999) Minimal residual disease in breast cancer. Cancer Metastasis Rev 18:101–108. doi: 10.1023/A:1006216504892
7. Chambers AF, Groom AC, MacDonald IC (2002) Dissemination and growth of cancer cells in metastatic sites. Nat Rev Cancer 2(8):563–572. doi:10.1038/nrc865
8. Mundy GR (2002) Metastasis to bone: causes, consequences and therapeutic opportunities. Nat Rev Cancer 2:584–593. doi: 10.1038/nrc867
9. Holmgren L, O'Reilly MS, Folkman J (1995) Dormancy of micrometastases: balanced proliferation and apoptosis in the presence of angiogenesis suppression. Nat Med 1:149–153. doi: 10.1038/nm0295-149
10. Welch DR, Steeg PS, Rinker-Schaeffer CW (2000) Molecular biology of breast cancer metastasis: genetic regulation of human breast carcinoma metastasis. Breast Cancer Res 2(6):408–416. doi:10.1186/bcr87
11. Chambers AF, MacDonald IC, Schmidt EE et al (1995) Steps in tumor metastasis: new concepts from intravital videomicroscopy. Cancer Metastasis Rev 14:279–301. doi:10.1007/BF00690599
12. Chambers AF, Naumov GN, Vantyghem SA et al (2000) Molecular biology of breast cancer metastasis. Clinical implications of experimental studies on metastatic inefficiency. Breast Cancer Res 2:400–407. doi:10.1186/bcr86
13. Steeg PS (2000) Molecular biology of breast metastasis: 'has it spread?' disarming one of the most terrifying questions. Breast Cancer Res 2(6):396–399. doi:10.1186/bcr85
14. Chambers AF, MacDonald IC, Schmidt EE et al (2000) Clinical targets for anti-metastasis therapy. Adv Cancer Res 79:91–121. doi:10.1016/S0065-230X(00)79003-8
15. Welch DR (1997) Technical considerations for studying cancer metastasis in vivo. Clin Exp Metastasis 15:272–301. doi:10.1023/A:1018477516367
16. Schmeichel KL, Bissell MJ (2003) Modeling tissue-specific signaling and organ function in three-dimensions. J Cell Sci 116(12):2377–2388. doi:10.1242/jcs.00503
17. Rose GG (1966) Cytopathophysiology of tissue cultures growing under cellophane membranes. In: Richter GW, Epstein MA (eds) International review of experimental pathology. Academic Press, New York, pp 111–178
18. Rose GG, Pomerat CM, Shindler TO et al (1958) A cellophane-strip technique for culturing tissue in multipurpose culture chambers. J Cell Biol 4(6):761–764. doi:10.1083/jcb.4.6.761
19. Vogler EA (1989) A compartmentalized device for the culture of animal cells. J Biomater Artif Cells Artif Organs 17:597–610
20. Dhurjati R, Liu X, Gay CV et al (2006) Extended-term culture of bone cells in a compartmentalized bioreactor. Tissue Eng 12(11):3045–3054. doi:10.1089/ten.2006.12.3045
21. Sorkin AM, Dee KC, Knothe Tate ML (2004) "Culture shock" from the bone cell's perspective: emulating physiological conditions for mechanobiological investigations. Am J Physiol Cell Physiol 287(6):C1527–C1536. doi:10.1152/ajpcell.00059.2004
22. Cailleau R, Olive M, Cruciger QV (1978) Long-term human breast carcinoma cell lines of metastatic origin: preliminary characterization. In Vitro 14(11):911–915. doi:10.1007/BF02616120
23. Rusciano D, Burger M (2000) In vivo cancer metastasis assays. In: Welch D (ed) Cancer metastasis: experimental approaches: Elsevier, pp 207–242
24. Kinder M, Chislock E, Bussard KM et al (2008) Metastatic breast cancer induces an osteoblast inflammatory response. Exp Cell Res 314(1):173–183. doi:10.1016/j.yexcr.2007.09.021
25. Lian JB, Stein GS (1992) Concepts of osteoblast growth and differentiation: basis for modulation of bone cell development and tissue formation. Crit Rev Oral Biol Med 3(3):269–305
26. Page DL, Anderson TJ, Sakamoto G (1987) Diagnostic histopathology of the breast, pp 219–222
27. Pitts WC (1991) Carcinomas with metaplasia and sarcomas of the breast. Am J Clin Pathol 95:623–632
28. Friedl P, Wolf K (2003) Tumour-cell invasion and migration: diversity and escape mechanisms. Nat Rev Cancer 3(5):362–374. doi:10.1038/nrc1075
29. Mercer R, Miyasaka C, Mastro AM (2004) Metastatic breast cancer cells suppress osteoblast adhesion and differentiation. Clin Exp Metastasis 21(5):427–435. doi:10.1007/s10585-004-1867-6
30. Chou YF, Dunn JC, Wu BM (2005) In vitro response of MC3T3-E1 pre-osteoblasts within three dimensional apatite-coated PLGA scaffolds. J Biomed Mater Res B Appl Biomater 75(1):81–90. doi:10.1002/jbm.b.30261
31. Franz-Odendaal TA, Hall BK, Witten PE (2006) Buried alive: how osteoblasts become osteocytes. Dev Dyn 235(1):176–190. doi:10.1002/dvdy.20603
32. Stetler-Stevenson WG (1993) Tumor cell interactions with the extracellular matrix during invasion and metastasis. Annu Rev Cell Biol 9(1):541. doi:10.1146/annurev.cb.09.110193.002545

33. Visser Kd, Coussens L (2006) The inflammatory tumor microenvironment and its impact on cancer development. Contrib Microbiol 13:118–137
34. Marriott I (2004) Osteoblast responses to bacterial pathogens: a previously unappreciated role for bone-forming cells in host defense and disease progression. Immunol Res 30:291–308. doi:10.1385/IR:30:3:291
35. Fritz EA, Glant TT, Vermes C et al (2002) Titanium particles induce the immediate early stress responsive chemokines IL-8 and MCP-1 in osteoblasts. J Orthop Res 20:490–498. doi:10.1016/S0736-0266(01)00154-1
36. Kinder M, Chislock E, Bussard KM et al (2008) Metastatic breast cancer induces an osteoblast inflammatory response. Exp Cell Res 314(1):173–183. doi:10.1016/j.yexcr.2007.09.021
37. Papanicolaou DA (1998) The pathophysiologic roles of interleukin-6 in human disease. Ann Intern Med 128(2):127
38. Roodman GD, Kurihara N, Ohsaki Y et al (1992) Interleukin 6. A potential autocrine/paracrine factor in Paget's disease of bone. J Clin Invest 89(1):46–52. doi:10.1172/JCI115584
39. Devlin RD, Bone HG 3rd, Roodman GD (1996) Interleukin-6: a potential mediator of the massive osteolysis in patients with Gorham-Stout disease. J Clin Endocrinol Metab 81(5):1893–1897. doi:10.1210/jc.81.5.1893
40. Klein B, Zhang XG, Lu ZY et al (1995) Interleukin-6 in human multiple myeloma. Blood 85(4):863–872
41. Kozlowski L, Zakrzewska I, Tokajuk P et al (2003) Concentration of interleukin-6 (IL-6), interleukin-8 (IL-8) and interleukin-10 (IL-10) in blood serum of breast cancer patients. Roczniki Akademii Medycznej W Bialymstoku (1995) 48:82–84
42. Benoy I, Salgado R, Colpaert C et al (2002) Serum interleukin 6, plasma VEGF, serum VEGF, and VEGF platelet load in breast cancer patients. Clin Breast Cancer 2(4):311–315
43. Mettler L, Salmassi A, Heyer M et al (2004) Perioperative levels of interleukin-1beta and interleukin-6 in women with breast cancer. Clin Exp Obstet Gynecol 31(1):20–22
44. Salgado R, Junius S, Benoy I et al (2003) Circulating interleukin-6 predicts survival in patients with metastatic breast cancer. Int J Cancer 103(5):642–646
45. Zhang GJ, Adachi I (1999) Serum interleukin-6 levels correlate to tumor progression and prognosis in metastatic breast carcinoma. Anticancer Res 19(2B):1427–1432
46. Bozcuk H, Uslu G, Samur M et al (2004) Tumour necrosis factor-alpha, interleukin-6, and fasting serum insulin correlate with clinical outcome in metastatic breast cancer patients treated with chemotherapy. Cytokine 27(2–3):58–65. doi:10.1016/j.cyto.2004.04.002
47. Kozlow W, Guise TA (2005) Breast cancer metastasis to bone: mechanisms of osteolysis and implications for therapy. J Mammary Gland Biol Neoplasia 10(2):169–180. doi:10.1007/s10911-005-5399-8
48. Sanchez-Sweatman OH, Lee J, Orr FW et al (1997) Direct osteolysis induced by metastatic murine melanoma cells: role of matrix metalloproteinases. Eur J Cancer 33(6):918–925. doi:10.1016/S0959-8049(97)00513-3
49. Phadke PA, Mercer RR, Harms JF et al (2006) Kinetics of metastatic breast cancer cell trafficking in bone. Clin Cancer Res 12(5):1431–1440. doi:10.1158/1078-0432.CCR-05-1806
50. Stewart AF, Vignery A, Silverglate A et al (1982) Quantitative bone histomorphology in humoral hypercalcemia of malignancy: uncoupling of bone cell activity. J Clin Endocrinol Metab 55:219–227
51. Sasaki A, Boyce BF, Story B et al (1995) Bisphosphonate risedronate reduces metastatic human breast cancer burden in bone in nude mice. Cancer Res 55(16):3551–3557
52. Lipton A (2000) Bisphosphonates and breast carcinoma: present and future. Cancer 88:3033–3037. doi:0.1002/1097-0142(20000615)88:12+<3033::AID-CNCR20>3.0.CO;2-C
53. Mastro A, Gay C, Welch D et al (2004) Breast cancer cells induce osteoblast apoptosis: a possible contributor to bone degradation. J Cell Biochem 91(2):265–276. doi:10.1002/jcb.10746

A Three-Dimensional Osteogenic Tissue Model for the Study of Metastatic Tumor Cell Interactions with Bone

Andrea M. Mastro[2,3] and Erwin A. Vogler[1,3]

[1]Department of Materials Science and Engineering; [2]Department of Biochemistry and Molecular Biology, Materials Research Institute; and [3]The Huck Institutes of Life Sciences, The Pennsylvania State University, University Park, Pennsylvania

Abstract

A specialized bioreactor based on the principle of simultaneous growth and dialysis permits growth of three-dimensional (3D), multiple-cell-layer osteogenic tissue from isolated osteoblasts over long, continuous-culture intervals (tested up to 10 months with no sign of necrosis). The resulting tissue recapitulates the stages of bone development observed *in vivo*, including phenotypic maturation of cobblestone-shaped osteoblasts into stellate-shaped osteocytes interconnected by many intercellular processes. Gene expression profiles parallel cell-morphologic changes with time, ultimately leading to increased expression of osteocyte-associated molecules such as E11, DMP1, and sclerostin. Contiguous, cm^2-scale macroscopic mineral deposits that form within the bioreactor are consistent with bone hydroxyapatite. The simple to use bioreactor system provides an *in vitro* model that permits the study and manipulation of cancer cell interactions with bone tissue in real time. Metastatic human breast cancer cells, MDA-MB-231^{GFP}, introduced into the model grow and colonize osteoblastic tissue in a manner reflecting various characteristics of pathologic tissue observed in the clinic. Specifically, MDA-MB-231^{GFP} cells are observed to penetrate the thick extracellular matrix in which osteoblasts are embedded and to form chains reminiscent of "Indian files," described for infiltrating lobular or metaplastic breast carcinomas. Osteoblasts appear to be marshaled into a parallel alignment with cancer cells, followed by erosion of extracellular matrix structural integrity. Tissue degradation appears to be accompanied by increased expression of osteoblast inflammatory cytokines. [Cancer Res 2009;69(10):4097–100]

The skeleton is a favored site for the metastatic spread of breast, prostate, lung, and multiple myeloma cancers (1). Metastasis to the bone often progresses with significant morbidity related to substantial bone loss (osteolytic cancers) or gain (blastic cancers), bone pain, hypercalcemia, pathologic fractures, and spinal cord compression (2). Bone metastasis is particularly pernicious because early-stage detection is obscured by the refractory nature of bone; once bone colonization occurs, the cure rate drops precipitously (1–3). Inaccessibility also hampers a full understanding of the cellular and molecular mechanisms underlying cancer colonization of bone, thereby slowing drug development. Whole animal models are thus too complex for detailed mechanistic studies and, although excised tissue faithfully captures the end stages of bone metastasis associated with fully developed tumors, the critical initial stages of disease remain substantially obscured in this surrogate (4, 5). Standard monolayer cell culture sharply reduces complexity and permits direct access to bone cells; however, in so doing, the biological relevance of a fully developed tissue architecture is lost. For these reasons, as well as for reducing the use of animals for research, three-dimensional (3D) tissue models have become a focus of recent investigation (6, 7) and a challenging target for tissue engineering (8).

Effective *in vitro* bone models must strike a difficult balance between experimental efficiency and retention of biological complexity. For example, the metaphysis region of long bone, where cancer cells are known to traffic early in the metastasis process (9), is chiefly comprised of cancellous bone in the form of thin trabeculae intertwined with blood vessels, connective tissue, and hematopoietic cells of the bone marrow. Trabeculae, in turn, are comprised of a calcified collagenous matrix populated and lined by osteoblasts, which are responsible for bone accretion, interacting with osteoclasts, which are responsible for bone resorption. A minimal model of bone accretion consisting of only osteoblasts must simulate the microenvironment wherein spatially and temporally sequenced secretion of growth factors and cytokines associated with bone development can occur (10) over long periods measured in months. Generally speaking, neither conventional cell culture nor advanced bioreactor systems that rely on scheduled or continuous culture refeeding can reproduce this microenvironment because removal of spent growth medium also eliminates, or significantly perturbs, pericellular concentration gradients.

We have adapted a specific type of bioreactor (11), based on the principle of simultaneous growth and dialysis first pioneered by G.G. Rose (12), for the purpose of developing an *in vitro* model of bone with systematically increasing biological complexity (6, 13). The core idea behind this compartmentalized bioreactor is to continuously feed cells with low-molecular-weight nutrients by dialysis through a cellulose membrane that also retains cell-secreted macromolecules within a cell-growth compartment bounded by this membrane. In this way, metabolic waste products such as lactic acid continuously dialyze out of the cell-growth compartment and into a basal-medium compartment for eventual removal and replacement with fresh growth medium. Growth and feeding functions are thus separated (compartmentalized), and the pericellular space is not perturbed by wholesale growth medium removal. The result is an extraordinarily stable culture environment wherein concentration gradients can develop.

Using this method of culture, we have grown multiple-cell-layer osteogenic tissue from two lines of osteoblasts: human fetal hFOB1.19 (ATCC CRL-11372) and mouse calvaria MC3T3-E1 (ATCC CRL-2593) (ref. 13). Focusing on MC3T3-E1-derived tissue, we have observed *in vitro* the progression of osteoblast development as it

Requests for reprints: Andrea M. Mastro, 431 S. Frear Laboratory, University Park, PA 16803. Phone: 814-863-0152; Fax: 814-863-7024; E-mail: a36@psu.edu.

doi:10.1158/0008-5472.CAN-08-4437

occurs in natural bone; i.e., from proliferation and differentiation to engulfment of osteoblasts in a thick cell-secreted mineralized matrix, followed by subsequent phenotypic maturation into a network of osteocytes with a distinctive stellate shape (Fig. 1*A* and *B*). In some cultures, contiguous, cm^2-scale macroscopic mineral deposits were formed that proved consistent with bone hydroxyapatite, as shown by X-ray scattering and infrared spectroscopy. In addition, the gene-expression profiles of characteristic osteoblast proteins such as Type 1 collagen, alkaline phosphatase, osteonectin, osteopontin, and osteocalcin mirrored that observed *in vivo*. After several months, the cultures also expressed molecules indicative of osteocytes, i.e., E11, DMP1, and sclerostin. RNA recovery from these mature cultures was low compared to less mature bioreactors, consistent with decreased cell density (due to apoptosis) and the reduced metabolic activity attributed to osteocytes. To our knowledge, these are the first *in vitro* observations of massive osteoblast-mediated ossification and phenotypic transformation into osteocytes reported in the literature. The compartmentalized bioreactor thus presents itself as an *in vitro* model for studies of bone biology and pathology.

The bioreactor is amenable to real-time live-cell analysis by fluorescence confocal microscopy. We have labeled osteoblasts with Cell Tracker Orange, for example, and followed cell morphology over time. At the end of the culture period, the tissue can be fixed, and the cells can be stained for alkaline phosphatase or with phalloidin, and/or labeled with other fluorescent molecule probes (Fig. 1). Tissue can be further processed by using conventional histologic methods, including conventional light and electron microscopies (13). We have combined fluorescence with TEM by using fluorescent, electron-dense Quantum Dots (In Vitrogen-Molecular Probes). Following a protocol similar to that discussed below, we introduced MDA-MB-231 metastatic cancer cells that had internalized Q Tracker 655 dots (10 nm nominal diameter with cadmium cores) into osteoblast cultures and followed cancer cell-osteoblast interactions by confocal microscopy before processing the tissue for TEM. The electron-dense dots were observed to collect within perinuclear vacuoles only in the cancer cells and did not transfer to the osteoblasts. In this way, we were able to distinguish cancer cells from osteoblasts and study cell-cell interactions at the TEM level. Finally, all or part of the culture can be released from the membrane for RNA isolation suitable for gene expression by PCR or lysed for protein expression by western blot.

Introduction of MDA-MB-231^{GFP} human metastatic breast cancer cells (genetically engineered to produce green-fluorescent protein, GFP, and known to invade the murine skeleton 14) onto MC3T3-E1 osteoblastic tissue grown in the compartmentalized bioreactor to various stages of phenotypic maturity allowed us to follow early stages of cancer cell colonization in real time by confocal microscopy (Fig. 1*C–E*). In this way, we observed cancer cell-osteoblast tissue adhesion, cancer cell proliferation, tissue penetration, the formation of nonvascularized microtumors, and the ultimate degradation of osteoblast-derived extracellular matrix (ECM). Cancer cells proliferated and formed into columns of cells that penetrated the collagenous tissue matrix and organized into rows similar to the "Indian files," described for infiltrating lobular or metaplastic breast carcinomas (Fig. 1*E* and *F*) (ref. 15). Migration of cancer cells along tracks of remodeled ECM produced by a preceding invading cell(s) apparently results in characteristic cell-alignment patterns (16). Invasion by chains of tumor cells linked together by cell-cell contacts is considered to be an effective penetration mechanism (17), conferring high metastatic capacity and commensurately poor prognosis (15, 16). The observation of filing in the osteoblastic tissue model suggests a considerable degree of physiologic relevance. Indian filing is common in soft tissue, but it is also found in bone metastasis (Fig. 1*G–I*).

We also observed an increased expression of inflammatory cytokines such as IL-6 in the presence of the breast cancer cells, as well as a decrease in secretion of soluble (newly formed) collagen and osteocalcin (a marker of osteoblast maturity) (ref. 6). A strong osteoblastic stress response and a decrease in collagen production correlated with the loss of ECM integrity seen after 7 days of coculture with MDA-MB-231^{GFP}. These results parallel previous studies in conventional culture showing that exposure of osteoblasts to MDA-MB-231^{GFP}-conditioned medium produced an osteoblastic inflammatory stress response with sharply increased expression of the inflammatory cytokines IL-6, IL-8, and MCP-1 (18). These cytokines are known to attract and activate osteoclasts, and they are likely to contribute to the tumor-host microenvironment *in vivo*. In particular, IL-6, a pleiotropic cytokine, has been implicated in the pathogenesis of osteolysis associated with Paget's disease, Gorham-Stout syndrome, and multiple myeloma. IL-6 levels in breast cancer patients have been found to correlate to the clinical stage of the disease as well as to the rate of recurrence. High IL-6 serum levels in breast cancer patients have been found to be an unfavorable prognosis indicator (see [6] and citations therein). IL-8 and the murine-related molecules KC and MIP-2 have also been found to correlate with increased bone metastasis *in vivo* and with stimulation of osteoclast differentiation followed by bone resorption. Interestingly, MCP-1, a principal chemokine involved in normal bone remodeling, is produced primarily by osteoblasts and not by the metastatic MDA-MB-231^{GFP} cells upon interaction. Thus, the osteoblastic response to the cancer cells, even in the absence of osteoclasts, changes the tumor microenvironment to favor osteolysis in this particular cancer cell model (6).

Interestingly, we found that the above-described pattern of cancer colonization was dependent on osteoblastic tissue maturity (Fig. 1B, table portion). MDA-MB-231^{GFP} cells failed to penetrate immature osteoblast tissue (less than 30 days in culture), instead forming colonies substantially on, not in, tissue. Significant penetration, remodeling, and characteristic cancer-cell-alignment patterns were observed only in relatively mature osteoblastic tissue. Cancer-cell-induced changes in osteoblast shape and in the production of inflammatory cytokines were seen after as few as 3 days of coculture. We speculate that cancer cell penetration was slowed by close contacts among osteoblasts comprising immature tissue and that it becomes more efficient as the cell/ECM ratio decreases, creating a more permeable tissue.

Comparison of results obtained with tissue grown in the bioreactor to cells grown with conventional tissue culture clearly showed that 3D tissue was superior in modeling details of cancer cell colonization. In the first place, osteoblasts do not grow into more than 1-2 cell layers in conventional cell culture. Furthermore, these cultures usually did not remain healthy for more than about 1 month before showing signs of necrosis or sharply increased apoptosis (13). These substantially 2D cultures never achieved the phenotypic maturity observed in the bioreactor, and, in particular, there was no evidence of an osteoblast-to-osteocyte transition. In the second place, although the MDA-MB-231^{GFP} cells proliferated in contact with 2D osteoblast monolayers and formed colonies, these cancer cells did not penetrate the osteoblast monolayers and did not form cell files. It is thus apparent that the 3D osteoblastic tissue model is a better tool for the discovery of therapeutic interventions to cancer colonization of bone.

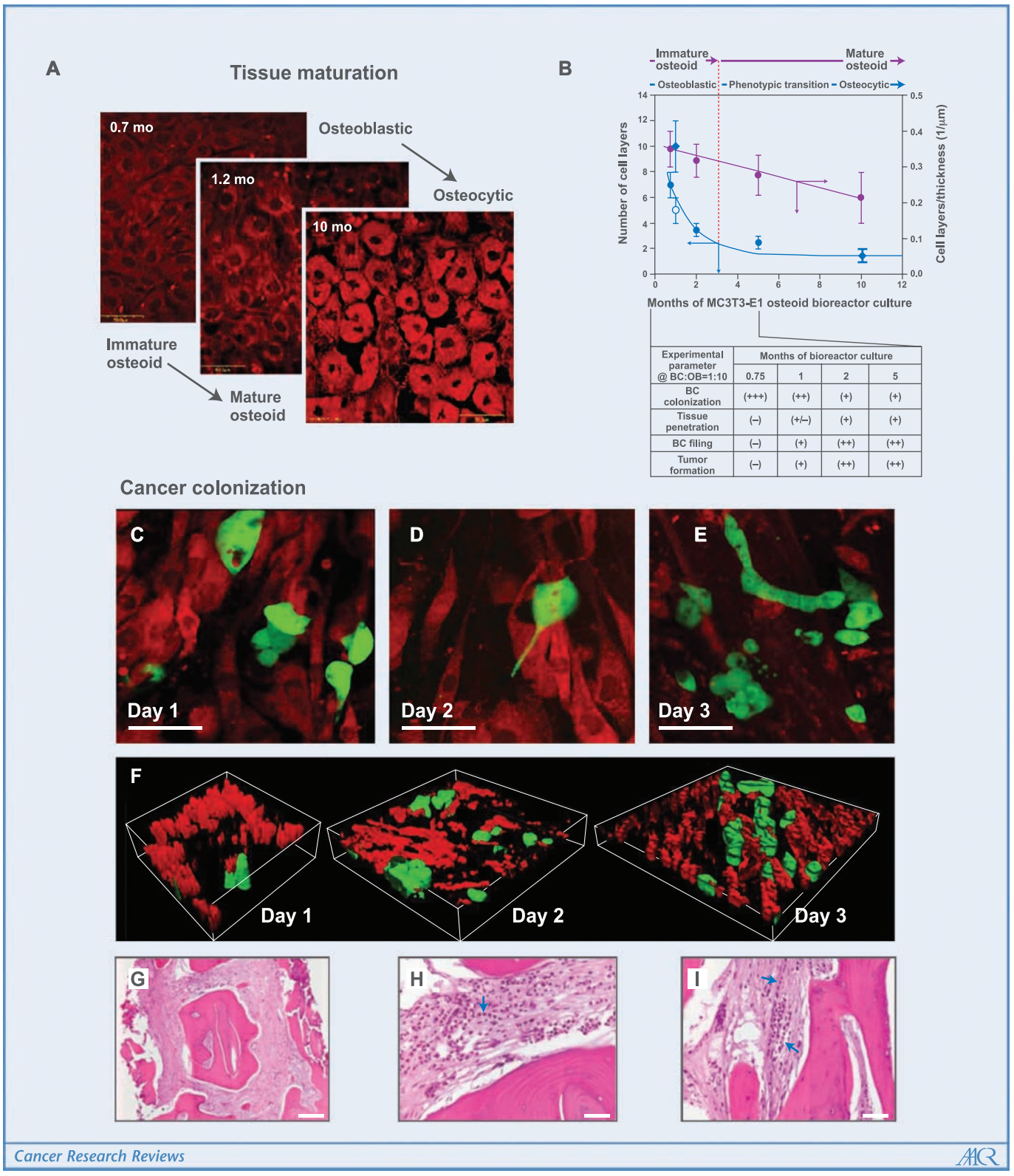

Figure 1. *A,* osteogenic tissue maturation in the bioreactor recapitulates development of native bone by systematic and reproducible phenotypic maturation of preosteoblasts through mineralizing osteoblasts to terminally differentiated osteocytes. *B,* MC3T3-E1 cells produce and mineralize a thick, engulfing extracellular matrix (ECM) that slowly decreases in thickness and number of cell layers through progressive apoptosis to a final stable state exhibiting no sign of tissue necrosis over 10 months of continuous culture (graph). *C-F*, interaction of MDA-MB-231^{GFP} human cancer cells (green, GFP) with osteogenic tissue (red, osteoblasts; black, ECM) depends on tissue maturity (*B*, table) and exhibits stages of cancer cell adhesion (*C*), penetration (*D*), and alignment of cancer cell into files (*E*) that are reminiscent of events observed in pathologic tissue. *F,* filing is especially evident in corresponding 3D confocal reconstructions. *G-I,* for comparison, Indian Filing is shown in a section from bone (*solid pink*) with metastatic breast cancer (rows of cells with dark purple nuclei). The scale bars in *A, C*, and *D* represent 50 μm, the scale bar in *F* represents 100 μm, the scale bar in *G* represents 200 μm, and the scale bars in *H* and *I* represent 50 μm.

In summary, we have found that the easy to use bioreactor design based on the principle of simultaneous growth and dialysis permitted *in vitro* culture of 3D, multiple-cell-layer osteoblastic tissue from isolated cells and their maintenance for much longer periods than in conventional culture (demonstrated up to 10 months with no indication of tissue necrosis). This osteoblastic tissue exhibited important hallmarks of the osteoblast-to-osteocyte phenotypic transition and deposition of macroscopic bone. We conclude that the resulting tissue is a relevant *in vitro* model of osteoblasts within regions of growing bone, such as the metaphysial areas of long bone that are otherwise difficult to access *in vivo*. Challenge with breast cancer cells known to invade skeleton permitted, for the first time, direct and real-time observation of cancer cell colonization of the osteoblast tissue. Important pathologic events such as cancer cell filing and colony (microtumor) formation observed clinically were reproduced *in vitro*. These studies have revealed that breast cancer cell colonization strongly depends on osteoblastic tissue maturity, and point to a potentially important point of therapeutic intervention for cancer metastases in bone. Comparison of breast cancer cell interactions with osteoblasts in conventional culture to interactions with osteoblastic tissue in the bioreactor strongly suggested that monolayer cell culture is not the optimal model for studying the cancer cell colonization of bone.

In the future, we plan to use primary osteoblasts (especially human) as source cells for the growth of osteogenic tissue. In addition, we plan to increase the biological complexity of the system by adding other cell types, including osteoclasts. We have already successfully cultured primary osteoblasts isolated from mouse calvaria in the bioreactor. After 3 months, these cells formed a multilayer complex that expressed characteristic osteoblast-differentiation proteins, in a manner similar to that obtained with the pure MC3T-E1 osteoblast cell line. Once we have a human-derived 3D osteogenic tissue model in hand, we plan to study interactions with other metastatic bone cancers (e.g., blastic prostate cancer cells or osteolytic multiple myeloma cells) to determine if human cancer colonization of human osteoblastic tissue parallels pathogenesis *in vivo*. We intend to explore the development of an *in vitro* bone-remodeling unit by coculture of primary osteoclasts with osteogenic tissue. Challenging such a mimic with cancer cells should permit the close examination of how cancer cells influence osteoblast-osteoclast interactions and upset normal bone remodeling. Toward the goal of ultimate biological complexity in an *in vitro* bone model, we aim to recreate the hematopoietic-cancer cell niche by culturing osteoblastic tissue in the presence of mesenchymal stromal cells from bone marrow cells. There is strong evidence in the literature that osteoblasts provide the endosteal niche for hematopoietic stem cells (19), and that this niche both receives and harbors metastatic cancer cells early in the colonization process. Finally, although this bioreactor system is not an appropriate tool for rapid drug screening, it can serve as an efficient system by which to test therapeutics at a level above that of 2D cell culture but below costly and slow animal testing. Although the described compartmentalized device is not commercially available, engineering plans have been published (11), and the bioreactor is straightforward enough to make in a standard engineering shop.

Disclosure of Potential Conflicts of Interest

No potential conflicts of interest were disclosed.

Acknowledgments

Received 11/21/08; revised 2/16/09; accepted 2/22/09.

Grant support: U.S. Army Medical and Material Command Breast Cancer Research Program (WX81XWH-06-1-0432) and The Susan G. Koman Breast Cancer Foundation (BCTR 0601044). This work was a contribution from the Osteobiology Research Group, The Pennsylvania State University.

We thank Ravi Dhurjati, Laurie Shuman, Venkatesh Krishnan, and Donna Sosnoski for their work with various aspects of this project. We also thank Dr. Elizabeth Frauenhoffer of the Penn State Hershey Medical Center for images of metastatic breast cancer in bone.

References

1. Rubens RD, Mundy GR. Cancer and the skeleton. London: Martin Dunitz; 2000.
2. Nielsen OS, Munro AJ, Tannock IF. Bone metastases: pathophysiology and management policy. J Clin Oncol 1991;9:509–24. PubMed.
3. Rubens RD. Bone metastases-the clinical problem. Eur J Cancer 1998;34:210–3. PubMed doi:10.1016/S0959–8049(97)10128–9.
4. Nemeth JA, Harb JF, Barroso U, Jr., He Z, Grignon DJ, Cher ML. Severe combined immunodeficient model of human prostate cancer metastasis to human bone. Cancer Res 1999;59:1987–93. PubMed.
5. Welch DR. Technical considerations for studying cancer metastasis *in vivo*. Clin Exp Metastasis 1997;15: 272–301.
6. Dhurjati R, Krishnan V, Shuman LA, Mastro AM, Vogler EA. Metastatic breast cancer cells colonize and degrade three-dimensional osteoblastic tissue *in vitro*. Clin Exp Metastasis 2008;25:741–52. PubMed doi:10.1007/s10585–008–9185_z.
7. Schmeichel KL, Bissell MJ. Modeling tissue-specific signaling and organ function in three dimensions. J Cell Sci 2003;116:2377–88.
8. Rose FR, Oreffo RO. Bone tissue engineering: hope vs hype. Biochem Biophys Res Commun 2002;292:1–7. PubMed doi:10.1006/bbrc.2002.6519.
9. Phadke PA, Mercer RR, Harms JF, et al. Kinetics of metastatic breast cancer cell trafficking in bone. Clin Cancer Res 2006;12:1431–40. PubMed doi:10.1158/1078–0432.CCR_05–1806.
10. Lian JB, Stein GS. Concepts of osteoblast growth and differentiation: basis for modulation of bone cell development and tissue formation. Crit Rev Oral Biol Med 1992;3:269–305. PubMed.
11. Vogler EA. A compartmentalized device for the culture of animal cells. Biomater Artif Cells Artif Organs 1989;17:597–610.
12. Rose GG. Cytopathophysiology of tissue cultures growing under cellophane membranes. Int Rev Exp Pathol 1966;5:111–78.
13. Dhurjati R, Liu X, Gay CV, Mastro AM, Vogler EA. Extended-term culture of bone cells in a compartmentalized bioreactor. Tissue Eng 2006;12:3045–54. PubMed doi:10.1089/ten.2006.12.3045.
14. Rusciano D, Burger M. *In vivo* cancer metastasis assays. In: Welch D, editor. Cancer metastasis: experimental approaches. Amsterdam, The Netherland: Elsevier; 2000. p. 207–42.
15. Page DL, Anderson TJ, Sakamoto G. Infiltrating carcinoma: major histological types. In: Anderson Thomas J, editor. Diagnostic histopathology of the breast. Edinburgh: Churchill Livingstone; 1987. p. 219–22.
16. Friedl P, Wolf K. Tumor-cell invasion and migration: diversity and escape mechanisms. Nat Rev Cancer 2003; 3:362–74. PubMed doi:10.1038/nrc1075.
17. Friedl P, Wolf K. Tube travel: the role of proteases in individual and collective cancer cell invasion. Cancer Res 2008;68:7247–9. PubMed doi:10.1158/0008–5472. CAN_08–0784.
18. Kinder M, Chislock E, Bussard KM, Shuman L, Mastro AM. Metastatic breast cancer induces an osteoblast inflammatory response. Exp Cell Res 2008; 314:173–83. PubMed doi:10.1016/j.yexcr.2007.09.021.
19. Taichman RS. Blood and bone: two tissues whose fates are intertwined to create the hematopoietic stem-cell niche. Blood 2005;105:2631–9. PubMed doi:10.1182/blood_2004–06–2480.

In Vitro Cell.Dev.Biol.—Animal (2010) 46:28–35
DOI 10.1007/s11626-009-9238-x

Osteogenesis in vitro: from pre-osteoblasts to osteocytes

A contribution from the Osteobiology Research Group, The Pennsylvania State University

Venkatesh Krishnan · Ravi Dhurjati · Erwin A. Vogler · Andrea M. Mastro

Received: 8 May 2009 / Accepted: 3 September 2009 / Published online: 14 October 2009 / Editor: J. Denry Sato

Abstract Murine calvariae pre-osteoblasts (MC3T3-E1), grown in a novel bioreactor, proliferate into a mineralizing 3D osteoblastic tissue that undergoes progressive phenotypic maturation into osteocyte-like cells. Initially, the cells are closely packed (high cell/matrix ratio), but transform into a more mature phenotype (low cell/matrix ratio) after about 5 mo, a process that recapitulates stages of bone development observed in vivo. The cell morphology concomitantly evolves from spindle-shaped pre-osteoblasts through cobblestone-shaped osteoblasts to stellate-shaped osteocyte-like cells interconnected by many intercellular processes. Gene-expression profiles parallel cell morphological changes, up-to-and-including increased expression of osteocyte-associated genes such as E11, DMP1, and sclerostin. X-ray scattering and infrared spectroscopy of contiguous, square centimeter-scale macroscopic mineral deposits are consistent with bone hydroxyapatite, showing that bioreactor conditions can lead to ossification reminiscent of bone formation. Thus, extended-term osteoblast culture (≤10 mo) in a bioreactor based on the concept of simultaneous growth and dialysis captures the full continuum of bone development otherwise inaccessible with conventional cell culture, resulting in an in vitro model of osteogenesis and a source of terminally differentiated osteocytes that does not require demineralization of fully formed bone.

Keywords Osteocyte · Osteoblast · Bone formation · Bioreactor · Three-dimensional cell culture model

Venkatesh Krishnan and Ravi Dhurjati contributed equally.

Electronic supplementary material The online version of this article (doi:10.1007/s11626-009-9238-x) contains supplementary material, which is available to authorized users.

R. Dhurjati · E. A. Vogler
Departments of Materials Science and Engineering,
Pennsylvania State University,
University Park, PA 16802, USA

V. Krishnan · A. M. Mastro (✉)
Biochemistry and Molecular Biology,
Pennsylvania State University,
431, South Frear,
University Park, PA 16802, USA
e-mail: a36@psu.edu

E. A. Vogler
Materials Research Institute, Pennsylvania State University,
University Park, PA 16802, USA

V. Krishnan · E. A. Vogler · A. M. Mastro
The Huck Institutes of Life Sciences,
Pennsylvania State University,
University Park, PA 16802, USA

Introduction

Diseases of bone such as osteoarthritis, osteomalacia, and osteoporosis negatively affect the quality of life for millions and cause commensurate socioeconomic burden (Rodan and Martin 2000; Service 2000). Likewise, cancers in bone are pernicious diseases with characteristically high levels of morbidity and mortality (Rubens 1998; Rubens and Mundy 2000). Resolution of these healthcare issues, as well as development of therapeutic approaches to bone restoration (Rodan and Martin 2000), depends, in part, on a firm understanding of the cellular-and-molecular basis of osteogenesis.

Osteoblasts, cells of mesenchymal origin, are responsible for bone accretion (Ducy et al. 2000) through a tightly regulated, spatiotemporal sequence (Lian and Stein 1992) that includes proliferation of pre-osteoblasts, differentiation

into functional osteoblasts capable of depositing collagenous matrix, and progressive mineralization of that matrix. In the final stage of bone development, mature osteoblasts either undergo apoptosis, become bone lining cells or terminally differentiate into osteocytes that inhabit lacunar spaces within hard bone (Knothe Tate et al. 2004). Throughout this sequence, cells maintain extensive intercellular networks through gap junctions (osteoblasts) or intercellular processes (osteocytes; Doty 1981). Thus, bone tissue is a functional syncytium that transduces mechanochemical stimuli through dynamic cell–cell contacts (Palumbo et al. 1990). This syncytium is disrupted by bone diseases (Knothe Tate et al. 2002), including metastases of cancers in bone (Dhurjati et al. 2008), emphasizing the importance of 3D tissue organization in osteopathologies.

Conventional cell culture has proven to be a valuable tool for studying the physiology of bone-forming cells. In particular, enzymatic isolation of osteoblasts has yielded reproducible and widely applied methods for studying osteoblast biology in vitro (Nijweide and Burger 1990). However, osteoblasts grown by conventional-culture methods are limited to a 2D monolayer and do not emulate the 3D network that characterizes bone tissue. Also, conventional culture is not generally suitable for maintaining cells over the long period required for completion of all stages of bone development. Importantly, the pericellular microenvironment, perturbed by the periodic replacement of the medium, prevents development of chemical gradients (cytokines and other factors) thought to mediate phenotypic development (Chaudhuri and Al-Rubeai 2005). As a consequence, differentiation of osteoblasts into osteocytes has not been reproduced under in vitro conditions conducive to probing with modern genomic and proteomic tools.

We have developed a novel bioreactor (Vogler 1989; Dhurjati et al. 2006) based on the principle of simultaneous growth and dialysis (Rose 1966) that permits extended-term, uninterrupted growth of a 3D mineralizing osteoblastic tissue (Dhurjati et al. 2006). This system permits phenotypic

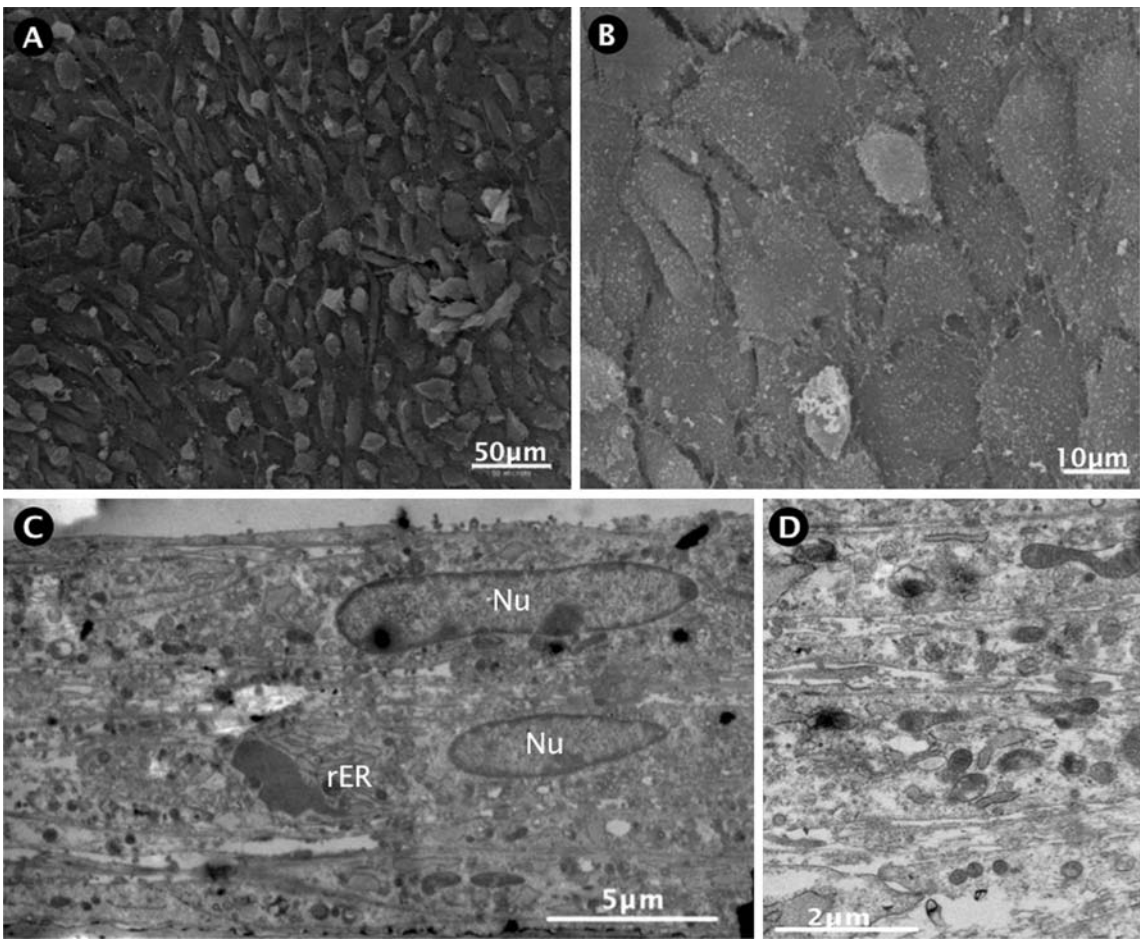

Figure 1. MC3T3E-1 pre-osteoblasts grown for 15 d within the bioreactor. (*A*, *B*) SEM images of a dense 3D tissue about 22 µm thick. (*C*, *D*) Cross-sectional TEM images showing six to eight layers of actively mineralizing and densely packed cells with close cell contacts (*Nu* nucleus, *rER* rough endoplasmic reticulum).

maturation of pre-osteoblasts into terminally differentiated osteocytes. Bioreactors have occasionally exhibited mineralization yielding contiguous, square centimeter-scale mineral deposits that prove to be consistent with bone hydroxyapatite. Simultaneous-growth-and-dialysis culture has thus provided unprecedented access to osteocyte biology.

Materials and Methods

Bioreactor. Bioreactors based on the principle of simultaneous growth and dialysis (Rose 1966) were implemented as described previously (Vogler 1989; Dhurjati et al. 2006, 2008; see also Supplementary Figure 1). Briefly, the cell-growth compartment (5 mL) was separated from a 30-mL medium reservoir by a dialysis membrane. Cells were inoculated into the growth chamber in complete medium including serum. The reservoir was filled with basal medium without serum. Serum constituents or macromolecules synthesized by cells with molecular weights in excess of the dialysis membrane cutoff (6–8 kDa) were retained and concentrated within the growth compartment.

Cells and cell culture. Murine calvarial pre-osteoblasts (MC3T3-E1), a gift from Dr. Norman Karin, Pacific Northwest National Laboratories, Richland, WA were inoculated into the growth chamber (10^4cells/cm^2) and cultured with growth medium [alpha-minimum essential medium (Mediatech, Herdon, VA), 10% neonatal fetal bovine serum (Cansera, Roxdale, Canada), 100 U/mL penicillin 100 µg/mL streptomycin (Sigma Aldrich, St. Louis, MO)]. The reservoir contained the same medium but without serum. Once the cells reached confluence, usually 4–5 d, the medium in the growth chamber was replaced with differentiation medium containing 50 µg/mL ascorbic acid and 10 mM β-glycerophosphate (Sigma Aldrich). Every 30 d, the basal medium within the medium reservoir was refreshed. This medium change prevented the buildup of metabolic wastes. Bioreactors were maintained at 37°C in a humidified 5% CO_2 incubator.

Reverse transcriptase polymerase chain reaction. After indicated times, MC3T3-E1 were harvested and RNA isolated (RNeasy, Qiagen, Valencia, CA). All RNA samples had a A260/280 ratio >1.8. CDNA was generated from 0.5 µg RNA using the SuperScript® VILO™ kit (Invitrogen, Carlsbad, CA). PCR was carried out with a thermo cycler (DeltaCycler 1™ System, Ericomp, San Diego, CA) as described previously (Dhurjati et al. 2008). The sequences of the primer pairs are available in Supplementary Table 1. Expression levels for each gene were normalized by determining the ratio of the band volume to that of β-actin.

Table 1 Temporal gene expression of differentiation markers in MC3T3-E1 cultured in the bioreactor

Markers	Months in culture			
	0.7	1	2	10
Osteocalcin	0.54[a]	0.14	0.55	0.015
Osteonectin	0.53	0.53	0.34	0.19
Osteopontin	0.21	0.054	0.51	0.11
Type I collagen	1.49	1.36	1.21	0.76
MMP13	0.11	0.23	1.46	na
E-11	1.15	0.93	1.01	0.78
DMP-1	0.09	0.04	0.63	0.06
Sclerostin	nd	nd	–[b]	–[b]
Yield of RNA	1,100 ng/µL	160 ng/µL	180 ng/µL	12 ng/µL

MC3T3-E1 cells were cultured in the bioreactor for various intervals (22, 30, 60 d, 10 mo). Cells were harvested and RNA isolated (RNeasy, Qiagen) as described in the "Materials and Methods" section. PCR was carried out on a thermocycler (DeltaCycler 1™ System, Ericomp). PCR reactions were run on a 2% agarose gel, stained with ethidium bromide and imaged under UV illumination. Gel documentation was performed on the Kodak Gel Logic 100 Imaging System (Eastman Kodak, Rochester, NY) and band volume quantitation was done by ImageQuant software (Molecular Dynamics, Sunnyvale, CA)

n=2, *nd* not detected, *na* not assayed

[a] Shown are expression levels of each gene normalized by determining the ratio of the band volume for each message relative to the band volume for β-actin for the same cDNA

[b] Detected at faint levels that could not be quantified

Confocal microscopy. The cells were fixed with 2.5% glutaraldehyde in cacodylate buffer and stained with Alexa Fluor 568 phalloidin according to the manufacturer's instructions (Molecular Probes, Invitrogen). In situ laser scanning was performed using an Olympus FV-300 laser scanning microscope (Olympus America Inc., Center Valley, PA; Dhurjati et al. 2008).

Fourier transform infrared spectroscopy and X-ray analyses. A bone chip from the bioreactor or from bovine bone was placed in a stainless steel vial along with a large ball bearing and then put in a Wig-L-Bug vibrating mill. The bone was ground for 30 s. A small amount of oven-dried KBr powder (International Crystal Laboratories, Garfield, NJ) was added, the ball bearing removed, and the materials mixed for 30 s. A translucent 7-mm pellet was pressed (Quick-Press, Buck Scientific, East Norwalk, CT) and analyzed in transmission mode using a Fourier transform infrared spectroscopy (FTIR) spectrometer (Bruker IFS 66/s, Bruker Optics, Billerica, MA). Other bone chips were dried with hexamethyldisilazane and ground in a ball mill into a powder. The X-ray diffraction pattern of the powder was collected using a Phillips MPD theta-2-theta powder

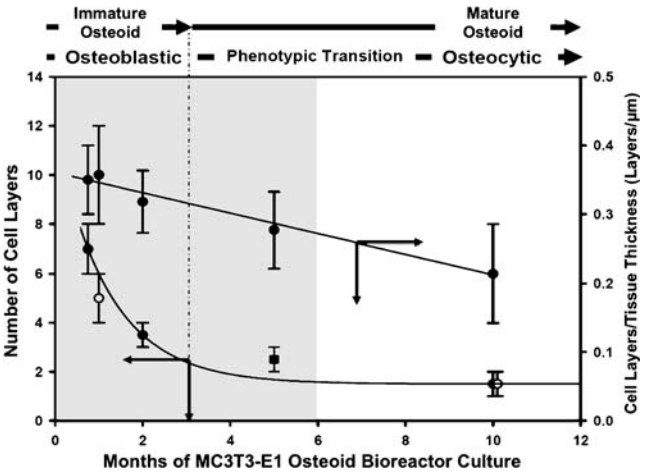

Figure 2. Phenotypic maturation of MC3T3E-1 within the bioreactor over 10 mo continuous culture. An exponential-like decrease in the number of cell layers with time (*left-hand axis*) translated into a linear-like decrease in cell-layer/tissue-thickness ratio (*right-hand axis*). This finding was consistent with the process of bone maturation that resulted in transformation of proliferating pre-osteoblasts into nondividing osteoblasts that become engulfed in mineralized matrix and mature into osteocytes (Eriksen et al. 2007). Data within *gray box* were previously reported in (Dhurjati et al. 2008).

diffractometer (PANalytical Inc., Westborough, MA) and compared to that of authentic bone.

Scanning and transmission electron microscopy. Tissue from the bioreactor was fixed overnight with 2.5% glutaraldehyde in 0.1 M sodium cacodylate buffer at 4°C and processed for transmission electron microscopy (TEM) as described previously (Dhurjati et al. 2008). For scanning electron microscope (SEM), the tissues were further incubated with 1% osmium tetroxide in cacodylate (Dhurjati et al. 2008).

Results

Osteoblastic tissue growth and maturation under continuous long-term culture. MC3T3E-1, developed into 3D tissue about 22 μm thick within 15 d (Fig. 1*A*, *B*), comprised of six to eight layers (Fig. 1*C*, *D*) of actively mineralizing (positive for alkaline phosphatase activity and for mineralization by von Kossa stain), differentiated osteoblasts (Dhurjati et al. 2006, 2008). TEM showed that this tissue

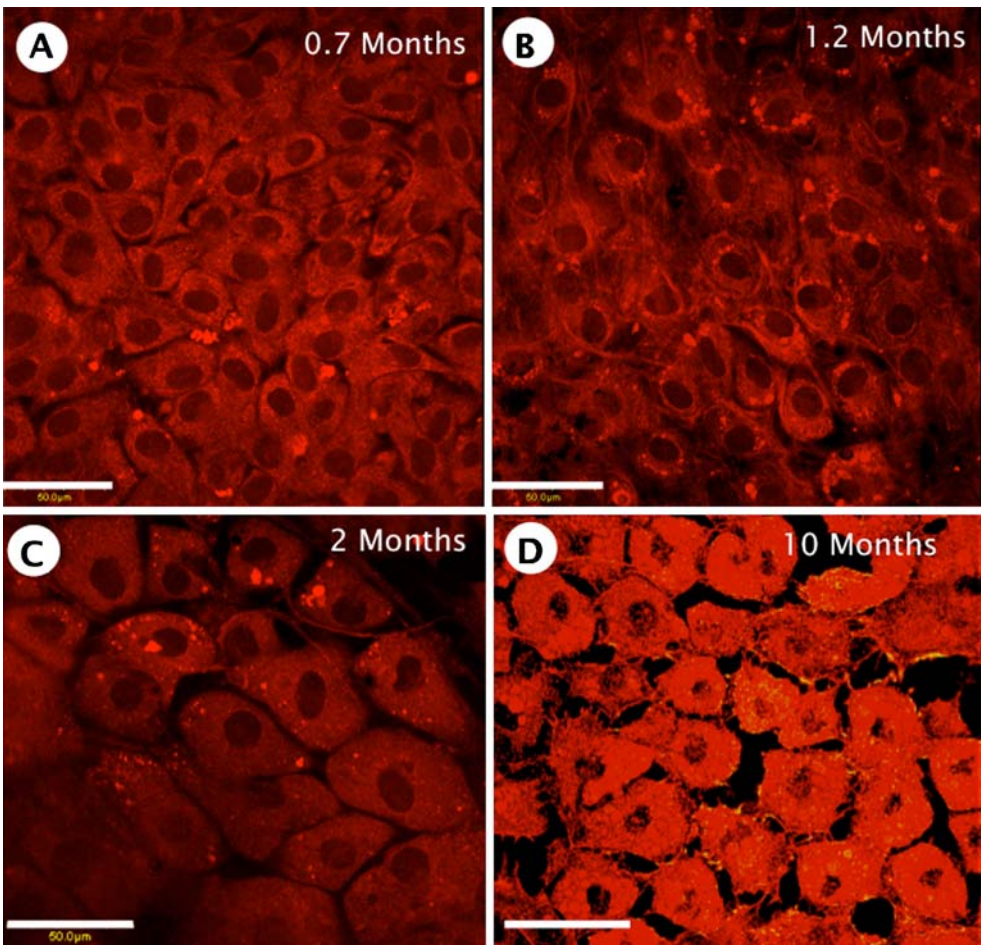

Figure 3. Progression in cell morphology monitored by confocal microscopy of Alexa Fluor 568 phalloidin stained MC3T3E-1 within the bioreactor over 10 mo of culture (compare with Fig. 2). (*A*) "Cobblestone"-shaped osteoblast-like cells matured from fibroblastic pre-osteoblasts within 3 wk. (*B*) Elongated cells appeared with development of many cellular processes within 1.2 mo. (*C*) Density of cells enmeshed in a dense collagenous matrix (appears *black* and see Figs. 4 and 8 in Dhurjati et al. (2006)) decreased over 2 mo. (*D*) One to two layers of stellate cells with many intercellular contacts after 2–10 mo of continuous culture. *Scale bar* represents 50 μm.

was densely packed with close cell contacts (Fig. 1*C*, *D*). Continuous culture reproducibly resulted in transformation of spindle-shaped pre-osteoblasts into cobblestone-shaped osteoblasts that secreted and mineralized an extensive, collagenous extracellular matrix that completely enveloped the cells (Dhurjati et al. 2006, 2008).

Quantitative evaluation of ~30–50 histological and ultrastructural sections taken from bioreactor cultures at different times (Fig. 2) revealed continuous transformation of tissue. Initially, the cells were closely packed (high cell/matrix ratio) but transformed into a more mature phenotype (low cell/matrix) after about 5 mo. Confocal microscopy (Fig. 3*A–D*) further revealed that this transformation was associated with a progression in cell morphology from cuboidal to stellate with many intercellular contacts (indicated by arrows).

SEM images of a bioreactor after 10 mo of continuous culture (Fig. 4*A*, *B*) showed that tissue was about 50 μm thick and was comprised of stellate cells interconnected with many processes with different lengths ranging from about one cell diameter ("short") to many cell lengths ("long"). Examination of many TEM images (e.g., Fig. 4*D*) revealed that intercellular connections terminated in overlapping protrusions (see arrows). From these images and molecular biology (Table 1), we concluded that the entire tissue was substantially comprised of osteocytic cells. However, we cannot discount the possibility that there was a mixed population of osteoblasts and osteocytes at various stages of genotypic and phenotypic transition.

We counted 36 osteocytes in a 4-μm^2 confocal images field (Fig. 4*C*), suggesting that there were about 9×10^4 osteocytes/cm^2. This value further translated into two million osteocytes/bioreactor; assuming that the 27-μm tissue shown was uniform across the entire 25-cm^2 growth space (see Fig. 5*D*). We further estimated that there were about 3.4×10^4 osteocytes/mm^3, which compared favorably with 1.3×10^4 osteocytes/mm^3 measurements on human bone (Mullender et al. 1996; Sugawara et al. 2005).

Gene expression. The phenotypic progression suggested by cell morphology was reflected in the characteristic expression of genes such as type I collagen, osteonectin, osteocalcin, and osteopontin (Table 1; Lian and Stein

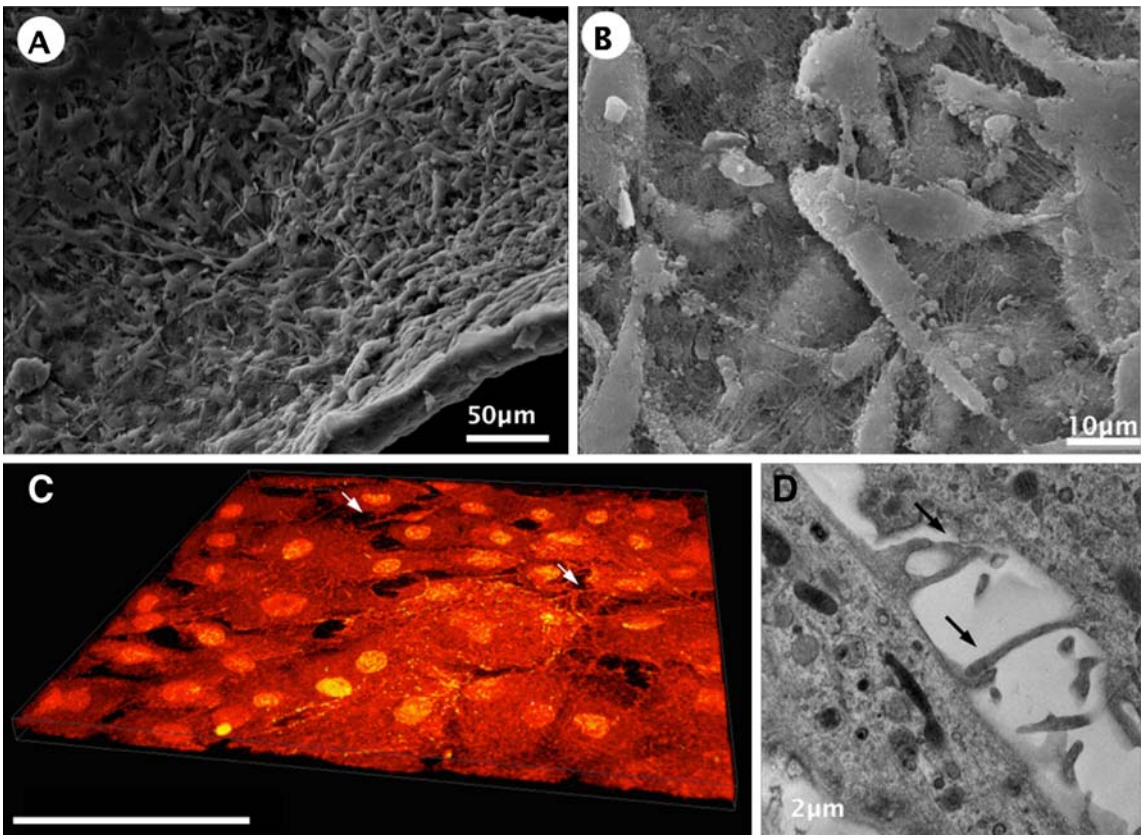

Figure 4. Osteocyte-like cells mature within the bioreactor over 10 mo continuous culture. (*A*, *B*) SEM image of ~23-μm-thick tissue showing closely packed stellate cells interconnected with many cellular processes. (*C*) Confocal image of Alexa Fluor 568 phalloidin stained osteocytes showing one to two cell layers with many intercellular processes. (*D*) High-magnification TEM image of overlapping cell protrusions (*arrows*) typical of osteocytes.

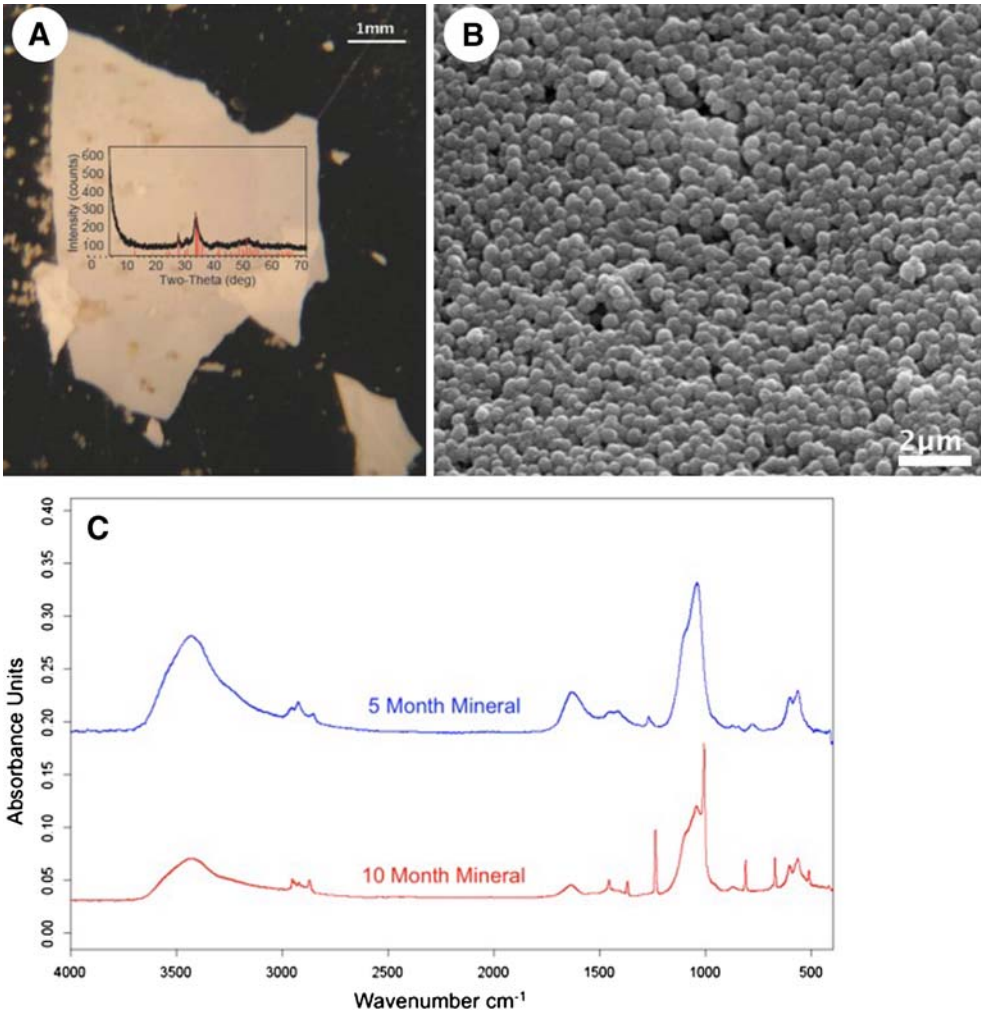

Figure 5. Macroscopic mineral deposits on the growth chamber side of the bioreactor dialysis membrane. Mineral chip taken from a 10-mo bioreactor dialysis membrane were prepared for X-ray diffraction or FTIR spectral analyses as described in the "Materials and Methods" section. (*A*) The X-ray diffraction pattern was similar to bovine bone (*inset*). (*B*) The chip was comprised of close-packed spherical nodules. (*C*) FTIR spectra of chips recovered from 5 and 10 mo bioreactors showing changes in chemical composition with deposition time.

1992). Upregulation of matrix metalloproteinase (MMP)-13 (indicative of extracellular matrix remodeling) and the proteins E11, DMP-1, and sclerostin, indicative of osteocytic transformation (Franz-Odendaal et al. 2006), occurred in more mature cultures. However, these results do not guarantee that the culture contained mature osteocytes exclusively, possibly accounting for the low yield of sclerostin detected. Moreover, in spite of the fact that there were numerous viable cells within the bioreactor after 10 mo, RNA recovery was lower than that of younger bioreactors (Table 1), consistent with fewer cells and perhaps related to the relatively low metabolic activity attributed to osteocytes (see "Discussion" section).

Formation of macroscopic bone. After about 2 mo of continuous culture, bioreactors occasionally exhibited contiguous, square centimeter-scale macroscopic mineral deposits on the growth chamber side of the dialysis membrane (see Supplementary Figure 1). Dialysis membranes from bioreactors without visually apparent mineral were found by FTIR spectroscopy to produce weak signals consistent with hydroxyapatite (data not shown), suggesting that osteoblasts may have passed too quickly through the mineral-deposition phase to produce visually apparent aggregates. Too few bioreactors have been studied to date to discover the exact conditions that led to bioreactor ossification, but there was no doubt that unknown experimental factors (e.g., inoculum concentration, precise timing of media replacement, etc.) occasionally led to deposition of macroscopic bone-like mineral. This material did not appear in bioreactors kept with differentiation medium alone in the absence of cells. X-ray diffraction of a mineral "chip" (Fig. 5*A*) also was consistent with bovine bone (see inset of Fig. 5*A*). SEM of the chip revealed that the deposit was comprised of many nodules (Fig. 5*B*), consistent with a nucleation-and-growth deposition phenomenon. Comparison of FTIR spectra of chips recovered from 5 to 10 mo bioreactors suggested an evolution of chemical composition with deposition time (Fig. 5*C*), although the FTIR spectra were not further interpreted in detail.

Discussion

Osteoblastic tissue growth and phenotypic maturation under continuous long-term culture. Cell and tissue morphological evidence (Figs. 1, 2, 3, and 4) combined with gene expression data (Table 1) has led us to conclude that growth and maturation of MC3T3-E1 derived osteoblastic tissue over 10 mo of continuous culture in the bioreactor recapitulated the normal sequence of bone deposition characterized by stages of proliferation, matrix maturation, mineralization and terminal differentiation into osteocytes (Lian and Stein 1992). In particular, the tissue progressed through these stages (Fig. 2) showing no apparent signs of necrosis. In fact, microscopy revealed that tissue recovered from 10 mo bioreactors was quite similar to 5 mo tissue (not shown), suggesting that viability through the phenotypic transition stage (Fig. 2) was nearly constant. We therefore speculate that osteoblastic tissue can be sustained indefinitely within the bioreactor with only occasional refreshment of basal media in the reservoir, but we have not yet experimentally examined cultures longer than 10 mo. Gene expression was likewise consistent with phenotypic maturation into osteocytes indicated by the expression E-11, DMP-1, and sclerostin.

Osteocytes developed to densities similar to that seen in calvarial bone (Sugawara et al. 2005). If this osteocytic tissue has an architecture similar to authentic bone (Fig. 4*A*), then at least calvarial osteocytes are quite closely packed in bone in a way that is different from osteocytes in shafts of long bone where they are separated by several cell diameters interconnected by long processes (Eriksen et al. 2007). Textbook images convey the idea that osteocytes are rather sparse in bone. Neither our data nor measurements of osteocyte density in authentic bone (Mullender et al. 1996; Sugawara et al. 2005) support such a perspective for calvaria-derived bone. Since carrying out this work, we became aware of a paper by (Murshid et al. 2007) comparing primary chicken osteoblasts to MC3T3-E1 grown in a 3D matrigel matrix. The cells that grew in both cultures were similar but not identical. This group did not assay for osteocyte proteins, i.e., sclerostin, DMP-1, or E-11, so we cannot compare our work directly with theirs.

Formation of macroscopic bone. Deposition of contiguous, square centimeter-scale macroscopic mineral is, to our knowledge, unprecedented in the culture of bone cells in vitro. Failure to routinely reproduce bioreactor ossification suggests uncontrolled variable(s) in the culture that once discovered may help understand critical variables involved in bone restoration after trauma or disease. We were struck by the observation that this cell-mediated mineral deposition formed on the cell side of the dialysis membrane (see Supplementary Figure 1). Osteoblasts exocytose vesicles containing enzymes responsible for mineral formation (Anderson et al. 2005) which were observed in TEM sections of osteoblastic tissues (e.g., Fig. 1*C*). Presumably, these secreted enzymes caused nucleation of mineral nodules on the dialysis membrane that aggregated into a contiguous layer with time. This mineral deposit had the X-ray and FITR characteristics of bone and did not appear to be due to the microcrystalline apatite deposition described by Cisar et al. (2000). Clearly, more research is required to fully trace steps involved in formation of macroscopic mineral deposits by osteoblasts in the environment of the bioreactor.

Implications for osteobiology. We suggest that the ability to monitor and control the maturation of osteoblastic tissue in vitro is useful to the study of osteogenesis and osteopathologies. Foremost is the ability to create readily accessible osteocytes that are otherwise accessible only by extraction from bone using rigorous extraction protocols (Nijweide and Burger 1990). Growth of osteocytes from isolated pre-osteoblasts offers the distinct advantage that demineralization is not required. Furthermore in the bioreactor, cells can be directly observed by microscopy. Moreover, the conditions of culture can be controlled and modified to better understand the process of osteogenesis. We have already used the bone model to study the affect of metastatic breast cancer known to invade skeleton on osteoblastic tissue (Mastro and Vogler 2009). We directly observed cancer cell adhesion, penetration, colony formation, and osteoblast reorganization heretofore only inferred in 2D culture models. This result encourages use of 3D tissue models in the study of other pathologies, such as osteoarthritis, osteomalacia, and osteoporosis.

The bioreactor employed in this work is probably only one of many that can produce bone tissue with varying phenotype ranging from pre-osetoblast to terminally differentiated osteocytes. However, a critical attribute of this method is creation of a pericellular microenvironment that mimics growing bone. The simultaneous-growth-and-dialysis method is crucial in this regard because it allows concentration gradients to form that guide cell maturation.

Acknowledgments This is supported by U.S. Army Medical and Material Command Breast Cancer Program WX81XWH-06-1-0432, Susan G. Komen for the Cure BCTR 0601044, with additional support from the National Foundation for Cancer Research. Authors appreciate the expert technical assistance of Ms. Donna Sosnoski and the Cytometry and the Electron Microscopy Facilities at Penn State. We thank Dr. Carol Gay for her thoughtful discussions and critique.

References

Anderson H. C.; Garimella R. et al. The role of matrix vesicles in growth plate development and biomineralization. *Front Biosci* 10: 822–837; 2005.

Chaudhuri J.; Al-Rubeai M. Bioreactors for tissue engineering: Principles, design and operation. Springer, Berlin; 2005.

Cisar J. O.; Xu D. Q. et al. An alternative interpretation of nanobacteria-induced biomineralization. *Proceedings of the National Academy of Sciences* 97: 11511–11515; 2000.

Dhurjati R.; Krishnan V. et al. Metastatic breast cancer cells colonize and degrade three-dimensional osteoblastic tissue in vitro. *Clin Exp Metastasis* 25: 753–763; 2008.

Dhurjati R.; Liu X. et al. Extended-term culture of bone cells in a compartmentalized bioreactor. *Tissue engineering* 12: 3045–3054; 2006.

Doty S. B. Morphological evidence of gap junctions between bone cells. *Calcif Tissue Int* 33: 509–512; 1981.

Ducy P.; Schinke T. et al. The osteoblast: A sophisticated fibroblast under central surveillance. *Science* 289: 1501–1504; 2000.

Eriksen E. F.; Eghbali-Fatourechi G. Z. et al. Remodeling and vascular spaces in bone. *J Bone Miner Res* 22: 1–6; 2007.

Franz-Odendaal T. A.; Hall B. K. et al. Buried alive: How osteoblasts become osteocytes. *Developmental Dynamics* 235: 176–190; 2006.

Knothe Tate M. L.; Adamson J. R. et al. The osteocyte. *The International Journal of Biochemistry & Cell Biology* 36: 1–8; 2004.

Knothe Tate M. L.; Tami A. et al. Micropathoanatomy of osteoporosis—indications for a cellular basis for bone disease. *Advances in Osteoporotic Fracture Management* 2: 9–14; 2002.

Lian J. B.; Stein G. S. Concepts of osteoblast growth and differentiation: basis for modulation of bone cell development and tissue formation. *Crit Rev Oral Biol Med* 3: 269–305; 1992.

Mastro A. M.; Vogler E. A. A three-dimensional osteogenic tissue model for the study of metastatic tumor cell interactions with bone. *Cancer Res* 69: 4097–4100; 2009.

Mullender M. G.; van der Meer D. D. et al. Osteocyte density changes in aging and osteoporosis. *Bone* 18: 109–113; 1996.

Murshid S. A.; Kamioka H. et al. Actin and microtubule cytoskeletons of the processes of 3D-cultured MC3T3-E1 cells and osteocytes. *J Bone Miner Metab* 25: 151–158; 2007.

Nijweide P. J.; Burger E. H. Mechanisms of bone formation in vitro. In: Hall B. K. (ed) Bone. Volume 1: The osteoblast and osteocyte. The Teleford, Caldwell, pp 303–326; 1990.

Palumbo C.; Palazzini S. et al. Morphological study of intercellular junctions during osteocyte differentiation. *Bone* 11: 401–406; 1990.

Rodan G. A.; Martin T. J. Therapeutic approaches to bone diseases. *Science* 289: 1508–1514; 2000.

Rose G. G. Cytopathophysiology of tissue cultures growing under cellophane membranes. *Int. Rev. Exp. Pathol.* 5: 111–178; 1966.

Rubens R. D. Bone metastases—the clinical problem. *European Journal of Cancer* 34: 210–213; 1998.

Rubens R. D.; Mundy G. R. Cancer and the skeleton. Informa Health Care, London; 2000.

Service R. F. Tissue engineers build new bone. *Science* 289: 1498–1500; 2000.

Sugawara Y.; Kamioka H. et al. Three-dimensional reconstruction of chick calvarial osteocytes and their cell processes using confocal microscopy. *Bone* 36: 877–883; 2005.

Vogler E. A. A compartmentalized device for the culture of animal cells. *J. Biomater. Artif. Cells Artif. Organs* 17: 597–610; 1989.

Bisphosphonate Effects on Breast Cancer Colonization of Three-Dimensional Osteoblast Tissue

Genevieve N. Miller, McNair Scholar
The Pennsylvania State University

McNair Faculty Research Advisors:
Erwin A. Vogler, Ph.D.
Professor of Materials Science and Engineering
Departments of Materials Science and Engineering and Bioengineering
College of Engineering
The Pennsylvania State University
Andrea M. Mastro, Ph.D.
Professor of Microbiology and Cell Biology
Department of Biochemistry and Molecular Biology
Eberly College of Science
The Pennsylvania State University

ABSTRACT

The purpose of this study was to characterize the effect of zoledronic acid (a bisphosphonate used clinically to treat bone metastasis) on osteoblasts and a model of breast cancer metastasis to bone *in vitro*. Murine calvarial pre-osteoblasts (MC3T3-E1) were grown to various stages of maturity in tissue culture and continuously treated with zoledronic acid (ZA) at 0.05, 0.50 or 5.00 μM concentrations. Drug effects on osteoblast proliferation, differentiation and mineralization were assessed. Additionally, mineralized 3D osteoblastic tissue was grown in a specialized bioreactor based on the principle of simultaneous-growth-and-dialysis. This 3D bone model provides a unique test system in which cancer cell interactions with osteoblastic tissue at controlled phenotypic maturities can be monitored in real time. Using this system, human metastatic breast cancer cells (MDA-MB-231) were co-cultured for 6 days with osteoblastic tissue in the actively-mineralizing phase (120 days of continuous culture). Without added ZA, cancer cells were observed to attach, penetrate, and colonize osteoblastic-tissue in a continuous process that ultimately marshaled osteoblasts into linear files similar to that observed in authentic pathological tissue. A single dose of ZA (at 0.50 μM and 0.05 μM administered 3 days after co-culture was initiated) delayed cancer-cell penetration and colony formation, with osteoblasts retaining the characteristic cuboidal shape observed in controls for the first 2 days of co-culture. Thereafter, cancer-cell colonization progressed to the filing stage.

INTRODUCTION

Breast Cancer in Bone

Breast cancer is the second most commonly diagnosed cancer in women in the United States, with an estimated 192,370 new cases of invasive breast cancer in 2009 [1]. Breast cancer also ranks second as the cause of cancer deaths, with an expected 40,610 breast cancer deaths this year [1].

Breast cancer may progress to become invasive, i.e. cancer cells spread throughout the breast tissue, or metastatic, i.e. cancer cells spread to other organs in the body [2]. Breast cancer frequently metastasizes to bone [3], where it disrupts the normal balance between the function of osteoblasts (bone-forming cells) and osteoclasts (bone-resorbing cells), favoring osteolysis [4]. Tumor cell production of parathyroid hormone-related protein (PTHrP) signals osteoblasts to increase expression of receptor activator of nuclear factor κB ligand (RANKL), which activates osteoclasts to begin bone resorption [5]. Transforming growth factor-β (TGF-β) is released from the bone matrix as it is degraded, which further stimulates cancer cell production of PTHrP [6], generating a "vicious cycle" between breast cancer and the bone environment.

Osteoblasts also contribute to bone loss during metastasis. Breast-cancer cells disrupt normal osteoblast function [7, 8] and suppress the production of matrix proteins. In addition they elicit an osteoblast stress response in which osteoblasts release inflammatory cytokines known to activate osteoclasts [9].

Bisphosphonate Therapy

A family of drugs called bisphosphonates has been widely used clinically for the management and prevention of skeletal complications from bone metastases [10]. Bisphosphonates are chemically stable synthetic analogues of inorganic pyrophosphate (P-O-P), a molecule that inhibits calcification [11], in which the oxygen atom has been replaced by a carbon atom (P-C-P). The third-generation, nitrogen-containing bisphosphonates, such as zoledronic acid, target the "vicious cycle" of breast cancer metastasis to bone in two ways – by reducing osteoclast activity and exhibiting direct antitumor effects on cancer cells. Bisphosphonates bind avidly to bone mineral, where they are internalized by osteoclasts during dissolution [12]. Once internalized, nitrogen-containing bisphosphonates inhibit the enzyme farnesyl diphosphate (FPP) synthase in the mevalonate pathway and interfere with functions essential for osteoclast survival [12, 13]. Bisphosphonates also directly affect tumor cells by inhibiting proliferation, inducing apoptosis, and interfering with adhesion, invasion, and angiogenesis [14].

The effects of bisphosphonates on tumor cells and osteoclasts have been well documented, but reported effects on osteoblasts vary among studies. Proliferation and differentiation of human fetal osteoblasts (hFOB 1.19) was reportedly enhanced by pamidronate coated cellulose scaffolds [15], while direct treatment of hFOB cells with pamidronate and zoledronate was found to decrease cell proliferation but enhance differentiation [16]. Treatment of human osteoblast-like cells derived from trabecular bone explants with zoledronic acid (ZA) promoted differentiation and mineralization but induced apoptosis at concentrations of 0.5 μM or greater [17]. The proliferation of primary human osteoblasts cultured on ZA-coated implants was not affected by concentrations up to 100 μM, while cells directly treated with 50 μM ZA were significantly reduced in number [18]. The proliferation and osteogenic differentiation of human bone marrow

stromal cells (BMSC) were enhanced by 10^{-8} M concentrations of alendronate, risedronate and zoledronic acid [19]. Zoledronic acid (1 μM – 1 nM) treatment of human mesenchymal stem cell (hMSC)-derived osteoblasts reportedly has little effect on differentiation but inhibits mineralization in a dose-dependent manner [20]. Studies using MG63 human osteoblast-like cells indicate that aledronate and pamidronate promote both proliferation and differentiation [21, 22], but zoledronic acid decreases proliferation in a dose-dependent manner [23].

In vitro studies using murine cell lines also produce various results. Treatment of MC3T3-E1 osteoblasts in tissue culture plates with 0.1-50 μM concentrations of zoledronic acid decreased cell proliferation [23], while the viability and mineralization of MC3T3-E1 cells cultured on calcium phosphate discs were unaffected by the same concentrations [24]. Researchers using aminobisphosphonates on primary rat osteoblasts and primary mouse osteoblasts found that nanomolar concentrations of each inhibited osteoblast mineralization while micromolar concentrations were toxic to the cells [25, 26]. Cells cultured on dentine substrates responded similarly to bisphosphonate treatment but at higher concentrations [25].

The results of these studies suggest that the effects of nitrogen-containing bisphosphonates on osteoblasts vary according to tissue complexity. To study the effects of these drugs on osteoblasts *in vitro* in a manner relevant to clinical applications, a sophisticated model of bone tissue is required.

Compartmentalized bioreactor

Modeling the bone environment to gain an understanding of the mechanisms underlying breast cancer colonization of bone is difficult. Cell systems must create an environment that provides biological relevance as well as experimental control [27]. The previous lack of a sophisticated bone model has not only hindered breast cancer metastasis research, but also has hindered the development and understanding of therapeutic treatments for bone metastases.

This research utilizes a compartmentalized cell culture device [28] based on the concept of simultaneous growth and dialysis pioneered by G.G. Rose [29] to grow and develop three-dimensional osteoblastic tissue for extended culture [30]. This compartmentalized cell culture device, hereafter referred to as the "bioreactor", consists of a cell growth chamber separated from a larger medium reservoir by a dialysis membrane. Waste from the growth compartment and nutrients from the medium reservoir are capable of dialyzing, while macromolecules synthesized by the cells as they develop are maintained in the cell growth space. Media is exchanged in the medium reservoir, thereby reducing drastic environmental changes cells experience in conventional tissue culture. The bioreactor creates an extraordinarily stable cellular environment that allows for the growth of multiple-cell layer osteoblastic tissue. Three-dimensional osteoblastic tissue has been maintained for over 10 months of continuous culture using this device [30].

The 3D osteoblastic tissue grown in the bioreactor can be challenged with metastatic breast cancer cells to model the initial stages of breast cancer colonization of bone. Human metastatic breast cancer cells (MDA-MB-231) introduced into existing cultures of murine osteoblasts (MC3T3-E1) were observed to adhere to and penetrate osteoblastic tissue and form colonies

within the cultures [31]. Furthermore, breast cancer cells were observed to align into "Indian files", chains of single cancer cells, characteristic of cancer invasion [31, 32]. This system allows for the real time monitoring of breast cancer colonization of osteoblastic tissue.

The purpose of this study was to characterize the effect of a nitrogen-containing bisphosphonate, zoledronic acid, on osteoblasts in conventional tissue culture and osteoblasts challenged with metastatic breast cancer cells in the compartmentalized bioreactor.

MATERIALS AND METHODS

Cells and tissue culture conditions

Murine calvaria pre-osteoblast (MC3T3-E1) cells were a gift from Dr. Norman Karin at the Pacific Northwest National Laboratories (ATCC CRL-2593). MC3T3-E1 were cultured in an incubator at 37^{o}C with 5% CO_2 and maintained in alpha minimum-essential medium (α–MEM) (Mediatech, Herdon, VA) supplemented with 10% heat-inactivated neonatal fetal bovine serum (FBS) (Cansera, Roxdale, Ontario) and 1% 100 U/ml penicillin and 100 μg/ml streptomycin (Sigma, St. Louis, MO), hereafter referred to as growth medium. MC3T3-E1 were passaged every 3-4 days using 0.002% pronase in phosphate buffered saline (PBS). Cells were not used above passage 20. Growth medium further supplemented with 50 μg/ml ascorbic acid and 10mM β-glycerophosphate (Sigma, St. Louis, MO), hereafter referred to as differentiation medium, was used to develop mineralized, differentiated osteoblasts.

Human metastatic breast cancer (MDA-MB-231) cells genetically engineered to produce green fluorescent protein (GFP) were a gift from Dr. Danny Welch at the University of Alabama at Birmingham (ATCC-HTB 26). MDA-MB-231^{GFP} cells are capable of forming bone metastases [33]. MDA-MB-231^{GFP} were cultured at 37^{o}C with 5% CO_2 and maintained in Dulbecco's Modified Eagle's medium (DMEM) (Mediatech, Herdon, VA) supplemented with 5% heat-inactivated neonatal FBS and 1X non-essential amino acids.

Zoledronic acid

Zoledronic acid (2-(imidazol-1-yl)-hydroxyehtylidene-1,1-bisphosphonic acid, disodium salt) was purchased from Toronto Research Chemicals, North York, Ontario and dissolved in 0.1 N NaOH to make a 5 mM stock solution.

Tissue culture

MC3T3-E1 were plated at a sub-confluent density (10^4 cells/cm^2) onto 24-well plates (Corning, Corning, NY). Differentiating cells were maintained with periodic media changes every 3-4 days.

Bioreactor design and implementation

Compartmentalized bioreactors based on the principal of simultaneous growth and dialysis were constructed as described previously [30]. Briefly, 316L stainless steel stock rings were tightly secured together by stainless steel screws to create the body of the device. Two compartments – a cell growth chamber (5 ml volume) and a larger (30 ml volume) medium reservoir – were formed with two outer gas-permeable and liquid-impermeable films and an inner dialysis membrane. The films forming the outer barriers were approximately 3 mm thick and made by hot pressing Surlyn 1702 resin (DuPont, Wilmington, DE) using simultaneous application of heat (220^{o}C) and pressure (245 Pa) in a laboratory hot press. The inner film was cellulosic-dialysis membrane (Spectrapor-13266; Spectrum Medical Industries, Rancho Dominguez, CA) and was hydrated in de-ionized water for 2 hours prior to assembly of the device. Assembled bioreactors had a cell-growth area of 25 cm^2. Once assembled, bioreactor chambers were filled with 0.1% sodium azide in PBS, packaged in plastic bags, and sterilized using 10 Mrad γ-ray irradiation at the Breazeale Nuclear Reactor Facility at the Pennsylvania State University. Sterile bioreactors were rinsed 3 times with PBS and incubated overnight with basal medium (aMEM, 1% penicillin-streptomycin) prior to cell inoculation.

MTT assay for cell proliferation

MC3T3-E1 were plated at 10^4 cells/cm^2 in growth medium. Following overnight incubation, zoledronic acid was added at 0.05, 0.50 and 5.00 μM concentrations for 24, 48, and 72 hours, upon which cell viability was assessed with an MTT assay. MTT (3-(4,5-Dimethylthiazol-2-yl)-2,5-diphenyltetrazolium bromide) (Sigma, St. Louis, MO) at 5 mg/ml in PBS was added to the cultures equivalent to $1/10^{th}$ of the culture volume (50 μl/500 μl per well). Cells were incubated at 37^{o}C in 5% CO_2 for 2 hours. Cells were then rinsed once with PBS and 1 ml solubilization solution (0.1 N HCl, 1% Triton X-100 in isopropanol) was added to dissolve the formazan crystals. Samples were read at 570 nm on a spectrophotometer with 650 nm background subtraction. Viable cell numbers were used to determine proliferation over time.

Alkaline phosphatase activity

MC3T3-E1 were plated at 10^4 cells/cm^2 in differentiation medium and maintained with periodic media changes for 17 days. After 17 days, differentiation medium was exchanged with zoledronic acid in concentrations of 0.05, 0.50 and 5.00 μM diluted from a 5 mM stock concentration with differentiation medium. Cells were cultured an additional week in the presence of zoledronic acid with two medium changes containing the drug. Following exposure to zoledronic acid for 7 days, MC3T3-E1 were stained for alkaline phosphatase activity. Culture medium was removed and the cells were rinsed twice with PBS. The cells were fixed for 10 minutes with 10% formaldehyde in PBS and then rinsed three times with PBS. Cells were

stained for alkaline phosphatase with a solution consisting of napthol, pre-warmed dH_2O, 0.2 M Tris (Sigma, St. Louis, MO) and Fast Blue RR Salt (Sigma, St. Louis, MO) and then incubated at 37^oC (no CO_2) for 30 minutes.

Von Kossa stain for mineralization

MC3T3-E1 were plated at 10^4 cells/cm^2 in differentiation medium and maintained with periodic media changes exactly as described for the alkaline phosphatase assay except the cells were grown for 28 days. After 28 days, differentiation medium was exchanged with zoledronic acid in concentrations of 0.05, 0.50 and 5.00 μM. Following exposure to zoledronic acid for 7 days, MC3T3-E1 were stained for calcium phosphate and calcium carbonate salts. Culture medium was removed and the cells were rinsed twice with PBS. The cells were fixed for 10 minutes with 10% formaldehyde in PBS and then rinsed three times for five minutes each with dH_2O. A 5% silver nitrate solution (diluted in dH_2O) was added to the cells, and they were incubated in the dark for 30 minutes at room temperature. The cells were rinsed three times with dH2O, a final volume of 0.5 mL dH2O was added to the cells, and they were incubated for 2 hours under a fluorescent lamp.

Bioreactor co-cultures

MC3T3-E1 were inoculated into bioreactor cell growth chambers at 10^4 cells/cm^2 and were cultured for 120 days with medium changes to the medium reservoir every 30 days. After 120 days, osteoblast tissue was stained with Cell Tracker Orange™ (Invitrogen, Carlsbad, CA) for live confocal imaging to monitor osteoblast morphology throughout the experiment. MDA-MB-231^{GFP} cancer cells were inoculated into the cell growth chambers containing osteoblast tissue at a 1:10 ratio of breast cancer cells to osteoblasts (10^5 cancer cells/bioreactor). Cancer cells were observed using confocal microscopy. Zoledronic acid was added to bioreactor cell growth chambers in concentrations of 0.05 and 0.5 μM after 72 hours, a time when the cancer cells and the osteoblasts were re-organizing into files. Cultures were monitored for an additional 72 hours using confocal microscopy. On day 6, bioreactors were disassembled and the film containing adherent osteoblast tissue was carefully cut into pieces for various assays. Medium from the cell growth space and medium reservoir was also collected for analysis.

Confocal microscopy

Cultures maintained in bioreactors were observed daily using an Olympus FV-300 laser-scanning microscope (Olympus America Inc., Center Valley, PA) at 20x and 40x magnifications. Cell Tracker OrangeTM was excited using a 543 nm helium-neon laser and collected through a 565 nm long-pass filter. GFP was excited using a 488 nm argon laser and collected through 510 nm long-pass and 530 nm short-pass filters. The emission was split through a 570 nm dichroic

long-pass filter. Adherent osteoblast tissue from disassembled bioreactors was fixed in 2.5% glutaraldehyde in PBS and stained for actin filaments with Alexa Fluor 568 phalloidin stain (Invitrogen, Carlsbad, CA) for further image analysis.

RESULTS

Zoledronic acid effects on osteoblast proliferation.

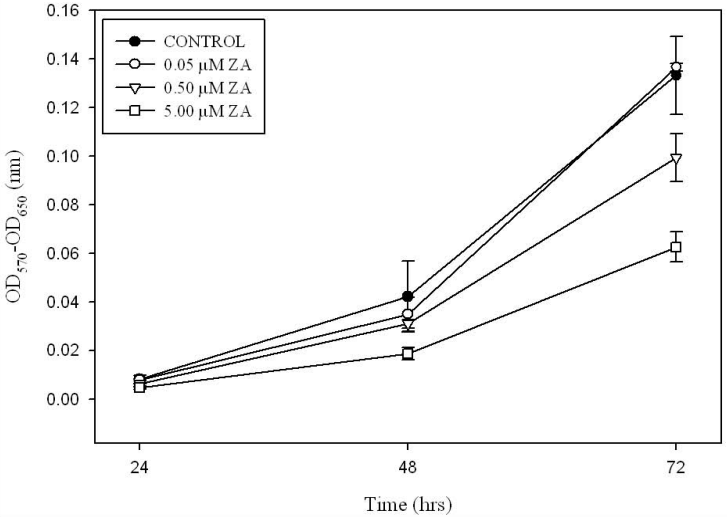

FIGURE 1. Effect of zoledronic acid (ZA) on osteoblast proliferation. MC3T3-E1 were plated at 10^4 cells/cm^2, incubated overnight, and treated with ZA at 0.05, 0.50 and 5.00 μM concentrations for 24, 48, and 72 hours (control cells were untreated). Cell proliferation was assessed with an MTT assay.

Osteoblast proliferation was measured by quantifying mitochondrial activity using an MTT assay. MC3T3-E1 were continuously treated with zoledronic acid in 0.05, 0.50 or 5.00 μM concentrations for 24, 48 or 72 hours. Results are reported as average optical density at 570 nm with a background subtraction of 650 nm, plus or minus standard deviation between triplicate samples (Figure 1). Continous exposure to zoledronic acid at 0.50 and 5.00 μM concentrations for 48 and 72 hours inhibited osteoblast proliferation. Treatment with low concentration (0.05 μM) zoledronic acid, however, did not result in the same inhibition; the optical densities at all times were similar to the untreated controls.

Zoledronic acid effects on osteoblast differentiation and mineralization.

Effects of zoledronic acid on osteoblast differentiation were measured by staining for alkaline phosphatase production. Alkaline phosphatase is an enzyme linked to osteoblast differentiation. Cells were cultured in differentiation medium for 17 days and then continously treated with zoledronic acid in 0.05, 0.50 or 5.00 μM concentrations for an additional 7 days. The culture dish was scanned to generate images of the tissue (Figure 2, A-D). Zoledronic acid at 5.00 μM (D) exhibited relatively strong inhibitory effects on alkaline phosphatase production.

Drug effects on mineralization were assessed by a Von Kossa stain for calcium phosphate and calcium carbonate salt deposits. Von Kossa's stain indirectly measures calcium in mineralized tissue. MC3T3-E1 were cultured in differentiation medium for 28 days and continuously treated for 8 days with zoledronic acid in 0.05, 0.50 or 5.00 μM concentrations. Images of the stained tissue were taken with a digital camera (Figure 2, E-H). All concentrations of zoledronic acid disrupted osteoblast mineralization (F-H) when compared to controls (E).

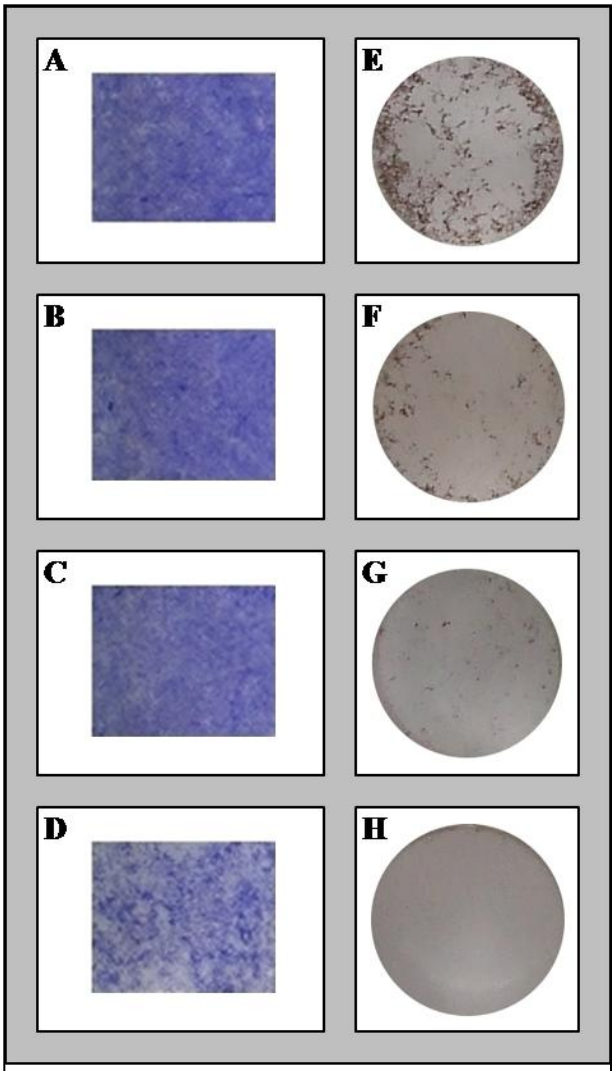

FIGURE 2. Effect of zoledronic acid (ZA) on osteoblast mineralization and differentiation. MC3T3-E1 were plated at 10^4 cells/cm^2 in differentiation medium and allowed to grow for 14 days (A-D) or 28 days (E-H) with periodic medium changes. Cells were then continuously treated with ZA at 0.05 (B,F), 0.50 (C,G) and 5.00 (D,H) μM concentrations for 8 days. Control cells (A,E) were untreated. Cell differentiation was assessed by alkaline phosphatase activity (A-D). Mineralization was determined with a Von Kossa stain (E-H).

Effects of zoledronic acid on breast cancer colonization of osteoblast tissue.

MC3T3-E1 were cultured in the bioreactor for 120 days with medium changes to the medium reservoir every 30 days. The osteoblast tissue was then challenged with metastatic breast cancer cells. Cancer cells were observed to colonize the tissue and organize into linear files after 48 hours, at which time zoledronic acid was added to the cultures in 0.05 and 0.5 μM concentrations. Cultures were maintained and monitored using confocal microscopy for an additional 72 hours.

Confocal images show breast cancer cells expressing green fluorescent protein (green) and osteoblasts stained with Cell Tracker Orange or Alexa Fluor 568 phalloiding (red) (Figure 3). Treatment with zoledronic acid reduced the formation of breast cancer cell colonies (Figure 3, compare A with B,C) and disrupted the alignment of breast cancer cells within the osteoblast tissue (Figure 3, compare D with E,F). Zoledronic acid also inhibited the penetration of breast cancer cells through the multiple-layer osteoblast tissue (Figure 3, table). Osteoblasts in cultures treated with zoledronic acid retained the characteristic cuboidal shape observed in the control (untreated) culture.

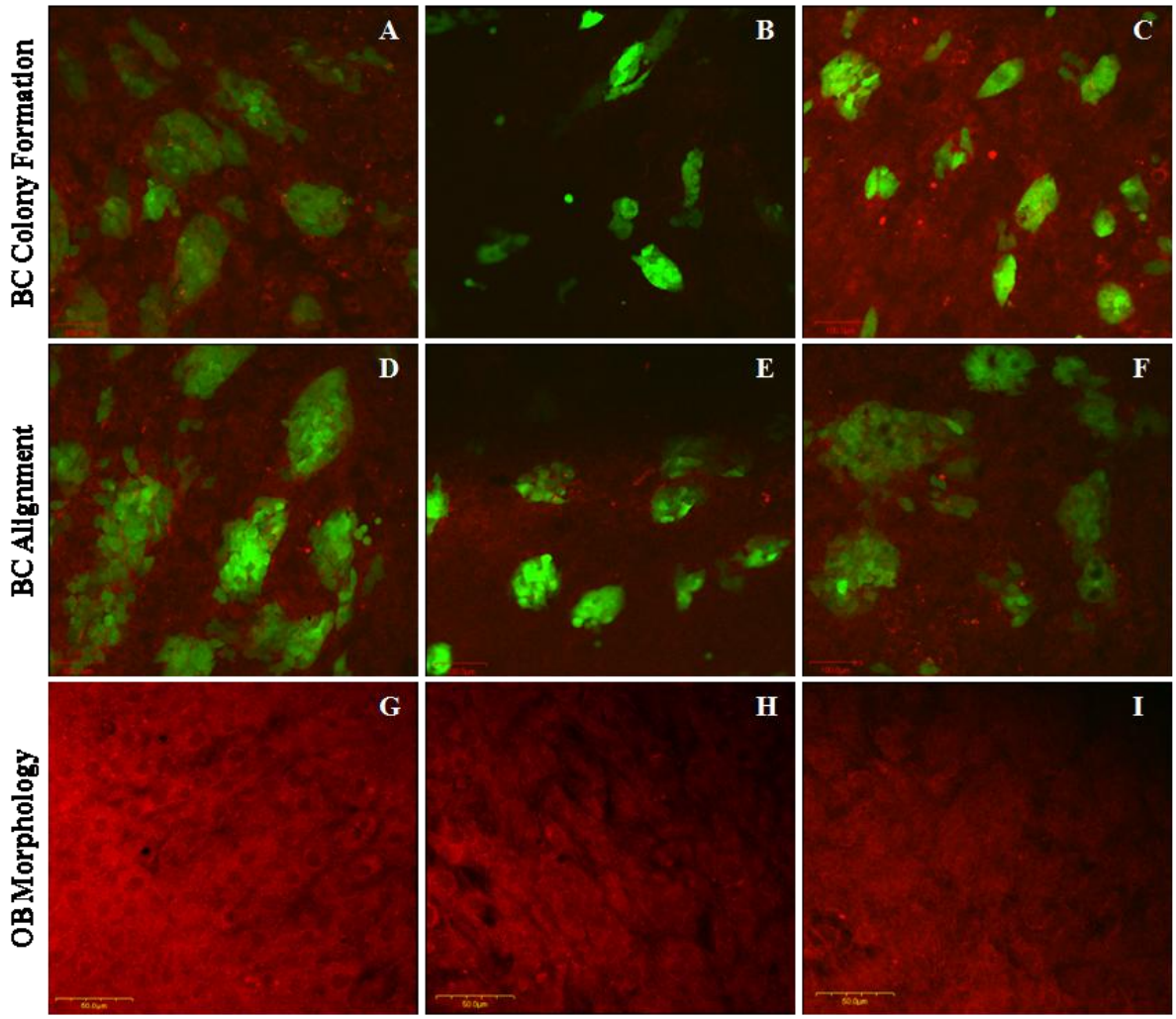

Experimental Parameter	Culture Conditions		
	OB + BC	OB + BC + 0.05 μM ZA	OB + BC + 0.50 μM ZA
BC Colony Formation	+++	+	++
BC Alignment	+++	+	++
Spindle-shaped OB Morphology	+++	+	++
Tissue Penetration	+++	+	++

FIGURE 3. Qualitative analysis of the effects of zoledronic acid (ZA) on MDA-MB-231 metastatic breast cancer cell (BC) colonization of osteoblast (OB) tissue. Cancer cells (green) were observed to penetrate and colonize osteoblast tissue (red) in the bioreactor (A,D,H). Addition of ZA to co-cultures in the bioreactor resulted in reduced breast cancer colony formation (B – 0.05 μM ZA, C – 0.50 μM ZA, 24 hr exposure) and disruption of cancer cell alignment with osteoblast tissue (E – 0.05 μM ZA, F – 0.50 μM ZA, 48 hr exposure). ZA delayed breast cancer cell penetration of osteoblast tissue (table) and osteoblasts retained characteristic cuboidal shape (I – 0.05 μM ZA, 72 hr exposure) consistent with controls (G). Scale bar = A-F: 100μM, G-I: 50 μM.

DISCUSSION AND FUTURE WORK

In this study, zoledronic acid was observed to have a notable effect on osteoblast proliferation, differentiation and mineralization. Treatment of sub-confluent MC3T3-E1 osteoblasts with zoledronic acid yielded a dose-dependent effect on proliferation (Figure 1), with higher concentrations of zoledronic acid inhibiting cell proliferation. Treatment with 0.50 μM zoledronic acid for 72 hours resulted in an approximate 25 percent reduction in osteoblast number, while treatment with 5.00 μM zoledronic acid for the same time inhibited proliferation by approximately 50 percent of the control. Exposure to a lower dosage (0.05 μM) of zoledronic acid had no statistically significant effect on osteoblast proliferation. However, these studies were carried out with cells grown in conventional tissue culture conditions.

Continuous treatment of 17- and 28-day old differentiated osteoblasts with zoledronic acid for one week resulted in decreased alkaline phosphatase production and calcium deposition, respectively (Figure 2). A continuous dose of zoledronic acid at 5.00 μM led to a reduction in alkaline phosphatase (Figure 2, D), while lower concentrations had little effect (Figure 2, B-C). All tested concentrations of zoledronic acid inhibited mineralization (Figure 2, F-H). Again, these tests were carried out with cells grown in tissue culture.

Exposure of three-month old osteoblasts grown in the bioreactor and challenged with metastatic breast cancer cells delayed the progression of cancer cells within the osteoblast tissue and temporarily maintained osteoblast tissue integrity (Figure 3). ZA treatment reduced the formation of breast cancer colonies (Figure 3, A-C) and inhibited breast cancer cell penetration of osteoblast tissue (Figure 3, table). Exposure of cancer cells to zoledronic acid also disrupted cancer cell alignment within the osteoblast tissue (Figure 3, D-F).

These results indicated that concentrations of zoledronic acid that minimally affect osteoblast function are capable of delaying breast cancer progression to bone. These data should be interpreted with caution, however. Other studies indicate that low concentrations (10 nM) of ZA do not significantly inhibit osteoblast proliferation until after 7 days of continuous culture [25]. Additionally, little is known about the adsorption kinetics of bisphosphonates. It is unclear whether ZA treatment of osteoblasts challenged with cancer cells in the bioreactor resulted in a true delay of breast cancer progression or occurred due to diffusion of ZA from the growth chamber to the medium reservoir. To address these concerns, future work will ensure that osteoblast proliferation is measured over an extended growth period and zoledronic acid is added to both bioreactor chambers.

Further analysis of the effects of zoledronic acid on breast cancer colonization of osteoblast tissue in the bioreactor is also required. RNA isolated from the bioreactor cultures will be

analyzed for expression of osteocalcin, Type I collagen, and other bone proteins. In addition, increases or decreases in cytokine production will be measured using medium collected from the bioreactor compartments.

Further studies will introduce the chemotherapeutic drug docetaxel into the bioreactor system, as literature suggests that zoledronic acid enhances the effects of docetaxel [34-39]. This study has shown that the bioreactor is a useful device for the study of drug effects on the early stages of breast cancer cell interactions with bone tissue.

ACKNOWLEDGEMENTS

This work was supported by the U.S. Army Medical Research and Material Command Breast Cancer Research Program WX81XWH-06-1-0432, the Susan G. Komen Breast Cancer Foundation BCTR 0601044, the Pennsylvania State University Office of Undergraduate Education, and the Penn State Ronald E. McNair Postbaccalaureate Achievement Program. I would like to thank Dr. Mastro, Dr. Vogler, and Donna Sosnoski for their guidance and assistance on this project. I would also like to thank Teresa Tassotti, Felicia Sanders and Judy Banker for their support.

REFERENCES

1. American Cancer Society. Cancer Facts & Figures 2009. Atlanta, GA: American Cancer Society, Inc. 2009; 1-72.
2. American Cancer Society. Breast Cancer Facts & Figures 2007-2008. Atlanta, GA: American Cancer Society, Inc. 2007; 1-36.
3. Rubens RD. Bone Metastases - The Clinical Problem. European Journal of Cancer 1998; 34 (2): 210-3.
4. Taube T, Elomaa I, Blomqvist C, et al. Histomorphometric evidence for osteoclast-mediated bone resorption in metastatic breast cancer. Bone 1994; 15 (2): 161-6.
5. Guise TA. Molecular mechanisms of osteolytic bone metastases. Cancer 2000; 88 (12 Suppl): 2892-8.
6. Bierie B, Moses HL. Tumour microenvironment: TGFβ: the molecular Jekyll and Hyde of cancer. Nat Rev Cancer 2006; 6 (7): 506-20.
7. Mercer RR, Miyasaka C, Mastro AM. Metastatic breast cancer cells suppress osteoblast adhesion and differentiation. Clinical and Experimental Metastasis 2004; 21: 427-35.
8. Mastro AM, Gay CV, Welch DR, et al. Breast Cancer Cells Induce Osteoblast Apoptosis: A Possible Contributor to Bone Degradation. Journal of Cellular Biochemistry 2004; 91: 265-76.
9. Kinder M, Chislock E, Bussard KM, et al. Metastatic breast cancer induces an osteoblast inflammatory response. Experimental Cell Research 2008; 314: 173-83.
10. Costa L, Lipton A, Coleman R. Role of bisphosphonates for the management of skeletal complications and bone pain from skeletal metastases. Supportive cancer therapy 2006; 3 (3): 143-53.
11. Fleisch H. Bisphosphonates: mechanisms of action. Endocrine reviews 1998; 19 (1): 80-100.
12. Green J. Bisphosphonates: Preclinical Review. The Oncologist 2004; 9(suppl 4): 3-13.
13. van Beek E, Pieterman E, Cohen L, et al. Farnesyl Pyrophosphate Synthase Is the Molecular Target of Nitrogen-Containing Bisphosphonates. Biochemical and biophysical research communications 1999; 264 (1): 108-11.
14. Green J. Antitumor effects of bisphosphonates. Cancer 2003; 97 (3 Suppl): 840-7.
15. Ponader S, Brandt H, Vairaktaris E, et al. In vitro response of hFOB cells to pamidronate modified sodium silicate coated cellulose scaffolds. Colloids and Surfaces B: Biointerfaces 2008; 64 (2): 275-83.

16. Reinholz GG, Getz B, Pederson L, et al. Bisphosphonates Directly Regulate Cell Proliferation, Differentiation, and Gene Expression in Human Osteoblasts. Cancer Res 2000; 60 (21): 6001-7.
17. Pan B, To LB, Farrugia AN, et al. The nitrogen-containing bisphosphonate, zoledronic acid, increases mineralisation of human bone-derived cells in vitro. Bone 2004; 34 (1): 112-23.
18. Greiner S, Kadow-Romacker A, Lbberstedt M, et al. The effect of zoledronic acid incorporated in a poly(D,L-lactide) implant coating on osteoblasts in vitro. Journal of biomedical materials research Part A 2007; 80 (4): 769-75.
19. von Knoch F, Jaquiery C, Kowalsky M, et al. Effects of bisphosphonates on proliferation and osteoblast differentiation of human bone marrow stromal cells. Biomaterials 2005; 26 (34): 6941-9.
20. Kellinsalmi M, Mnkknen H, Mnkknen J, et al. In vitro comparison of clodronate, pamidronate and zoledronic acid effects on rat osteoclasts and human stem cell-derived osteoblasts. Basic & clinical pharmacology & toxicology 2005; 97 (6): 382-91.
21. Panzavolta S, Torricelli P, Bracci B, et al. Alendronate and Pamidronate calcium phosphate bone cements: setting properties and in vitro response of osteoblast and osteoclast cells. Journal of inorganic biochemistry 2009; 103 (1): 101-6.
22. Xiong Y, Yang HJ, Feng J, et al. Effects of alendronate on the proliferation and osteogenic differentiation of MG-63 cells. The Journal of International Medical Research 2009; 37 (2): 407-16.
23. Peter B, Zambelli PY, Guicheux J, et al. The effect of bisphosphonates and titanium particles on osteoblasts: an in vitro study. Journal of Bone and Joint Surgery; British volume 2005; 87 (8): 1157-63.
24. Schindeler A, Little D. Osteoclasts but not osteoblasts are affected by a calcified surface treated with zoledronic acid in vitro. Biochemical and biophysical research communications 2005; 338 (2): 710-6.
25. Orriss IR, Key ML, Colston KW, et al. Inhibition of osteoblast function in vitro by aminobisphosphonates. J Cell Biochem 2009; 106 (1): 109-18.
26. Idris A, Rojas J, Greig I, et al. Aminobisphosphonates Cause Osteoblast Apoptosis and Inhibit Bone Nodule Formation In Vitro. Calcified Tissue International 2008; 82 (3): 191-201.
27. Mastro AM, Vogler EA. A Three-Dimensional Osteogenic Tissue Model for the Study of Metastatic Tumor Cell Interactions with Bone. Cancer Res 2009; 69 (10): 4097-100.
28. Vogler EA. A compartmentalized device for the culture of animal cells. Biomaterials, artificial cells, and artificial organs 1989; 17 (5): 597-610.
29. Rose GG. Cytopathophysiology of tissue cultures growing under cellophane membranes. Int Rev Exp Pathol 1966; 5: 111-78.
30. Dhurjati R, Liu X, Gay CV, et al. Extended-Term Culture of Bone Cells in a Compartmentalized Bioreactor. Tissue Engineering 2006; 12 (11): 3045-54.
31. Dhurjati R, Krishnan V, Shuman LA, et al. Metastatic breast cancer cells colonize and degrade three-dimensional osteoblastic tissue in vitro. Clin Exp Metastasis 2008.
32. Friedl P, Wolf K. Tumour-cell invasion and migration: diversity and escape mechanisms. Nat Rev Cancer 2003; 3 (5): 362-74.
33. Cailleau R, Oliv M, Cruciger QV. Long-term human breast carcinoma cell lines of metastatic origin: preliminary characterization. In vitro 1978; 14 (11): 911-5.
34. Brubaker KD, Brown LG, Vessella RL, et al. Administration of zoledronic acid enhances the effects of docetaxel on growth of prostate cancer in the bone environment. BMC Cancer 2006; 6 (15).
35. Fabbri F, Brigliadori G, Carloni S, et al. Zoledronic acid increases docetaxel cytotoxicity through pMEK and Mcl-1 inhibition in a hormone-sensitive prostate carcinoma cell line. Journal of Translational Medicine 2008; 6 (43).
36. Inoue K, Karashima T, Fukata S, et al. Effect of CombinationTherapy with a Novel Bisphosphonate, Minodronate (YM529), and Docetaxel on aModel of Bone Metastasis by HumanTransitional Cell Carcinoma. Clin Cancer Res 2005; 11 (18): 6669-77.
37. Karabulut B, Erten C, Gul MK, et al. Docetaxel/zoledronic acid combination triggers apoptosis synergistically through downregulating antiapoptotic Bcl-2 protein level in hormone-refractory prostate cancer cells. Cell Biology International 2009; 33: 239-46.
38. Kim S-J, Uehara H, Yazici S, et al. Modulation of Bone Microenvironment with Zoledronate Enhances the Therapeutic Effects of STI571 and Paclitaxel against Experimental Bone Metastasis of Human Prostate Cancer. Cancer Res 2005; 65 (9): 3707-15.
39. van Beek ER, Lowik CWGM, van Wijngaarden J, et al. Synergistic effect of bisphosphonate and docetaxel on the growth of bone metastasis in an animal model of established metastatic bone disease. Breast Cancer Res Treat 2008.